INVESTIGATIONS OF THE MICROSTRUCTURAL EVOLUTION IN Ti-6Al-4V ALLOY DURING CYCLIC HYDROGENATION AND DEHYDROGENATION HEAT TREATMENT

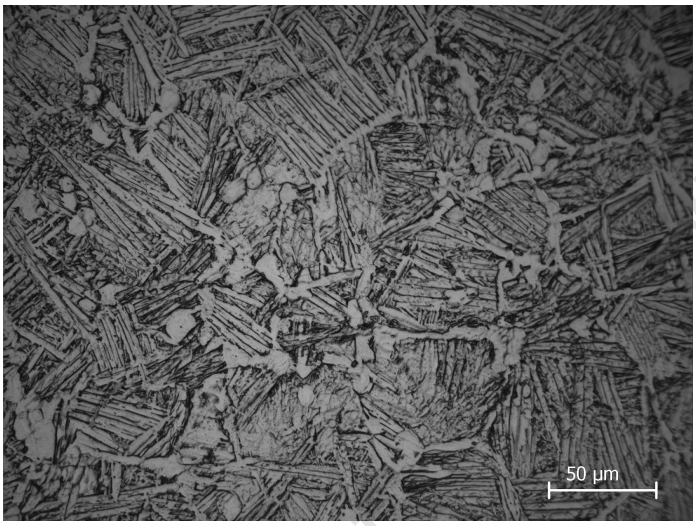

By

Jeremiah Chika Oguh

A thesis submitted to the Faculty of Engineering and the Built Environment of the University of Cape Town in fulfillment of the requirements for the degree of Master of Science in Engineering

Centre for Materials Engineering

Department of Mechanical Engineering

February 2008

DECLARATION

I, Jeremiah Chika Oguh, know the meaning of plagiarism and declare that all the work in this document, save for that which is properly acknowledged, is my own.

Signature: Date:

Abstract

The novel microstructures resulting from the temporary alloying of hydrogen in titanium 6 wt.-% aluminium 4 wt.-% vanadium alloy have been investigated. The temporary alloying process involves a two stage heat treatment during which hydrogen is firstly introduced into the titanium sample (hydrogenation), and secondly removed from the sample under vacuum annealing (dehydrogenation), thereby completing the cycle.

During the hydrogenation stage, the high diffusivity of hydrogen in titanium alloys at elevated temperatures is used to introduce hydrogen into the sample. Hydrogen being a β stabilizing element of titanium alloys, lowers the β → (α+ β) transition temperature and slows the kinetics of the β → α phase transformation. This leads to the generation of new microstructures. Fine α-grain structures and martensitic plates were observed upon completion of the hydrogenation treatment.

The dehydrogenation treatments were carried out in vacuum at constant isothermal time but different temperatures (550^{o}C, 650^{o}C and 750^{o}C). Widmanstätten structures with α-phase colonies were observed after dehydrogenation at 750^{o}C and 650^{o}C. Dehydrogenation at 550^{o}C produced more nucleation and further growth of the grain boundary allotriormorphs and a homogeneous microstructure consisting of globular α-grains in a β matrix. The hardness result from dehydrogenation at 550^{o}C was higher than after similar treatments at 750^{o}C and 650^{o}C.

Dehydrogenation at 550^{o}C and 650^{o}C for 18 hours produced greater volume fraction of equiaxed α-grains compared to the structure achieved from the 750^{o}C. Furthermore, it is more cost effective to process at the temperatures of 550^{o}C and 650^{o}C respectively. The lower dehydrogenation temperatures are therefore recommended.

Acknowledgements

I would want to express my sincere gratitude to the following people for their significant contribution in the course of this research:

- My supervisor, Professor R. D. Knutsen for his valuable suggestions, supervision and guidance throughout this work
- Glen Newins, Hubert Tomlinson and the workshop staff for their technical assistance
- Mrs P Park–Ross for her technical and logistical assistance in the laboratories.
- Mrs N S Africa for all the administrative assistance.
- Professor C.Lang for her advice and encouragement
- Professor F.H.Froes for his advice on the safer gas mixture to be used
- Dr. Remy Bucher and Dr. Mira Topic for their encouragement and the X-ray scan
- Mrs F D Young for helping us to maintain a clean working environment.
- The staff and students of the Centre for Materials Engineering for their constant words of encouragement
- The Centre for Materials Engineering and the faculty of engineering for their financial supports

I would also want to greatly thank my sister Mrs. Maureen Onyenacho and her family, my parents Mr & Mrs. P.A.Oguh and all the members of Oguh's family for their love, prayers and commitments throughout my life.

Finally and most importantly, I am thanking God for giving me the wisdom and strength throughout the course of this study.

Glossary

Ti64	Ti-6Al-4V (weight percent)
HCP	Hexagonal Close Packed
BCC	Body Centred Cubic
Ms	start of Martensite
Hv	Vickers Hardness
p.p.m	parts per million
THP	Thermo-hydrogen processing
TRIP	Transformation-induced plasticity
HG	Hydrogenation
DH	Dehydrogenation
AC	Air cooled
FC	Furnace cooled
XRD	X-ray diffraction
OM	Optical microscopy
TEM	Transmission electron microscopy
SEM	Scanning electron microscopy

Table of contents

Chapter 1

Introduction

1.1 Background

Microstructure plays a crucial role in the mechanical properties of alloys, such as strength, ductility, creep resistance, fracture toughness and crack propagation resistance [1]. It is known that microstructural or property enhancements rely mainly on the chemical composition, processing history and thermal treatment procedures used on the Alloy [1].

Research into an understanding of the evolution of microstructure in titanium alloys when subjected to a solution heat treatment, especially when treated temporarily with hydrogen as an alloying element, can be of great benefit to optimise titanium applications considering the mechanical property enhancement these treatments have enabled lately.

Titanium alloys are most widely used in chemical, automobile, aeronautical and biomedical industries because of its unique combination of biocompatibility, corrosion resistance and high specific strength [2]. Titanium alloy containing 6 wt.% aluminium and 4 wt.% vanadium (Ti-6Al-4V) is a well known, relatively low cost and most commercially viable amongst titanium alloys due to its attractive properties such as low density, high specific strength, workability, corrosion resistance, good creep and fatigue resistance. It is used in all product forms including valves, gears, bearings and castings, and possesses a high potential for production of pieces with good mechanical properties [3]. The mechanical properties of this alloy are often degraded by the adverse effects of hydrogen embrittlement [4]. Titanium and conventional titanium alloys have high affinity for hydrogen, being capable of absorbing up to 50 at.% hydrogen [5]. At higher temperatures, hydrogen as a temporary alloying element in titanium alloys could refine

the microstructure and improve the properties of the alloys due to the hydrogen enhanced–plasticity, hydrogen-induced phase transformations and the reversible reaction of hydrogen with titanium [6-8]. The reaction of hydrogen with titanium is reversible due to a positive enthalpy of solution in titanium, allowing hydrogen to be removed by vacuum annealing [5].

Recent researchers have shown that even a relatively low concentration of hydrogen introduced into titanium alloys as a temporary alloying element has a great effect upon phase transformation and subsequent modification of microstructure and mechanical properties [5]. This novel technique called thermo-hydrogen processing (THP) is based on the modifying effect of hydrogen as an alloying element on phase compositions, development of metastable phases, and kinetics of phase transformations in titanium alloys [5]. In this approach, the high diffusivity of hydrogen in titanium is used first to add hydrogen to the alloy by controlled diffusion from hydrogen environment and then, after processing, to remove it by controlled vacuum anneal [5]. It summarily involves the hydrogenation and dehydrogenation heat treatment technique of titanium alloys.

There are reported evidences of novel microstructures that result from this heat treatment. Little information is thus far available in open literature about the mechanism of the evolution of these resultant microstructures.

1.2 Motivation of the Research

This project is aimed at contributing towards the ongoing initiative, sponsored by the Advanced Manufacturing Technology Strategy (AMTS), towards building a lighter aircraft.

Improvements in the performance of aircraft have been closely linked to progress in materials. Reducing structural weights is one of the major ways to improve aircraft performance. Light and/or stronger materials allow greater range and speed and may also contribute to reducing operational costs [3].

Microstructure plays a crucial role in the mechanical properties of alloys, such as strength, ductility, creep resistance, fracture toughness and crack propagation resistance [1]. It is known that these enhancements rely mainly on the chemical composition, processing history and thermal treatment procedures. Ti-6Al-4V is a candidate material for aerospace application. Understanding of the evolution of the resultant microstructure which contributes to its modifications could be significant to the alloy usage. Besides, there is a motivation towards using hydrogen as a temporary alloying element in order to refine the grain size of cast titanium components.

1.3 Research Objectives

The following are the objectives of this research:

- To design an effective apparatus for hydrogenation and dehydrogenation of Ti-6Al-4V alloy
- To effect the diffusion of hydrogen in the titanium sample for microstructural modification
- To investigate the effect of hydrogen on phase transformation temperatures during hydrogenation
- To investigate the effect of varying heat treatment parameters on microstructure evolution during the hydrogenation/dehydrogenation cycles
- To identify the most effective processing variables to achieve grain size refinement

1.4 Thesis Layout

This research has been presented in the following sequence. The first chapter has been used to introduce the research. The second chapter contains the review of the works that have been done in the area of this research. The experimental technique which starts with the equipment design followed by the experimental approach is contained in chapter three. The results obtained from the experiments are presented and discussed in chapter four. The conclusions drawn from the results are stated in chapter five and finally the recommendations for future work are listed in chapter six.

Chapter Two

Literature Review

2.1 Titanium alloys and their usages in the aerospace industry [3]

Titanium and its alloys are excellent candidates for aerospace applications owing to their high strength to weight ratio and excellent corrosion resistance. Titanium usage is, however, strongly limited by its higher cost relative to competing materials, primarily aluminium alloys and steels. Therefore the advantages of using titanium must be balanced against this added cost.

There are three titanium alloy types based on the composition of the alloy and the resultant predominant room temperature (RT) constituent phase(s), and each of these families of alloys serves a specific role. The alloy types (conventional alloys only) include: (a) α and near- α alloys, (b) α/β alloys (c) β- alloys.

Alpha 'α' is the low temperature allotrope of titanium, and the microstructure of α and near- α alloys consists predominantly of the α- phase. The α/β alloys are, for the most part, still mostly α at room temperature, but they do have more of the β- phase, the high temperature allotrope, than the former class of alloys. The definition of β- alloys is not fully agreed upon, but in very general terms, they are capable of retaining 100% β when quenched from the β- phase field. There is some overlap in each of these "families" of alloys.

α and Near- α Alloys: There are two types of alloys in this category, the commercially pure grades of titanium (with O_2 and Fe as the primary alloying elements) and those with intentional additions of α- stabilizers, such as Al and Sn. Some of these do contain minor additions of β- stabilizers, such as Mo & V, but there is very little β retained at room

temperature. The commercially pure grades can be obtained with minimum yield strengths from 170 to 480 MPa, with the higher strength grades containing more O_2 & Fe. Their primary characteristics are good formability, with the formability decreasing as the strength increases, and excellent corrosion resistance. Strengths are comparable with the annealed 300 series stainless steels, but with about 40% decrease in density. The commercially pure titanium alloys are not heat treatable; hence they exhibit good weldability.

The α and near α- alloys include alloys such as Ti-3Al-2.5V (Ti-3-2.5), Ti-5Al-2.5Sn (Ti-5-2.5), Ti-8Al-1Mo-1V (Ti-8-1-1) and Ti-6Al-2Sn-4Zr-2Mo (Ti-6-2-4-2S). The "S" is added to the end of the composition for the latter alloy to denote the Si addition. Minor Si additions, in the range of 0.1 to 0.25, and higher, enhance the creep resistance of the high temperature alloys [3, 9, 10]. These mechanical properties of these alloys project it for elevated temperature applications.

α/β Alloy: The alloys include: Ti-6Al-4V (Ti-6-4), Ti-6Al-6V-2Sn(Ti-6-6-2) and Ti-6Al-2Sn-4Zr-6Mo(Ti-6-2-4-6). They are capable of somewhat higher strengths than the near-α alloys, have good combinations of properties, have a wide processing window, which means that processing requirements are not as stringent as for other types, and, depending on the alloy, are good for applications up to the range of about 315 to 400^{o}C. They can be strengthened, usually with a solution treatment below the β transus (the minimum temperature at which the alloy consists of 100% β- phase) to establish the hardenability, and a subsequent age. The amount of strengthening which can be achieved is a function of the alloy and section thickness. Alloys with the lower β- stabilizer contents such as Ti-6Al-4V, are highly weldable. As the β- stabilizer content increases, the hardenability increases but welding becomes more difficult.

Aluminium is an α-phase stabiliser while vanadium is a β-phase stabiliser. The effects of the two solutes on phase transformation of the titanium metal are depicted by the phase diagrams in figure 2.1a-b.

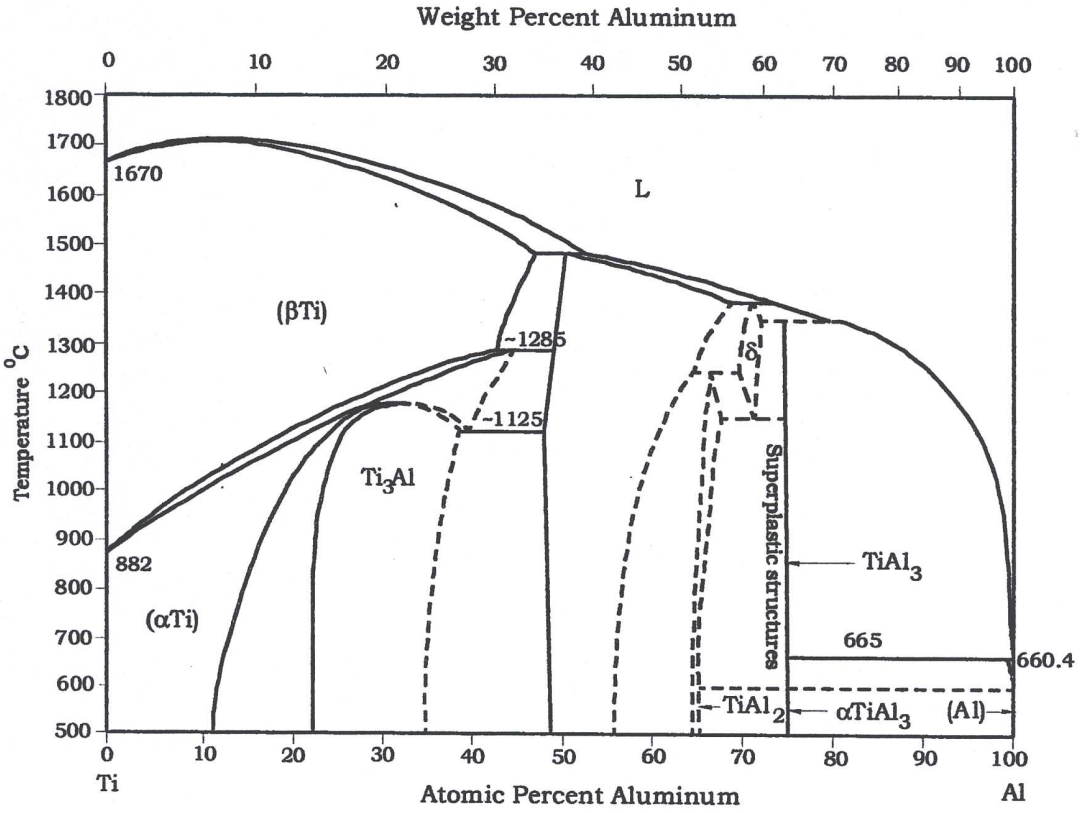

Figure 2.1a: Ti-Al binary phase system [11, 12]

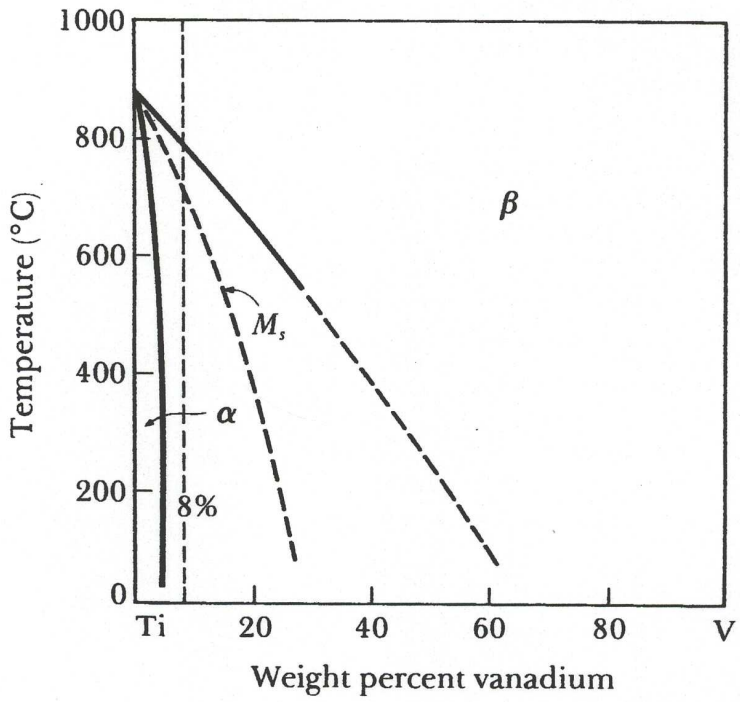

Figure 2.1b: Ti-V binary phase diagram [13]

Addition of controlled amounts of the two elements results in the stability of alpha and beta phases at room temperature. The annealed microstructure of the alloy shows the dark β-phase at the grain boundaries of the white α-phase as shown in figure 2.2**.**

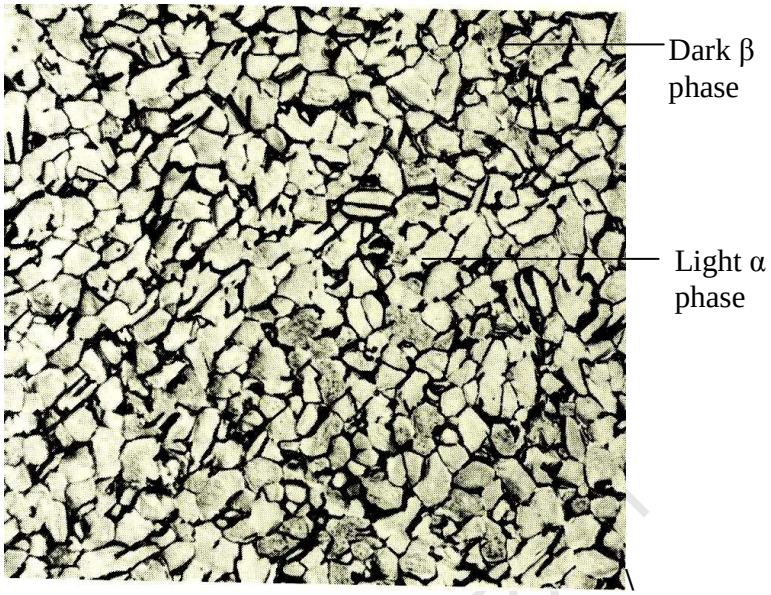

Figure 2.2: Ti-6Al-4V bar held for 1 hr at 956ºC and furnace cooled [14]

The two binary systems of Ti-Al and Ti-V indicate that titanium dissolves about 7% aluminium while complete solubility is noted for the titanium-vanadium binary system.

β -Alloys: This class of alloy which includes Ti-10V-2Fe-3Al (Ti-10-2-3), Ti-15V-3Cr-3Al-3Sn (Ti-15-3), Timetal 21S (Ti-15Mo-2.7Nb-3Al-0.2Si), and Ti-3Al-8V-6Cr-4Mo-4Zr (B-C), is capable of being heat treated to high strengths in excess of 1380 MPa. They can be heat treated over a broad range of strengths, permitting one to tailor the strength/fracture toughness properties combination that is desired. They generally have high stress corrosion resistance as well as fracture toughness. Beta alloys offer fabrication advantages, particularly for producing sheet, owing to their cold rolling capabilities. Owing to the limitations in reductions which can be achieved in α/β alloys, they must be hand rolled, which is a very labour intensive operation; the β alloys, on the contrary, can be strip rolled. Prior processing in terms of obtaining a given microstructure is not as important for the β alloys as solution treatment is normally done above the β transus. This is not, however, the case with α and α/β alloys which may require careful processing to obtain the correct microstructures for some of the more demanding applications.

2.1.2 Heat-Treatment of Titanium Alloys and Mechanical Properties of Ti-6Al-4V.

The occurrence of an allotropic transformation in pure titanium controls the type of structures which can be produced by the heat treatment of titanium-rich alloys and hence the increases in the range of mechanical properties which can be obtained from the alloys.

A number of contributions about the allotropic transformations of Ti-6Al-4V alloys have been put forward by some investigators.

Shivpuri et al. [15] reported that Ti-6Al-4V exhibits a β transus temperature at 890ºC. This was contrary to reports made by Kerr et al.[16] and Ilyn et al. [17] who studied the alteration of the β transus temperature with the additions of hydrogen on the Ti-6Al-4V alloy. However, both studies suggest a β transus temperature of around 1000 ºC for this alloy. At this temperature α and β phases transform into an "all β" system. There are several heat treatments that are used for titanium alloys. Titanium castings that are heat treated yield products of comparable or even higher mechanical properties to those of wrought products [18]. When the alloy is slowly cooled from the all β region, the α phase emerges in the shape of plates below the β transus temperature with the crystallographic morphology that is related to the parent β phase. The etching effect on the metal reveals white plates that correspond to the alpha phase while the thin dark regions between the alpha plates are the beta phase in the typical Widmansttäten structure. Different cooling rates from various temperatures result in distinct microstructures and mechanical properties. The α, α′ and the β phases are observed in various volume fractions and combinations owing to annealing temperatures and cooling rates. The α′ phase is formed during the martensitic transformation from quenching above the beta transus temperature. As the alloy crosses the Ms (start of martensite) line, the β microstructure transforms into titanium martensite. The basket weave structure of the air-cooled microstructure is shown in figure 2-3.

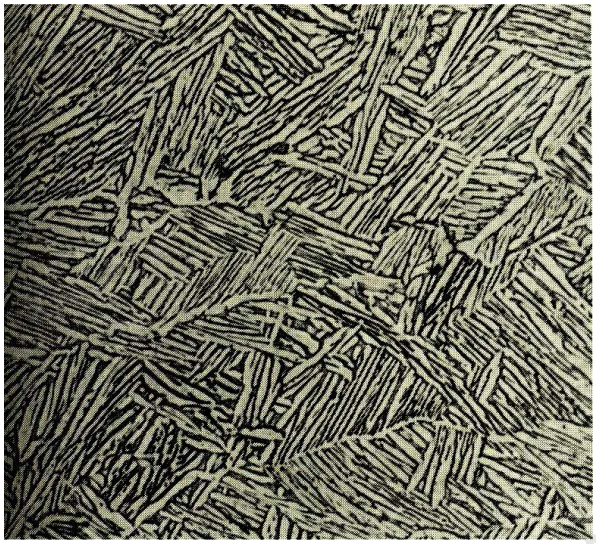

Figure 2-3: Ti-6Al-4V, forged at 1038ºC above the beta transus, air cooled, annealed for 2 hr at 704 ºC, and air cooled showing a Widmanstätten structure [14]

When titanium martensite is reheated, tempering will take place as β precipitates from the supersaturated α'. When highly alloyed α-β alloys are quenched from the β field, β' which is supersaturated in titanium is formed. When this supersaturated structure is aged, α will start to precipitate in a Widmanstätten structure shown in figure 2-3. Figure 2-4 provides a schematic for the two heat treatment paths.

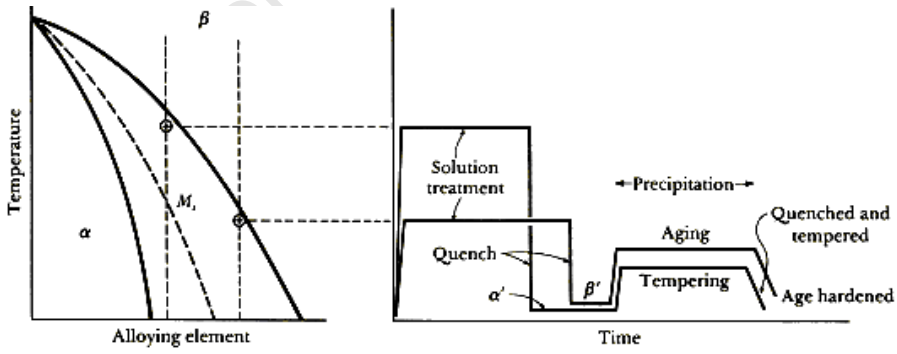

Figure 2-4: Heat treatment of the alpha- titanium alloys [19]

Volume fraction (%) of phases present upon different heat-treatments in a study conducted by Jovanovic et al. [18] is shown in table 2-1**.**

Table 2-1: Volume fraction (%) of phases present upon different heat-treatment [18]

T (°C)	Water-Quenching	Air-cooling	Furnace-cooling
1100	1.3 (β) ά = 98.7	14.7 (α) β+ α_{AC} = 85.3	95 (α) β= rest
1050	5 (β) ά = 95	34.5 (α) β+ α_{AC} = 65.5	97 (α) β= rest
1000	7.8 (β) ά = 92.2	50.9 (α) β+ α_{AC} = 49.1	90 (α) β= rest
950	42.2 (α) ά ≈ 50-57.8 β ≈ 8	72.2 (α) β+ α_{AC} = 28.8	95 (α) β= rest
900	61.3 (α) ά ≈ 26.9 β ≈ 10	81.3 (α) β+ α_{AC} = 18.7	95 (α) β= rest
850	80 (α) ά ≈ 10 β ≈ 10	84.5 (α) β+ α_{AC} = 15.5	95 (α) β= rest

where α_{AC} means acicular α phase and ά is the martensite phase.

Elemental composition analysis and mechanical properties for wrought and cast Ti-6Al-4V is shown in tables 2-2a and b respectively.

Table 2-2a: Elemental composition specifications for cast and wrought Ti-6Al-4V alloys [20]

	Weight (%)							
Standard	Ti	Al	V	N	C	O	H	Fe
ASTM F1108 – 97 (cast)	Balance	5.5 - 6.75	3.5 - 4.5	0.05 max	0.10 max	0.20 max	0.015 max	0.30 max
ASTM F136 – 96 (wrought)	Balance	5.5 - 6.75	3.5 - 4.5	0.05 max	0.08 max	0.20 max	0.012† max	0.25 max

† Section sizes of 0.813 mm and under may have a hydrogen content up to 0.0150 wt %

Table 2-2b: Mechanical properties of cast and wrought Ti-6Al-4V alloys [20]

Standard	Minimum Tensile strength (MPa)	Minimum 0.2% proof strength (MPa)	Minimum % elongation	Minimum % reduction on area	Hardness (Rockwell C)
ASTM F1108 – 97 (cast)	860	758	8	14	Unspecified
ASTM F1472 -93 (wrought)	930	860	10	20 – 25	Unspecified

2.1.2.1 Common Conventional Heat Treatments Used For Ti-6-4 Alloy [3]

- Mill anneal (MA or A)- this is the most common heat treatment, with a strength of about 896MPa, good fatigue properties, moderate fracture toughness (a typical value of about 66MPa√m) and reasonable fatigue crack growth rates (FCGR)
- Recrystallize anneal (RA) – this is a more damage tolerant heat treatment condition (usually used with what is termed as an extra low interstitial (ELI) grade with a reduced O_2 level to improve the fracture properties) which has a slightly lower strength than MA, slightly reduced fatigue properties, and improved fracture toughness and fatigue growth rate resistance. It is used for all fracture critical applications on the B-1 and B-2 bombers.
- Beta annealed (BA) – this is used with both the standard and ELI grades. For maximum damage tolerance properties, the ELI grade is used, and again, the strength is somewhat reduced, while FCGR resistance and fracture toughness are maximized but the fatigue strength is significantly degraded.
- Solution Treated and Aged (STA) – this provides the maximum strength, but full hardenability is limited to about 25mm. The STA heat treatment is not commonly used for shaped components as the thermal stresses induced by the required water quenching are not relieved during the ageing treatment, which can result in part

warpage during machining. Ti-6-4 has been the work horse of the titanium industry, and probably 80% - 90% of the titanium used on airframes has been this alloy. This is used in all sections of the aircraft – fuselage, nacelles, landing gear, wing, and empennage.

2.1.4 Titanium Alloy Applications [3]

Some of the more prominent aerospace applications include:

- α- Alloys- Commercially pure (CP) titanium, used in the annealed condition, is used primarily for their formability and corrosion resistance. Lower density of CP over annealed 300 series stainless steel which has similar characteristics gives it a better choice for application. It is used for non-structural applications requiring the above mentioned traits. Common examples are floor support structure in the galley and lavatory areas, tubes or pipes in the lavatory system, clips and brackets, and ducting for the anti-icing and environmental control systems (ECS). The ECS ducts operate at temperatures up to about 230^{o}C, which is too high for aluminium alloys. Stainless steel could be used but the CP offers about a 40% weight savings. Most of the US tonnage for the α- alloys (excluding CP Ti) in the aerospace industry, is for elevated temperature applications. They have good properties retention and creep resistance at elevated temperatures. The primary alloy for these applications is Ti-6-2-4-2S, and its chief consumer is the gas turbine engine industry. It is used for rotating components such as blades, discs and rotors at temperatures up to about 540^{o}C. The RT tensile strength is about 930MPa.

- **α/β Alloy:** Ti-6-4 is most frequently used in the titanium industry; it accounts for about 60% of the total titanium production. It is a forging alloy to work with; it is normally used at a minimum tensile strength of 896MPa, has good fatigue and fracture properties (which can be optimized through heat treatment) and is used in all product forms including forgings, bar, castings, foil, sheet, plate, extrusions, tubing and fasteners.

- **β Alloy:** Ti-13V-11Cr-3Al (Ti-13-11-3) was the first commercially significant β Alloy. It was used extensively on the SR-71 "Black bird" reconnaissance airplane. About 95% of the structural weight was reported to be titanium [21], the bulk of it being Ti-13-11-3; it was used for wing and body skins, frames, longerons, bulkheads, ribs, rivets and essentially the complete main and nose landing gears. One of the key reasons for selection of Ti-13-11-3 was its thermal stability. Some of the skins had to be spot welded on assembly, and the assembly could not be subsequently aged so the weld nugget would essentially be in the solution treated condition. Ti-13-11-3, the most stable of the commercial β Alloys (except for P & W's recently developed Alloy C, Ti-35V-15Cr) was the only heat treatable alloy which could be used at the operating temperatures, about 250-315^{o}C, which would not embrittle in the weld region [3]. Beta 21S is the only titanium alloy which is immune to hot hydraulic fluid. Hot hydraulic fluid is one of the very few corrosive media for titanium in the aerospace environment [3]. The hydraulic fluid used in commercial aircraft will break down and form an organo-phosphoric acid at temperatures in excess of ~130 ^{o}C which will etch the titanium, reducing the gauge, and, more importantly, pump in large amounts of hydrogen, which can cause severe embrittlement. The resistance is ascribed to the Mo and Nb contents- which seem to have a synergistic effect on corrosion resistance.

Alloy C: - the newly developed alloy by P&W. It has ignition resistance. It is used in areas previously requiring nickel-based alloys, primarily because there was a real concern of titanium fires in "hot" areas [3].

2.2 Concept of Thermo-hydrogen Processing (THP)

2.2.1 Basic Principles of THP

Thermohydrogen processing (THP) is a technique based on the modifying effect of hydrogen as an alloying element in titanium alloys on the phase compositions and the kinetics of phase transformations [5]. The THP technique allows enhancement of most of the processability/ fabrication techniques including working, machining, powder

production, sintering, compaction, etc., and also control of the microstructure leading to improved final mechanical properties. The decrease in the temperature of the (α+β)/β transformation that accompanies the hydrogen addition leads to a reduction in grain growth on heating into the (modified) β phase range [16, 22-24]. A hydrogen-induced increase in the temperature interval of the (α+β) range permits heat treatments to be performed that are not possible without hydrogen addition [23, 25, 26]. This leads to the generation of novel microstructures in conventional near-α alloys. The increased amount of the more workable β phase also improves the hot workability of the alloys and decreases the hot working temperatures [27, 28]. A shear modulus decrease in α titanium and an increase in β titanium by alloying with hydrogen affects the interaction/s of dislocations with obstacles and leads to softening of the α phase and strengthening of the β phase respectively [29].

A decrease in the critical cooling rate required for martensite formation brought about by the hydrogen addition improves the hardenability, increases the volume fraction of metastable phases, and leads to a completely martensitic structure in thicker sized articles [23, 30, 31]. As a result, a spectrum of novel microstructures can be obtained after aging and hydrogen removal. The hydrogen addition changes the volume fractions of phases present in a titanium alloy at a given temperature, which in turn changes the concentrations of other alloying elements in these phases.

The redistribution of alloying elements in different phases, because of the hydrogen addition, changes the specific volume of these phases. Thus, the difference in the specific volumes of these phases can be controlled by changing the amount of hydrogen addition, which in turn allows control of the morphology of these phases by heat-treatments (equiaxed structure when the difference in specific volume is small and elongated structure when the difference in specific volumes is large [28, 32]).

The retention of a large amount of the residual β phase at room temperature in conventional (α+β) titanium alloys as a result of hydrogen alloying can produce effects such as transformation-induced plasticity (TRIP) and non-linear elasticity [33]. The former is observed when the martensite transformation is induced by strain and the latter occurs when the transformation is induced by stress and is reversible during unloading [33].

Hydrogen-assisted cleaning and diffusion bonding of the metal surfaces can be used in the processing of powder metallurgy products and composites [34-36].

2.2.2 Reaction of Titanium with Hydrogen

The absorption of hydrogen by titanium is a reversible process, and when titanium is heated in a hydrogen atmosphere the reaction will therefore continue until the concentration of hydrogen in the metal attains an equilibrium value which depends on the specimen temperature and the pressure of the surrounding hydrogen atmosphere [37]. Any imposed temperature or pressure change causes rejection or absorption of hydrogen until a new equilibrium state is achieved [37]. Unlike the irreversible absorption of oxygen and nitrogen, therefore, the rate of absorption of hydrogen is dependent on the pressure of the gas as well as on the temperature and may be expressed in the form:

$d\omega/dt = c\,(p)^{0.5} \exp(-b/T)$ …….Equation. 1

Where ω is the amount of hydrogen absorbed in time t, p is the hydrogen pressure, T the absolute temperature, and c and b are constants, the values of which depend on the phases present in the metal [37].

Except at very low temperatures, the hydrogen concentration of the metal at the surface of the specimen will be the equilibrium value appropriate to the temperature and hydrogen pressure concerned [37]. The phase which will appear at the surface under any given conditions may, therefore, be ascertained by reference to figure (2- 1) in which the regions of temperature and pressure in which the three possible phases, i.e. the α solid solution, the β solid solution and the γ or hydride phase, can exist as outlined. The sequence of phases which would be observed on moving from the surface into the body of a titanium specimen heated in hydrogen may be obtained by observing the phase regions intersected by the isothermal line, corresponding to the temperature of the experiment, starting at the pressure of the hydrogen atmosphere and moving towards lower pressures [37]. A eutectoid reaction in which the β solid solution decomposes to form the α solid solution and the hydride phase occurs in the titanium – hydrogen system at about 300^{o}C, and no β-phase can, therefore, exist at lower temperatures [37]. Consequently the α /β and β/ γ boundaries in figure (2 – 1) would if produced meet at about 300^{o}C and thereafter, would form a single α / γ boundary [37].

The rates of diffusion of hydrogen in α- and β- titanium, which will influence the rate at which hydrogen can be absorbed by the metal, have been studied by wasilewski and kehl [37], who obtained the expressions:

$D_\beta = 1.95 \times 10^{-3} \exp \{(-6640 \pm 500) / RT\}\ cm^2/\ sec$ …. Equation. 2

And $D_\alpha = 1.8 \times 10^{-2} \exp \{(-12{,}380 \pm 680) / RT\}\ cm^2/sec$ ….Equation. 3

For the diffusion coefficients of hydrogen in β- titanium and in α- titanium respectively, R being the gas constant and T the absolute temperature [17, 37,]. wasilewiski and kehl were unable to establish any definite relationship between the diffusion coefficients and the hydrogen concentration [37].

According to Wasilewiski et al [37] , Gulbransel and Andrew have shown experimentally that provided the surface of titanium is oxide-free, the rate of absorption of hydrogen is appreciable at 300^{o}C and increases rapidly at higher temperatures. At temperatures above about 500 ^{o}C equilibrium is achieved in a matter of seconds [37]. If the experimental conditions are such that titanium hydride is formed on the surface of the metal as a result of titanium hydrogen -reaction, the hydrogen is absorbed at constant rate, as has been observed by wasilewski and kehl. These authors attributed their findings to the fact that the brittle hydride layer is porous, which is not unlikely, since the hydride has greater specific volume than the metal from which it was formed, and thus would probably crack under the internal stresses present [37].

The rate of hydrogen absorption and the rate of hydrogen evolution in vacuum are considerably reduced when the surface is contaminated by oxygen [37].

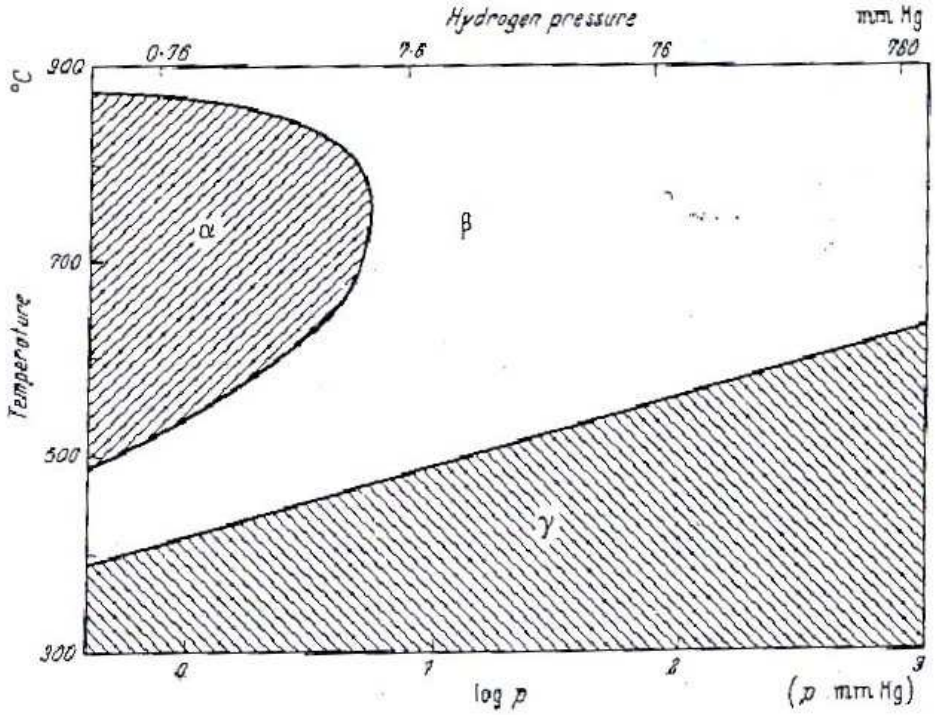

Figure 2 – 1: Diagram illustrating the phase which will be present in titanium-hydrogen alloys under any given conditions of temperature and hydrogen pressure. The two-phase regions are represented by the boundaries separating the single-phase regions [17]

2.2.3 Phase Transformations of Titanium Systems Using THP

The efficacy of THP is based on understanding how hydrogen as an alloying element affects the phases, phase compositions, and phase reactions in the alloy. Thus, it is necessary to determine the temperature - hydrogen concentration phase diagrams (both stable and metastable) of the titanium alloy-hydrogen system and the rates at which reactions occur (time-temperature-transformation diagrams) [5]. Over the past few years, phase diagrams have been determined for a number of titanium alloys-hydrogen systems, however only the Titanium- Hydrogen binary system and Ti-Al-V-H System will be discussed herein.

2.2.3.1 Titanium- Hydrogen Binary System

This is a simple eutectoid system with the terminal constituents being a solution of hydrogen in hexagonal closed packed (hcp) α titanium, and a δ hydride phase approaching the stoichiometric composition TiH_2, Figure 2-2 [5]. Hydrogen alloying stabilizes the high temperature body-centred cubic (bcc) β phase and creates a two phase α+β region [5]. The beta transus temperature (the lowest temperature at which only the beta phase is present) is decreased from 882°C for pure titanium to 300°C for the alloy with 39at.% hydrogen (eutectoid point) [5]. An interstitial solution of hydrogen in the α phase occurs to a maximum of approximately 6.72 at.% at the eutectoid temperature [6]. The solubility of hydrogen in the β phase is much higher; it is 39 at.% at the eutectoid point and increases with temperature up to 50 at.% [5]. The β phase is retained to a temperature of almost 550ºC below the pure metal β transformation temperature by the presence of hydrogen in solid solution (Figure2- 2). The β phase, however, cannot be retained at room temperature since it decomposes into α and δ phases at temperatures below 300ºC [5]. The hydride formation is associated with a 17.2% volume expansion, which produces high internal stresses in the α matrix [5]. Accommodation of this hydride-matrix misfit contributes significantly to the difference in hydride formation temperature (during cooling) and hydride decomposition temperature (during heating), resulting in a thermal hysteresis of the location of the α/(α+δ) phase boundary [38]. Hydrogen in solid solution decreases the shear and Young's moduli of the α phase and increases these parameters for the β phase [29].

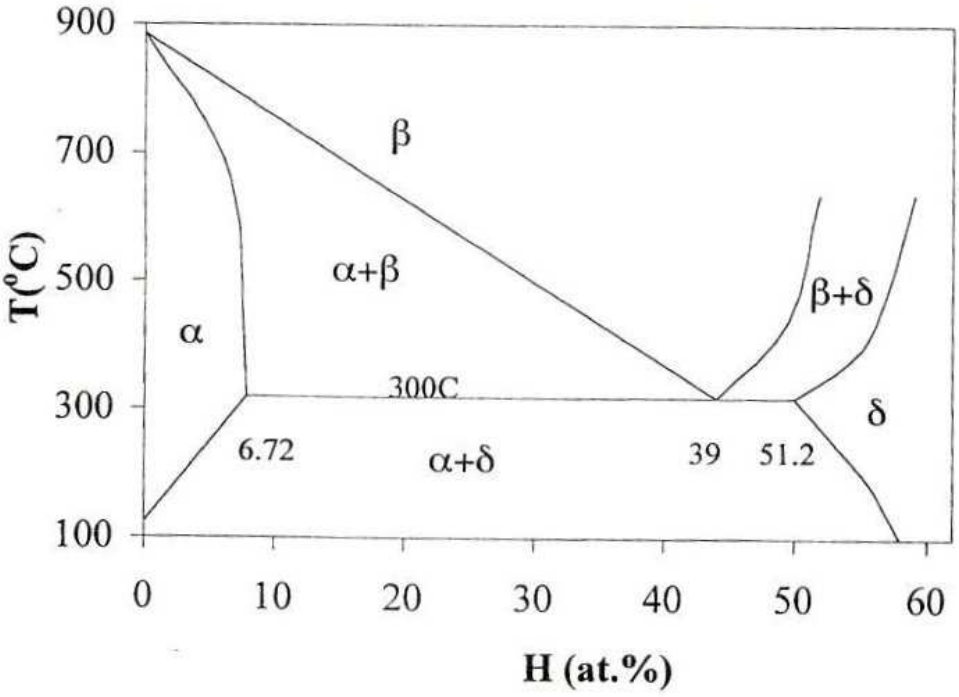

Figure 2-2: Binary Ti-H phase diagram [5]

2.2.3.2 Ti-Al-V-H System

Ti-6Al-4V alloy has the majority of work done on this system. Kerr and co-authors [28] were the first to conduct a detailed analysis of the effect of hydrogen on phase reactions in this alloy. The Ti-6Al-4V alloy is an α+β alloy which can have different volume fractions of α and β phases, depending on the heat treatment and interstitial (primarily oxygen) content [39]. The β phase is stable at room temperature only if it is enriched with more than 15 wt% of vanadium. Such enrichment is obtained when the alloy is slowly cooled or annealed below about 750 ^{o}C. Slow cooled Ti-6Al-4V contains about 90 vol. % of the α phase. This alloy can develop a large variety of microstructures with different morphological arrangements of the α and β phases, depending on the particular thermomechanical treatment utilized. These microstructures can be roughly classified into three different categories of alpha morphologies: lamellar, equiaxed, or a mixture of both (bimodal) [39]. Equiaxed microstructures can be obtained only after extensive

mechanical working of the material in the (α+β) field followed by annealing, while lamellar structures results from decomposition of the beta phase on cooling below the beta transus temperature [39].

Irrespective of the commercial and practical significance of the Ti-6Al-4V alloy, only a limited number of open literature publications are available on the effects of hydrogen on the phase compositions and reactions in this alloy [6, 28, 32]. Addition of hydrogen to the alloy was found to decrease the β transus temperature, for example a decrease from 1000 °C to 800 °C when 20 at.% H is added [28,]. Based on the work of Kerr et al.[28] the β transus temperature remained constant at this temperature from 20at.% H onwards up to 37 at.% H; however the data of Ilyn et al [17] showed a further decrease of the temperature down to 700 °C with an addition of 32 at.% H [6]. These investigators also disagree concerning the temperature of hydride transformation in this alloy. Based on metallographic examinations and X-ray diffraction (XRD) analysis, Kerr and co-authors [28] suggested the existence of an eutectoid decomposition of the β phase into α plus hydride at about 800 °C in alloys with hydrogen concentrations ≥15 at.% (Figure2-3) .

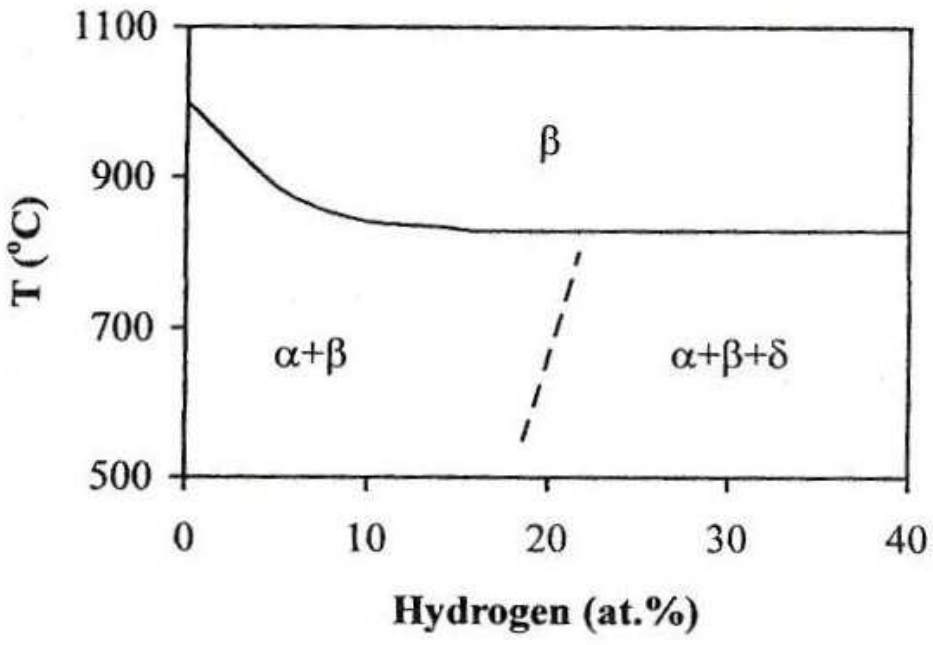

Figure 2-3: Phase boundaries in Ti-6Al-4V-H system as defined by Kerr et al.[28]

Ilyn and co-workers, on the other hand, reported [17] that the eutectoid transformation (β→α+δ) occurs at a temperature around 250°C in alloys containing ≥13at.% hydrogen, Figure 2-4

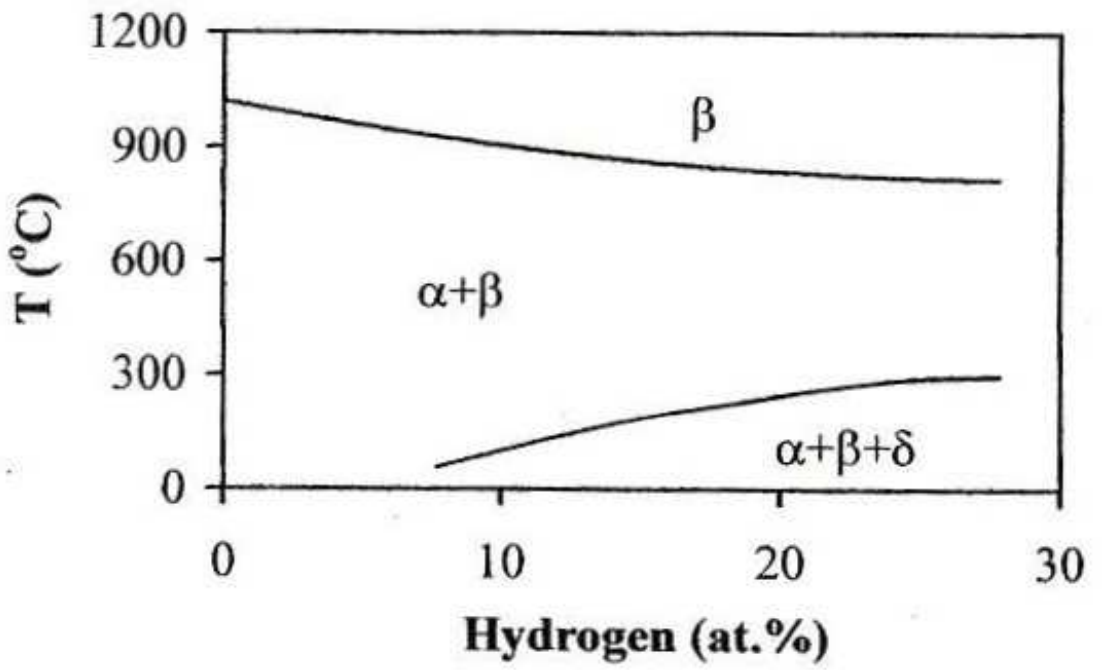

Figure 2-4:Phase boundaries in Ti-6Al-4V-H system as defined by Ilyn et al [17]

In a later detailed follow up study of the phase transformations in the Ti-6Al-4V-xH system using XRD, OM and TEM techniques, Qazi et al.[6] proposed a phase diagram, Figure 2-5, which supports and expands the work of Kerr et al.[28].

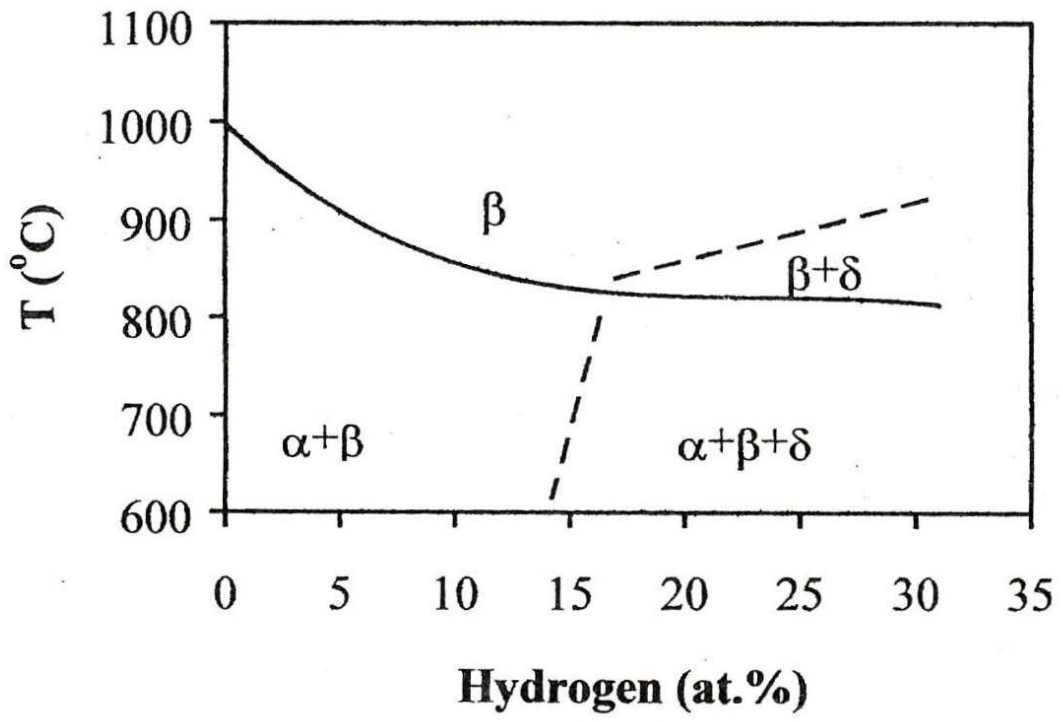

Figure 2-5: Phase boundaries in Ti-6Al-4V-H system as defined by Qazi et al [6]

It was shown that at hydrogen concentrations above 15 at.% the hydride phase is not only stable below the eutectoid temperature, which occurs approximately at 815ºC, but there also exists a two phase, β +δ, field above the eutectoid temperature. The presence of a hydride phase in the Ti-6Al-4V alloy containing 20 at.% H or higher at a temperature of 600ºC has been confirmed by Arkhipov et al. [31] by high temperature neutron diffraction; this result supports the diagram suggested by Kerr et al.[28] and Qazi et al. [6]. It was also concluded that [5] the discrepancy between the earlier results of Kerr et al. [28] , and Ilyn et al. [17] might be partially due to the very slow rate of β phase decomposition below the beta transus and eutectoid temperature. Hydrogen additions have been shown [40] to decrease the diffusion coefficient of the alloying elements in the beta phase; suggesting that the kinetics of the beta to alpha phase transformation will slow down. The kinetics of the β phase decomposition in the Ti-6Al-4V-xH system have been studied recently [6] and the β-TTT (time temperature transformation) diagrams for the Ti-6Al-4V alloy containing 10, 20 and 30at.% H have been reported. An increase in the hydrogen concentration from 0 to 30at.%H slowed down the kinetics of the β-phase transformation considerably,

resulting in an increase in the nose time for the start of the transformation from 12 seconds to 42 minutes, Figure 2- 6.

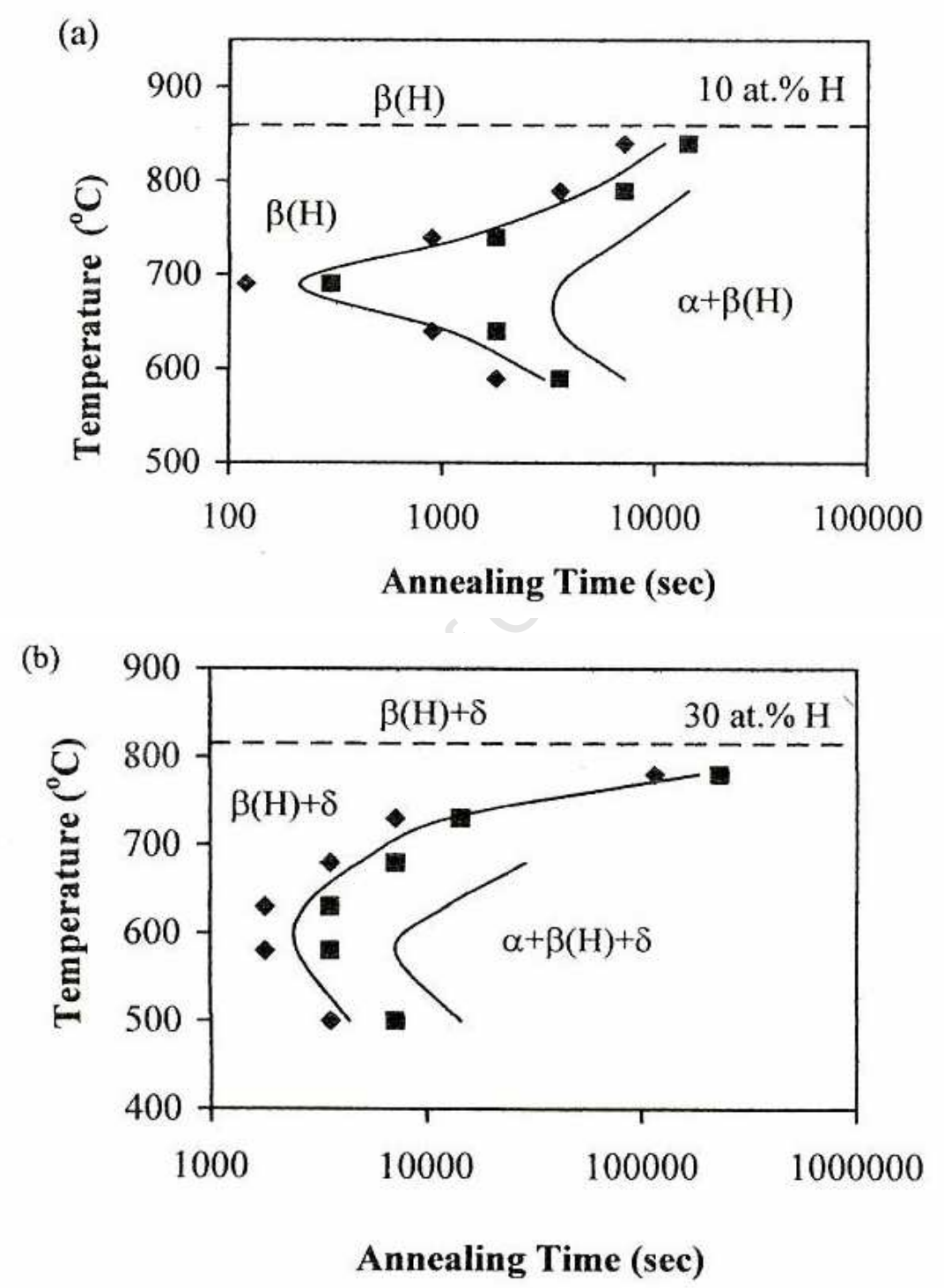

Figure 2- 6: TTT diagram for β phase decomposition in Ti-6Al-4V specimens with (a) 10at.-%H and (b) 30 at.-%H (Ref. [6])

The nose temperature, decreased linearly from 725°C to 580°C with an increase in hydrogen concentration from 0 to 30at. %, Figure 2 - 7.

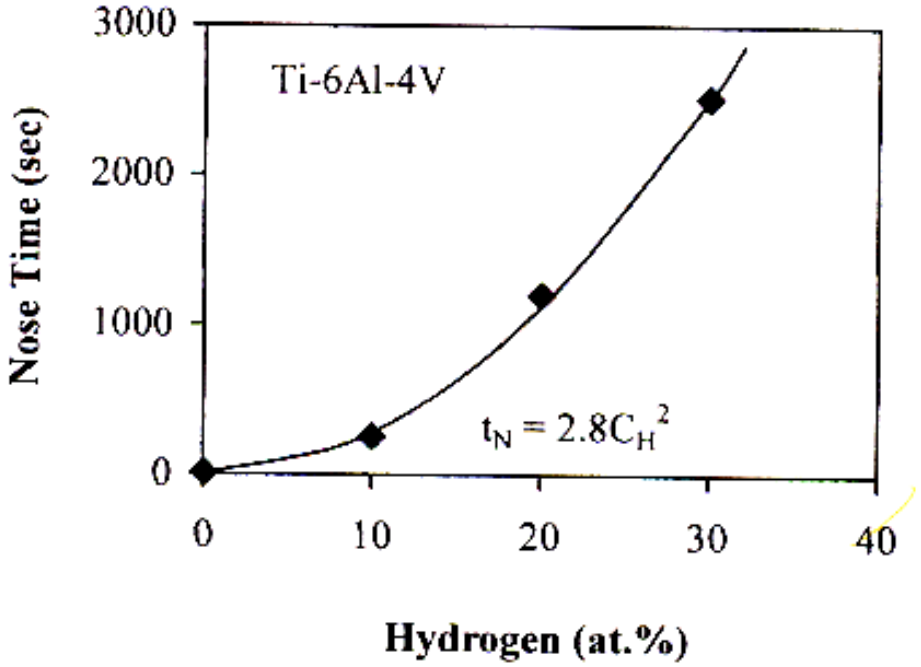

Figure 2 – 7: Nose time for beginning of β phase decomposition as function of hydrogen concentration [5]

The large increase in the nose time leads to a considerable decrease in the quench rate necessary to produce a 100% martensite structure. A cooling rate as low as 5°C/min in the alloy with 30 at.% H is sufficient while a cooling rate of 1000°C/min is required to produce a 100% martensite structure in the alloy with 0%H [5] . Slower cooling rates allow production of more homogenous microstructures after heat treatment, even in thicker sections, and also result in less warping of the components, because of the lower internal stresses developed during cooling [5].

The kinetics of martensite decomposition (aging) for Ti-6Al-4V-xH system has also been studied [41] and the following martensite decomposition sequence has been proposed. Aging at temperatures below M_s:

Martensite (aging) → equilibrium alpha + beta → (after quenching) equilibrium alpha + residual beta + martensite

Aging at temperatures above M_s:

Martensite (aging) → metastable beta + martensite → equilibrium alpha + beta → (after quenching) equilibrium alpha + residual beta + martensite

The amount of residual beta increases with the increasing hydrogen concentration and aging of samples containing 30at.% H at temperatures below 730ºC, all the β-phase formed during aging is retained on quenching to room temperature and, therefore no martensite forms [41].

Gong et al. [42] have reported precipitation of an ordered α_2 phase in the Ti-6Al-4V alloy containing 16 at.% H or higher after aging in the vicinity of 650°C, followed by furnace cooling through the temperature range of 650 to 550°C. These authors also found that the formation of the brittle α_2 phase in the hydrogenated alloys can be avoided by fast cooling through the temperature range of 650 to 550°C [42]. The α_2 phase was also detected by Zhang et al.[43] in the Ti-6Al-4V alloy after hydrogenation at 650°C with up to 22 at.% H followed by furnace cooling. The amount of the α_2 phase increased with an increase in the hydrogen concentration. Formation of the α_2 phase (Ti_3Al), which typically requires high (above 8%) Al concentrations, indicates that alloying with hydrogen leads to re-distribution of the alloying elements, in particular aluminium, between the α and β phases leading to enrichment of the α-phase with aluminium. There is however no explanation yet why the temperature range and the cooling rate are so critical for the α_2 phase formation in this alloy. The phase compositions of a number of other α+β alloys as influenced by the presence of hydrogen concentration, temperature and cooling rates are discussed in [31]; similar effects due to hydrogen were found as in the Ti-6Al-4V alloy.

2.2.4 Hydrogen-Induced Enhanced Processability

2.2.4.1 Hot Workability

Alloying with hydrogen increases ductility and reduces the flow stress of the α, α+β and intermetallic-base alloys in a wide temperature range, including the temperatures used for the conventional hot working of Ti-6Al-4V [27, 44], allowing the use of larger strains at lower temperatures. A typical example is the Ti-6Al-4V alloy hydrogenated with 16at.% (0.4wt.%) hydrogen, which showed a 30% decrease in forging stress at a constant forging temperature (760°C), or, alternatively, a 80°C decrease in the forging temperature at a constant forging stress [28]. Besides, a greater decrease in the forging temperature, from 950°C to 750°C, was reported by Anisimova et al. [36] for a VT6 alloy (Russian equivalent to the Ti-6Al-4V) after addition of 13-20 at.% H. Alloying of a Ti-8Al alloy with 20 at.% H allowed 78% deformation during forging at 950°C without cracking, while a sample with no hydrogen was completely fractured under the same forging conditions [36] Hydrogen alloying improves ductility of the β alloys in a wide temperature range, down to room temperature [23, 45]; although, their flow stresses increase with hydrogen addition [46].

It has generally been found [28, 47, 48] that for α and α+β alloys, the flow stress decreases, reaches a minimum, and then increases with an increase in the hydrogen concentration at a particular processing temperature.

Kerr et al. [28] suggested that the reduction in flow stress in Ti-6Al-4V was a result of the increased proportion of the β-phase. They also suggested that the flow stress increase at higher hydrogen contents could be attributed to the presence of hydrides in the microstructure. However, this suggestion does not explain the temperature dependence of the hydrogen concentration at the minimum flow stress. The decrease in the flow stress (fig.2-8) at lower hydrogen concentrations (α-phase region) was attributed to the softening of the α-phase due to hydrogen in solid solution [30, 46].

In the α+β two phase region the decrease in the flow stress with increasing hydrogen concentration was explained in terms of the combined effects of the softening of the α-

phase and increased volume fraction of the β-phase (which is softer than the α-phase). Hydrogen in solution in the α-phase decreases the elastic moduli of α titanium, figure 2-8b, and, thereby, lowers the strength of dislocation interactions with various obstacles [29]. About one-half of the observed softening can be attributed directly to this effect [29].

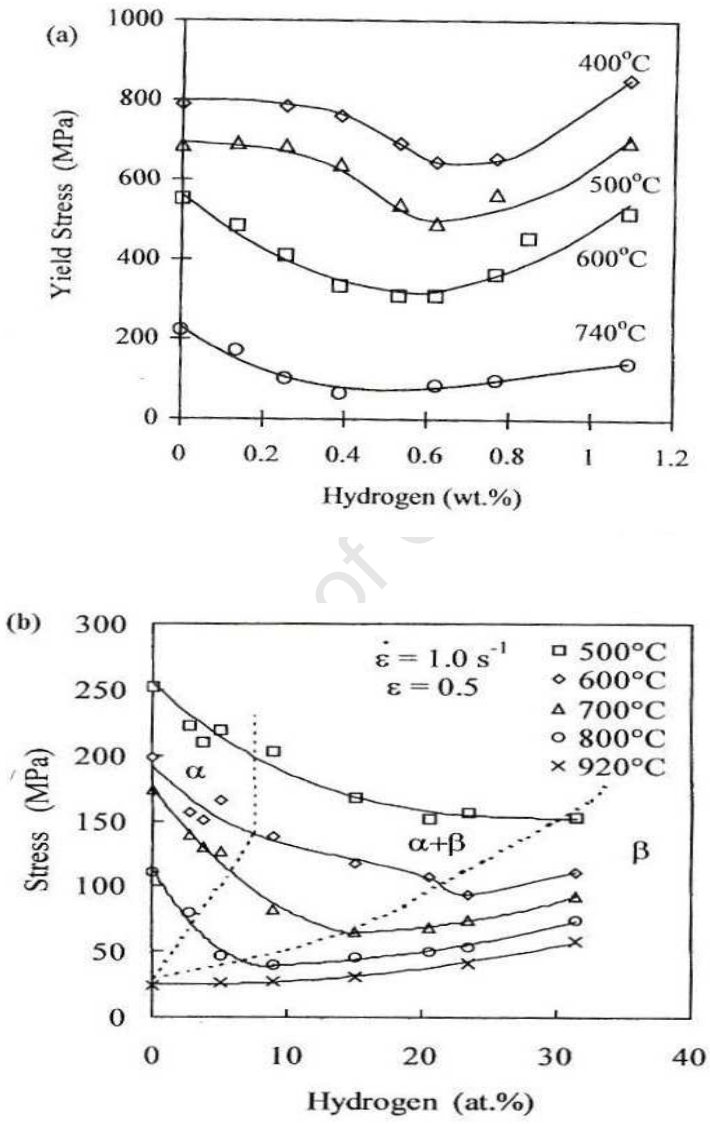

Figure 2- 8: Dependence of (a) the yield stress and (b) flow stress on hydrogen concentration at various temperatures: (a) VT20 alloy (Ti-6Al-2Zr-1.5V-1Mo) [49], (b) CP Ti [46]

Another reason, for α softening, is that the hydrogen in solution, being highly mobile and occupying interstitial sites near dislocations, prevents other solutes from segregating to the mobile dislocations [50] . An increase in the hydrogen concentration in the single β-phase field resulted in the β-phase hardening [48] and this was explained in terms of the hydrogen-induced retardation of the diffusion of substitutional atoms [51], leading to an increase in the flow stress. A detailed analysis of the hardening effect of hydrogen additions to β titanium led to the conclusion [7, 29, 52] that at least two mechanisms could be responsible for the minimum in the flow stress. Alloying with hydrogen increases the shear modulus of the β-Ti, Figure 2- 9a, [29].

This result in a decrease in the density of thermally activatable sites and to an increase in the heights of the barriers to glide [7, 29]; both changes harden the material. Additional hardening could be due to short range ordering, which occurs at high hydrogen concentrations [53].

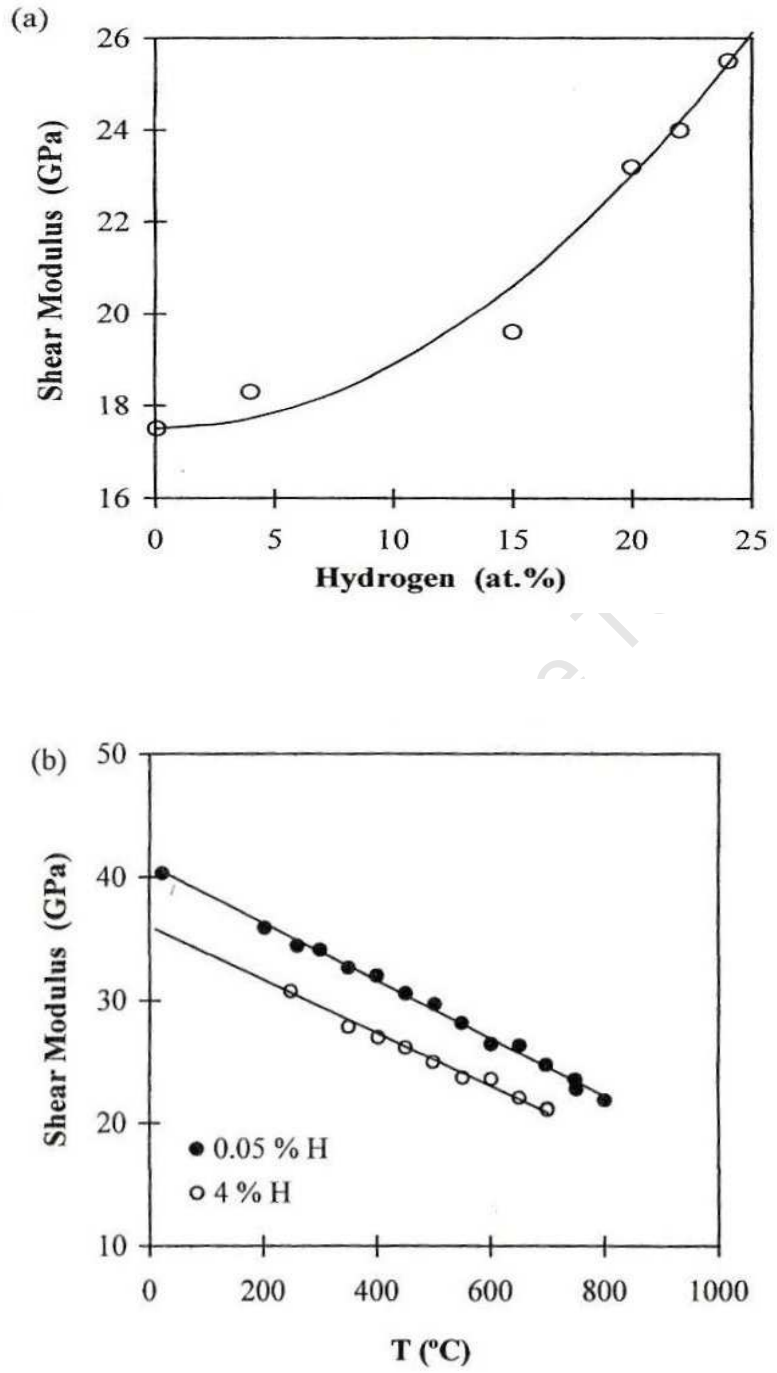

Figure 2-9: Dependence of shear modulus on (a) hydrogen concentration at T=960 °C (β-Ti) and (b) temperature (α-Ti containing two different hydrogen concentrations) [29]

2.2.4.2 Cold Workability

Improvement in cold formability due to THP has been observed and studied by Kolachev and co-workers [54] in pseudo-β and some α+β titanium alloys. The room-temperature ductility of these alloys increased considerably when 4.6-8.8at. % (0.1-0.2wt. %) hydrogen was added and the strength increased also. This behaviour was explained in terms of a reduction in the concentrations of the alloying elements in the β-phase (because of its increased volume fraction), by the increased dislocation mobility, and by the activation of additional slip systems and twining [54]. However, this explanation is in contradiction with the experimental observation that the material is strengthened by hydrogen addition [54]. Instead, the low-temperature increase in the ductility of the hydrogenated β-rich alloys is probably a manifestation of the transformation-induced plasticity (TRIP) that is well-known in steels (i.e. the strain-induced formation of martensite from the residual β-phase) [54]. Hydrogen-improved formability has been used to produce high-quality nuts and heading bolts of large diameter from pseudo-β alloys [45].

2.2.4.3 Machining

Improvement in the machinability of certain α and α+β titanium alloys has been reported by Kolachev and co-workers [54]. It was found that a certain hydrogen concentration interval exists for each alloy within which the hydrogen increases tool life, Table 2- 1. Within this hydrogen content interval, tool life increases 2-10 times depending on the alloy type. Table 2- 1 lists the decrease in the cutting area temperature, reduction in cutting force and increase in tool life for different titanium alloys along with the optimum hydrogen concentration interval. The improvement in machinability due to the presence of hydrogen allows the cutting rate to be increased by 1.5-2.0 times while maintaining the other cutting parameters or, alternatively, allows higher feeds and cutting depths to be used while keeping the cutting rate constant [54].

Table 2- 1: Hydrogen Influence on the Machinability Characteristics of Titanium Alloys [54]

Alloy	Optimum Hydrogen Concentration (at.%)	The change of machinability characteristics of Hydrogenated metal as compared to initial one		
		Decrease of cutting Area T(°C)	Reduction in Cutting force, Number of times	Increase in Tool Endurance Number of Times
VT1-0 (Ti 99.5)	10.7	100-150	1.6-1.7	3.5
VT5-1 (Ti-5Al-2.5Sn)	17.8-22.4	S	1.1	2-2.5
VT20 (Ti-6.1Al-1.9Zr-1.6V0.9Mo)	8.8-12.6	-	-	3.5
VT3-1 (Ti-6.3Al-2.6Mo-1.9Cr-0.6Fe-0.24Si)	12.6-19.4	100-120	1.4	8-12
VT6 (Ti-6Al-4V)	12.6-16.1	50-70	1.4	7-8
VT25 (Ti-6.8Al-2Mo-1.7Zr-1.3Sn-1V)	25.2-27.8	S	1.1	4-5
VT8 (Ti-6.7Al-3.4Mo-1.1Zr-0.8Sn-0.22Si)	6.7-8.8	S	1.3	8-10
VT8	25.2-26.2	S	1.3	8-10

S small change

2.2.5 Modification of Microstructure and Mechanical Properties

Titanium alloy castings have a large β grain size with a coarse lamellar structure and porosity. As a result, their mechanical properties, especially fatigue endurance (S-N), fall below desired levels. Thus, in many cases some kind of microstructural refinement treatment is required. Conventional microstructural refinement techniques involving mechanical working cannot be used with near net shapes (NNS). This opens up the possibility for use of THP which requires no working to refine the microstructure [5] . Thermohydrogen processing transforms the lamellar structure into an equiaxed fine grained morphology, decreases the porosity, and improves the tensile and fatigue strength substantially [54, 55], Table 2- 2.

Table 2- 2: Effect of THP on Mechanical Properties of Castings [54]

Alloy	Treatment	YS, MPa	UTS, MPa	El, (%)	RA, (%)	Kc, kJ/m2	$\tilde{N}_f$ [1] ($x10^4$)
Ti-5Al	As Cast	735	796	6.2	15.5	550	5.7
Ti-5Al	THP, 0.9 at.% H	863	910	13.5	32.3	600	12
Ti-6Al-4V	As Cast	870	940	8.8	18	460	4.9
Ti-6Al-4V	THP, 0.6 at.% H	1030	1090	12.8	20	450	9.7

$\tilde{N}_f$ [1] is the number of cycles to failure at the stress amplitude of 500 MPa.

Several types of THP have been reported, such as Hydrovac (HVC) [28], constitutional solution treatment (CST)[5], the hydrogenation/dehydrogenation of β quenched materials (βQ-HDH) [5], high temperature hydrogenation (HTH) [5] and other THP treatments [32, 42, 56], Table 2- 3. These methods, in general, consist of a β solution treatment before, during or after hydrogenation, a possible aging treatment below the hydrogenated β transus temperature and/or thermomechanical processing, then dehydrogenation by vacuum annealing at a lower temperature [5].

Table 2- 3: Types of Thermohydrogen Processing Treatments

Designation	Treatment	References
Hydrovac (HVC)	Hydrogenate- beta solution treat – water quench – age to form hydrides – dehydrogenate	[28, 32]
Constitutional Solution Treatment (CST)	Hydrogenate in beta region – cool to below eutectoid temperature and dehydrogenate	[5]
Beta quench and hydride-dehydride (BQ-HDH)	Beta solution treat – water quench – hydrogenate and dehydrogenate below eutectoid temperature	[5]
Hot isostatic pressing (HIP'ing) or vacuum hot press (VHP)	Hydrogenate – compact with hydrogen - dehydrogenate	[57, 58]
High temperature hydrogenation (HTH)	Hydrogenate in beta region – cool to room temperature – dehydrogenate below normal eutectoid temperature	[5]
Below β(H) transus hydrogenation	Hydrogenate just below β(H) transus – cool to room temperature – dehydrogenate at temperatures of α + β field	[42, 56]
Repeated eutectoid β phase decomposition	Hydrogenate above the β(H) transus – slow cool to below the eutectoid temperature – thermocycle to repeat the eutectoid β phase decomposition - dehydrogenate	[5]
Repeated martensitic β phase decomposition	Hydrogenate above the β(H) transus – quench to room temperature to produce α' martensite – thermocycle to repeat the martensitic β phase decomposition - dehydrogenate	[5]
HHWD-1	Hydrogenate – hot work in the α + β field – dehydrogenate below the hot working temperature	[5, 26]
HHWD-2	Hydrogenate – hot work just above β(H) transus – dehydrogenate below β(H) transus	[5]

2.2.5.1 Cast and Wrought Products

2.2.5.1.1 Conventional Alloys

Refinement in the microstructure of wrought alloys using THP has been reported by various researchers [24, 49, 56]. The refinement in α grain size led to an improvement in tensile properties of the Ti-6Al-4V alloy, and the strength and ductility values after different THP cycles are as tabulated in Table 2- 4 [56].

Table 2- 4: Mechanical Properties of As- Received (Coarse Equiaxed α Structure) and Various THP Treated Ti-6Al-4V [59]

Condition	0.2% YS MPa	UTS MPa	Elongation %.	RA %.
As received (Rolled and annealed)	829	876	15.0	31.7
HG (650°C, AC), β-Solution Treatment (900°C AC), Aging (565°C 8hr, AC) DH	1044	1071	12.8	23.0
HG (850°C, AC), Aging (650°C 2hr, AC) DH	1002	1081	11.2	27.5
HG (850°C, AC), Aging (650°C 2hr, AC) DH	921	991	10.6	15.5
HG (850°C, AC), DH	977	999	15.1	46.7
HG (780-750°C, AC), DH	955	991	16.0	49.5

HG: Hydrogenation; AC: Air Cooled; DH: Dehydrogenation done at 675°C (1247°F) for 8hr in vacuum

Increases in both strength and ductility have been achieved as a result of the THP treatments in comparison with non-treated coarse equiaxed Ti-6Al-4V material.

Table 2- 5 shows average α-grain sizes for Ti-6Al-4V produced as a result of different THP treatments [60]. The THP treatment did decrease the average α-grain size from 3.4µm in as forged-annealed condition to 0.91µm after THP treatment, Table 2- 5. The decrease in the average α-grain size did result in an increase in the yield strength, but at the same time decreased both the % elongation and reduction in area drastically, Table 2-5.

The THP treatments also resulted in a 9 to 13% increase in the fatigue strength of the Ti-6Al-4V, Table 2- 5 [60].

Table 2- 5: Summary of THP Treatments and Average α-Grain Produced by These Treatments in Ti-6Al-4V Alloy [60]

THP Cycle	Average α-Grain Size (μm)	0.2%YS MPa	UTS MPa	Elongation %.	RA %.	σ_{fat} * MPa
Forged-annealed	3.40	914	1000	17.7	39.6	590
HG, DH: 650°C	0.91	1119	1152	2.8	11.3	669
HG: Eutectoid decomposition: 590°Cin Ar / FC, DH: 775°C	1.26	974	1025	5.2	12.3	643

HG: Hydrogenation at 850°C and FC; DH: Dehydrogenation in Vacuum; FC: Furnace Cool. * Mean Fatigue Strength at N = 10^7

Hydrogenation of Ti-5Al-2.5Fe at 0-40°C (32-104°F) below the β-transus temperature followed by dehydrogenation at 673°C (1243.4°F) has been reported to result in fine α-grains leading to an improvement in both tensile strength and ductility [49].Qazi et al. in their later study reported a refinement in the as-cast coarse α-lamellar structure of Ti-6Al-4V by THP [6]. Qazi et al. used as-cast material (i.e. no mechanical working was done on the material) with an initial average prior beta grain size of 0.97mm [6]. By changing the THP parameters, microstructures varying from fine lamellar to equiaxed structures were produced. Qazi also reported that producing equiaxed α-grains using THP, requires alloying with 30at% H, beta solution treatment in the beta phase, step cooling and annealing below a critical temperature for complete decomposition of the beta phase, water quenched followed by dehydrogenation at 750°C [6].

Additional possible microstructural modifications can be achieved when a hot working step is included in the THP. Hot deformation in the (α+β) field accelerates phase and structure transformations and can produce very fine equiaxed grains [24, 61, 62]. Deformation at temperatures just above the β(H) transus temperature initiates dynamic recrystallization and β grain size refinement takes place [63].

Yoshimura and co-workers have reported refinement in the α-grains of the Ti-6Al-4V alloy by THP [56]. The THP treatment used included hydrogenation of the samples with 0.6wt.% hydrogen at 950°C, water quenching, hot rolling to a 85% reduction in thickness at 750°C followed by air cooling and finally dehydrogenation at 700°C in vacuum. The THP treatment resulted in an average α-grain size of 1-2µm with a tensile strength of 1000 MPa and elongation of 13% [56].

2.2.6 Other Areas of Thermo-hydrogen Process Applications

There are a few other areas where THP has either facilitated production and/or aided in grain refinement. Some of these areas are reported below:

2.2.6.1 Welds

Welding coarsens the microstructure in the welded region (fusion zone and heat affected zone) and can necessitate some microstructural refinement treatment to improve the mechanical properties of the joints. Conventional microstructural refinement treatments can not be used hence it requires mechanical working of the parts. Thermohydrogen processing has been used effectively with welded sheet articles [5] leading to a refinement of the microstructure in all regions of the part and to an increase in the strength of the joints. For example, spherical vessel of up to 1650 cm^3 capacity, made by welding 2 mm thick sheets of the VT23 alloy (Ti-6Al-4V-2Mo-1.2Cr-0.8Fe) and conventionally heat-treated, fractured under an internal pressure of 1080 MPa. But after a THP treatment, the vessel was able to withstand a pressure of 1119 MPa [5] . Additionally, THP minimized oxidation of the parts during heat treatment because of the lower heat-treatment temperatures used, which is particularly important in the case of articles made from thin sheets [5].

2.2.6.2 Powder Metallurgy Processing

Use of hydrogen as a temporary alloying element in powder metallurgy (P/M) allows production of high quality powders by the hydride-crush-dehydride (HDH) method [57, 64, 65], a reduction in the time of mechanical alloying for production of nanocrystalline alloys and composites, better sintering at lower temperatures, reduction in hot isostatic temperatures required for full density, thermal treatment of net-shape P/M products for grain refinement, property improvements, etc. [27, 66]. For example, Ti_3Al based hydrogenated powder during HIP'ing consolidates with less energy than when a non-hydrogenated powder is employed; this translated into a pressure reduction of 34-67 MPa or a temperature decrease of 110-140°C [67]. The sintering of injection moulded, blended elemental powder was found to occur more readily when it was hydrogenated [58]. It was suggested that hydrogen might clean the powder particles surfaces, promoting better bonding of adjacent powder particles. Thermohydrogen processing can be used to refine the microstructure of both titanium alloy powders and powder compact [44, 68]. Thermohydrogen processing treatment of HIP'd Ti-6Al-4V powder products resulted in over 40 % increase in the fatigue strength in comparison to non-treated Ti-6Al-4V P/M product [69]. Also hydrogenation of Ti-6Al-4V powder produced by the rotating electrode process (REP) led to improved compactability [70].

2.2.6.3 Metal Matrix Composites

Titanium-based composites are normally processed through solid-state diffusion bonding routes to minimize detrimental reactions at the matrix/reinforcement interfaces [5]. Unfortunately, such reactions occur at the temperatures at which the matrix is conventionally processed, which deteriorate the properties of the composite [5]. One possible way of reducing the reactivity is to use a matrix with a lower fabrication temperature [5], but little work has been conducted in this direction. THP has been effectively used in the processing of titanium matrix composites to reduce the consolidation temperature and to improve the final microstructure [71, 72]. Commercial foils of Ti-1100 (Ti-6Al-2.75Sn-4Zr-0.4Mo-0.45Si) and Ti-6Al-4V were used as the matrix

materials. The composite reinforcement consisted of two types of 100 µm diameter SiC fibres; these were either bare/or coated with a double-layer protective TiB_2/C coating.

Composites were produced by consolidation of alternately stacked fiber mats and matrix foils by vacuum pressing. Hydrogen was introduced into the foils before [71, 72] or during [5] consolidation. Unfortunately, the hydrogen concentration in the matrix was not determined. THP was found to substantially increase the rate of consolidation at a given temperature. This allowed full consolidation at temperatures about 100ºC lower (820ºC for Ti-6Al-4V and 920ºC for Ti-1100) than the conventional fabrication temperature without any detectable reactions at the interfaces. In particular, the long TiB needles that decorated the interfaces in conventionally processed samples did not form in the hydrogen-treated samples. Both reduced thermal activation at the low temperatures and hydrogen in solution in the matrix were suggested to inhibit boron diffusion through the matrix and thereby retarding the formation of borides [5]. Fully bonded fiber/matrix interfaces were observed in the THP treated samples, while conventionally processed samples displayed less well-bonded interfaces [5]. Besides, the matrix microstructure for the Ti-6Al-4V composite was refined after THP [71].

Chapter Three

Experimental Procedure

3.1 Design of an Effective Hydrogenation and Dehydrogenation Heat Treatment Apparatus

As a follow-up to the need, as articulated in the motivation for this research, a heat treatment apparatus was designed to provide safe and effective hydrogenation and subsequent dehydrogenation of titanium specimens after processing. Titanium and conventional titanium alloys have a high affinity for hydrogen within a hydrogen environment. The diffusion of hydrogen into titanium is temperature and pressure sensitive. The high diffusivity of hydrogen in titanium is used, first to add hydrogen to the alloy by controlled diffusion from hydrogen environment and then, after processing, to remove it by a controlled vacuum anneal. The rate of hydrogen absorption and the rate of hydrogen evolution in vacuum are considerably reduced when the surface is contaminated by oxygen. Therefore, effort has to be made to carry out the hydrogenation and dehydrogenation processes in a closed vacuum system connected to a heating apparatus.

3.1.1 Experimental Rig set-up

The following are required in order to conduct a safe and effective hydrogenation and dehydrogenation heat treatment study of titanium alloys:

- A high temperature heating system (furnace) with thermal stability
- An efficient vacuum pump to evacuate air from the system
- Pressure monitoring and control devices
- A source of hydrogen supply
- Flow rate control device
- Leak proof design of components
- Provision for adequate protection against mechanical damage on the hydrogen supply storage cylinder
- Provision for proper ventilation management to increase air flow and flush possible hydrogen leakage out of the building in the shortest possible path and time
- Ensuring that materials used in the design are non-combustible and non-reactive

This section outlines the essential component apparatus used for the set-up and describes the component designs and the experimental and/or operational methods for carrying out the experiments.

The general layout of the fixed part of the experimental rig is shown in figure (3-1A). It consists mainly of a horizontal heating furnace, vacuum pump, gas supply cylinders, a flow meter, pressure gauges, PIRANI gauge connected to the pump, cracking valves and quick release valves, copper coiled tube connected to the outlet, and a gas extractor connection (detailed in figure 3-1B).

Figure 3-1A: General experimental rig set-up

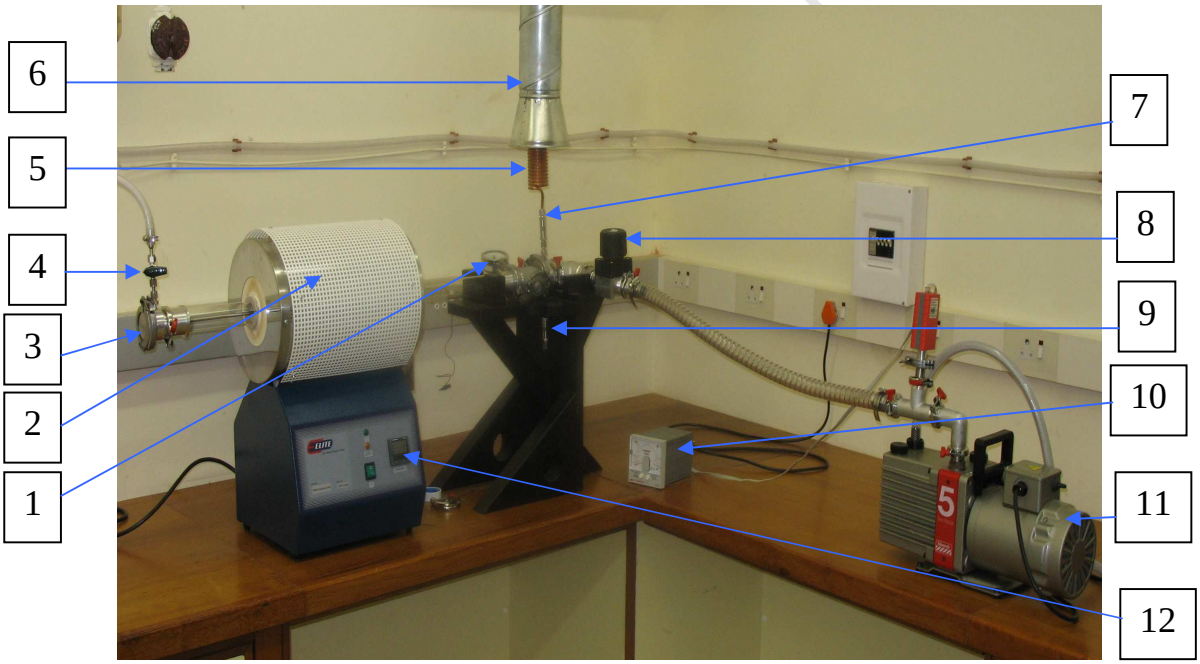

1 – Pressure meter
2 – Heating furnace
3 – Sample holder enclosure
4 – Gas control valve (inlet)
5 – Coiled copper tube
6 – Gas extractor connection
7 – Cracking valve (for gas outlet)
8 – Speedivalve
9 – Cracking valve (for backup)
10 –Peroni gauge
11 – Vacuum pump
12 – Furnace temperature display

Figure 3-1B: A detailed layout of the hydrogenation and dehydrogenation apparatus

3.1.1.1 The Heating System (Furnace)

A horizontal furnace, **model: TSH 12/50/300-2216E** with a maximum temperature of 1200^{o}C was supplied by Elite Thermal Systems LTD for the system set-up. A silica glass tube of approximately 2 meters in length with an internal and external diameter of 36mm and 40mm respectively was also supplied by Elite Thermal Systems LTD. Figure (3-2) shows this assembly of the heating furnace.

Figure 3-2: The heating furnace with the 2 meters silica glass (as supplied prior to set-up)

The heating system is central to the design set-up, as it provides the high temperature environment for the experiment. Temperature calibration tests were done on the furnace to determine the heating and cooling rates with respect to the specimen position during the experiment.

However, considering that a closed system is needed for the experiment under a constant hydrogen flow, additional modifications were made to the furnace set-up for sample positioning and end closure.

3.1.1.2 Specimen Holder

A specimen holder was designed from a high temperature, corrosion resistant AISI 316 stainless steel alloy. The material selection was in order to avoid material failure at high temperatures under the hydrogen environment. The specimen holder was designed to hold test pieces without obstructing gas flow inside the silica glass tube of the furnace. The specimen holder is firmly attached to an end closure that is designed to close the furnace system during the experiment. Figure (3-3) shows the full assembly design of the specimen holder. Details of the design are found in appendix (A)

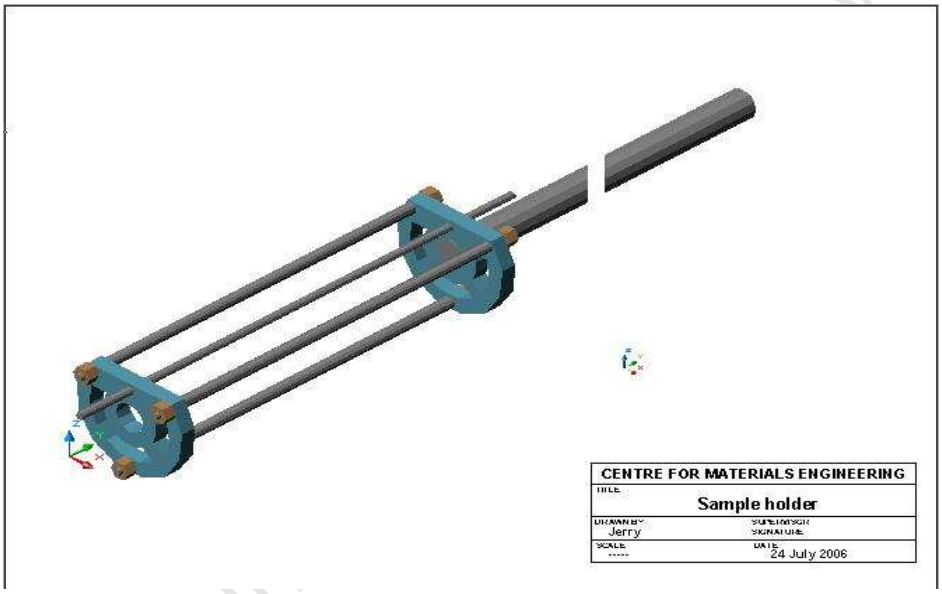

Figure 3-3: Assembly drawing of the sample holder

3.1.2 Pressure Control Devices Connected to the Furnace

Pressure control devices were connected to the furnace to prevent over pressuring of the system during the experiment. The pressure control devices used for the set-up were:

- Two one-way cracking valves;
- A pressure gauge and
- A manual one-way valve.

The cracking valves were set to crack at different gas pressures. One of the valves that was used on the system at the gas outlet, was set to crack at atmospheric pressure, while the other valve was set to crack at the pressure of 20kPa as a safety backup. Their relative positions are shown in figure (3-1B). The decision to set the cracking valves at the stated pressures was, firstly because the silica glass tube was manufactured to sustain pressures of up to approximately 50kPa and, secondly, the hydrogenation and dehydrogenation experiment was designed to be carried out at atmospheric pressure. The pressure gauge was mounted on the system to monitor pressure in the system during the experiment. The manual one-way valve was used to control gas inlet into the furnace system

3.1.2.1 Vacuum Pump

Air evacuation from the furnace system is very essential to the experiment owing to the fact that hydrogen is very explosive and flammable when in direct contact with air. Hydrogen has an auto-ignition temperature of about 585^{o}C with air. The Edwards vacuum pump was connected to the furnace apparatus in order to create the needed vacuum. The vacuum of approximately 10^{-2} Torr was achieved.

3.1.2.2 Copper coil tube and the gas extractor connections

At high temperatures and pressures hydrogen causes static ignition when in contact with air. Besides, there is danger of asphyxiation from the inhalation of hydrogen hence good ventilation and an extracting system are needed when working with hydrogen.

A copper coiled tube is connected to the gas outlet from the furnace so as to provide temperature drop of the escaping gas to below 580^{o}C before being exposed to the atmosphere. The escaping gas passes through the coiled tube which creates room for a longer distance of travel for the gas leading to its drop in temperature. A temperature confirmation test done with argon at 850^{o}C revealed a safe escaping gas temperature of about 100^{o}C.

The copper coiled tube is finally connected to the gas extraction system that extracts the escaping gas to the chimney.

3.1.2.3 Hydrogen Supply Source

A cylinder gas mixture of 5%H_2 and 95%Ar was supplied by Air liquid South Africa for the experiment. This percentage mixture was considered to be a safer working mixture for hydrogen at the elevated temperatures of the experiment. Also, a 99.998%Ar was supplied for the purpose of control experiments. Low pressure gas regulators were mounted on the gas cylinders to control the gas pressure from each cylinder bottle. A quick release valve was used to connect the gas flow line to the cylinders. The quick release valve enables easy and safe inter-connection of the gas pressure regulator onto the gas cylinder bottle. It also quickly locks up to atmospheric pressure on release for inter-connection.

3.1.2.4 The Gas Flow Meter

The diffusion of hydrogen into titanium alloys is sensitive to the rate of flow of hydrogen and the temperature of treatment. Thus, a gas flow meter was supplied to control the flow rate of the gas mixture. The gas flow meter was mounted vertically on the gas bottle pressure regular nozzle. Then the gas line connecting the heating chamber to the gas sauce is connected to the flow meter with a quick release valve. Figure (3-4) shows the general set-up/arrangement of the flow meter.

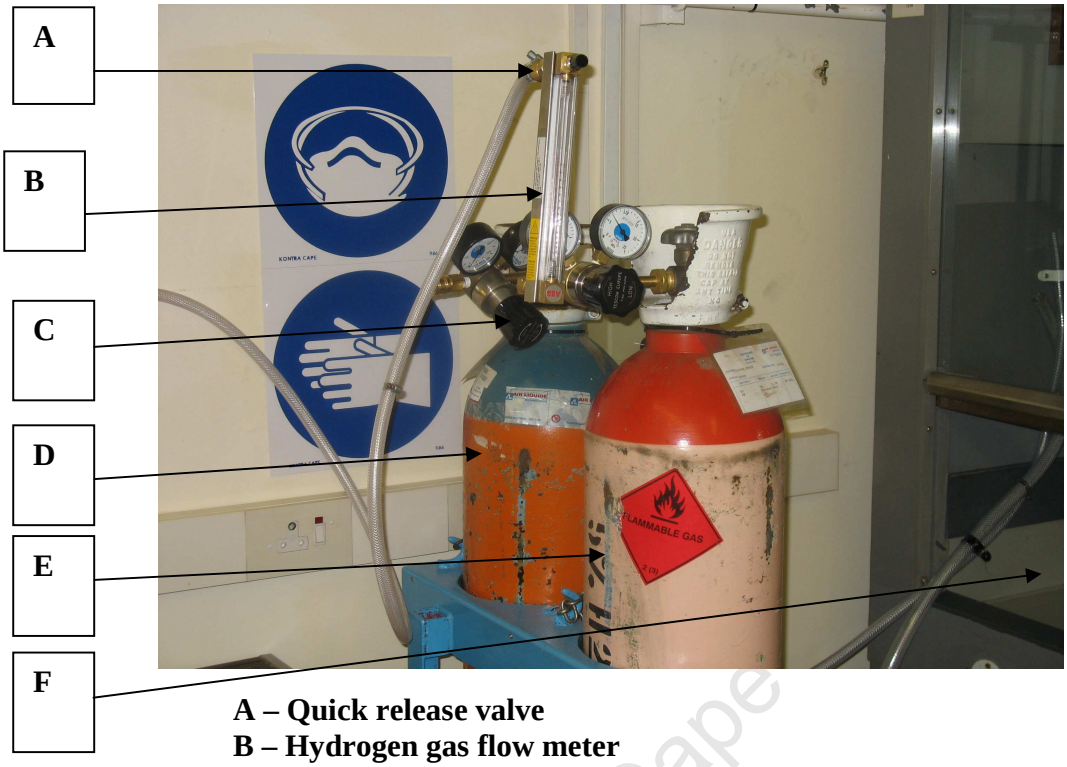

A – Quick release valve
B – Hydrogen gas flow meter
C – Gas regulator
D – Argon gas bottle
E – Hydrogen gas bottle
F – Fume cardboard

Figure 3-4: Gas supply arrangement

3.2 Background to Experimental Technique

The influence of hydrogen as a temporary alloying element in titanium alloys has been demonstrated on Ti-6Al-4V alloy. The so called Thermo-hydrogen Processing (THP) technique has enabled the modifying effect of hydrogen as an alloying element in titanium alloys on the phase compositions and the kinetics of phase transformation leading to evolution of novel microstructures. In this study, the evolution of microstructures during cyclic hydrogenation and dehydrogenation heat treatment has been investigated.

It has often been impossible to carry out conventional heat treatment on α/β alloys like the Ti-6Al-4V alloy due to the high temperature requirement which often results to grain growth. Thus, comparative control heat treatment cycles have been done with non-hydrogenated titanium samples versus the hydrogenated and dehydrogenated samples at similar heat treatment parameters with the treated specimens, with interest in the resultant microstructures at the temperature regions of treatment.

The investigation of the evolution of microstructures was done using light microscopy, scanning electron microscopy and x-ray diffraction (XRD) technique. The mechanical assessment of the specimens (the as-received and the treated) was done using hardness measurements. This section gives details of specimen preparation and the techniques used in this investigation.

3.3 Sample Preparation for Heat Treatment Experiments

Timetal 6-4 in the form of hot rolled and annealed bar of 16mm diameter was supplied by Goodfellow, Cambridge LTD, Huntington. This alloy has a nominal composition of 6wt. % Al, 4wt. % V and balance Ti, hence the designation Ti-6Al-4V (Ti-6-4). Cylindrical coupons of 16mm in diameter and thickness of 2mm were machined, with the precision cutting machine shown in fig (3-5), from the bulk materials and used as test pieces.

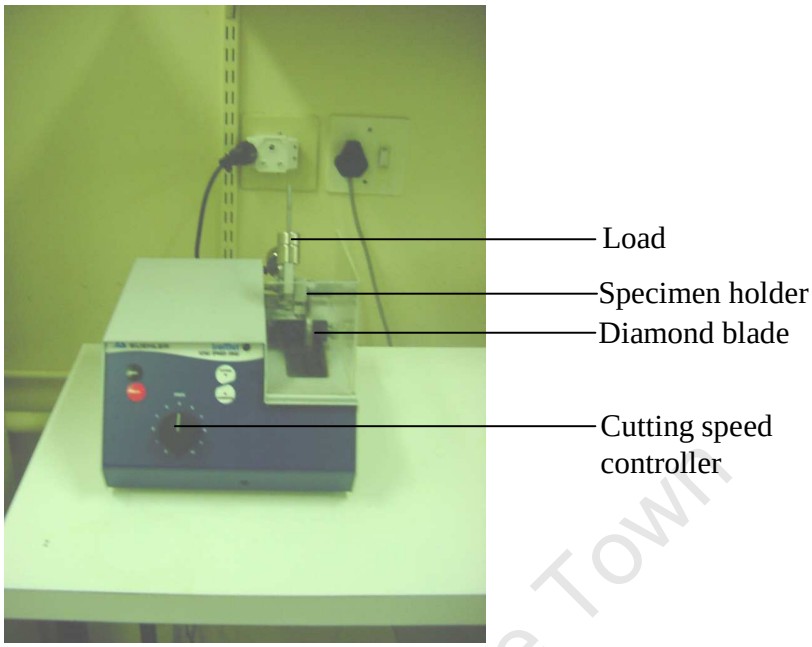

Figure 3-5: Isomet low speed saw used for precision cutting of the specimens

A hole of 3mm was drilled on the test pieces in order to accommodate test pieces on sample holder.

3.3.1 Heat Treatment Experiments

Heat treatments on test pieces were done in two stages: Hydrogenation and Dehydrogenation.

All test pieces underwent heat treatment first in a horizontal vacuum furnace as shown in figure (3-1A & B), for hydrogenation stage in a hydrogen environment or in argon environment to create inert environment for control samples which are not hydrogenated. Test pieces were subsequently subjected to dehydrogenation heat treatment in a vertical vacuum furnace shown in figure (3-7). The control samples were also subjected to the same heat treatment cycle in vacuum for comparison. Details of the two stages are as follows:

3.3.1.1 Hydrogenation (HG) Heat Treatment Process

Test pieces were inserted into the horizontal vacuum furnace using sample cradle as shown in the experimental set-up design. A vacuum of about $1x10^{-2}$ Torr was achieved for the experiment and subsequently the system is heated up first from room temperature to 430^{o}C. Then, hydrogen gas mixture of 95% Ar and 5% H_2 (percentages by volume) was introduced into the system at a flow rate of about 180Nml/min at one atmosphere. Subsequently, the furnace temperature was increased from 430^{o}C to 850^{o}C at 5^{o}C/min and remained isothermally at 850^{o}C for 3 hours. Then, the furnace was switched off to cool down to 430^{o}C at the cooling rate of about 5^{o}C/min with the gas still flowing. Finally, the gas flow was terminated and samples were brought out to cool in air at about 25^{o}C/min. It is important to state here that the essence of introducing hydrogen into the vacuum chamber at 430^{o}C instead of the isothermal temperature of 850^{o}C was to prevent possible auto-ignition of hydrogen in the system. Hydrogen experiences an auto-ignition at the temperature of 560 ^{o}C. Also the temperature for hydrogenation was chosen in order to simulate one of the standard types of thermohydrogen processes mentioned discussed earlier: Below β(H) transus hydrogenation, table 2-3. A schematic experimental diagram is shown in figure (3-6).

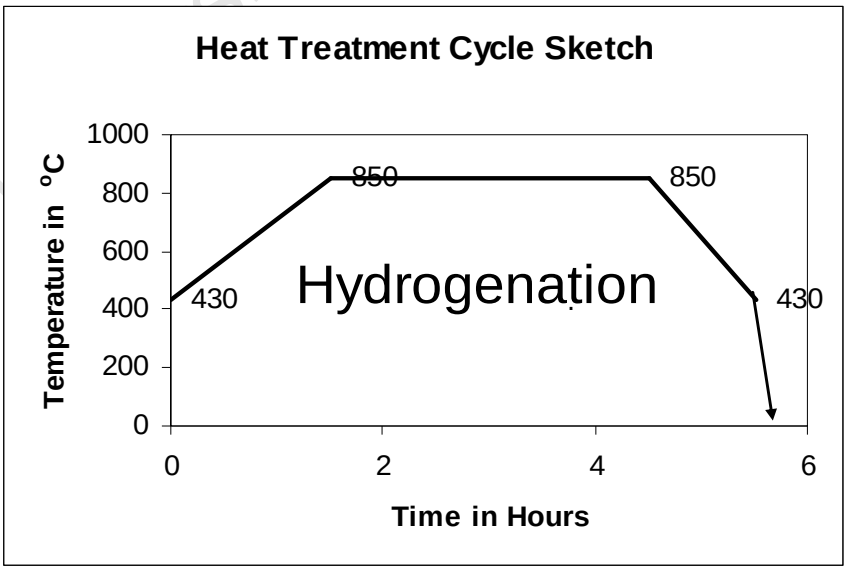

Figure 3-6: A schematic diagram of the hydrogenation heat treatment process on the Ti-6-4 specimens

Similar experimental steps were done on control samples in argon gas environment instead of hydrogen.

3.3.1.1.1 Partial Pressure Calculation

Experimental Data

Gas mixture by volume: 5%H_2 and 95%Ar
Working Temperature: 850^oC
System Pressure: 1 atmosphere = 760 Torr

Using the ideal gas equation where PV = nRT then, if volume V, is assumed to be equal to unity then, partial pressure at fixed temperature T, is proportional to volume fraction (or number of moles, n) of gas.
Therefore the partial pressure of hydrogen in the system,

$$P_{H_2} = 0.05x1atm = 38.0mmHg = 38.0Torr$$

Also partial pressure of argon,

$$P_{Ar} = 0.95x1atm = 721.99 = 723mmHg = 723Torr$$

3.3.1.2 Dehydrogenation (DH) Heat Treatment Process

After the HG stage, test pieces were ground on both sides with 320 grit SiC papers to remove oxide layers formed on surfaces during the hydrogenation heat treatment. Subsequently, samples were treated in a vertical vacuum furnace for dehydrogenation at different isothermal temperatures but constant isothermal times. A vacuum pressure of

about $1x10^{-6}$ Torr was maintained throughout the heat treatment processes. Both the hydrogenated and the control samples underwent the same conditions at this stage.

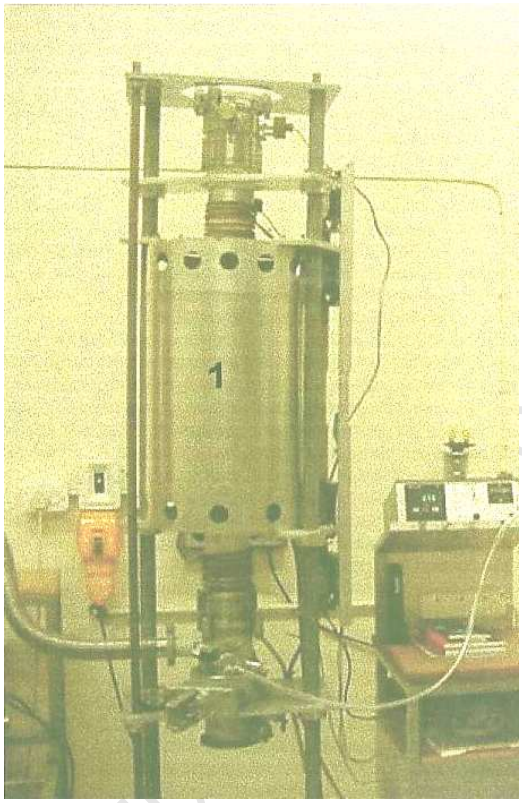

Figure 3-7: High temperature vacuum furnace used for the dehydrogenation process

3.3.2 Characterization of the Test Pieces

Various characterization techniques were used to investigate the evolution of microstructures from the cyclic hydrogenation and dehydrogenation heat treatment technique. All specimen preparations for characterization were done on both as-received and heat treated specimens.

3.3.2.1 Measurement of Hydrogen in the Ti-6-4 Specimens

The hydrogen concentrations in the test pieces were measured using sensitive electric weighing balance which measures up to 10^{-5}g. The Ti-6-4 specimen (as-received) were properly cleaned and weighed before and after hydrogenation and reweighed also after dehydrogenation to the nearest 0.1mg in order to compute the concentration of hydrogen in the specimen after each heat treatment. The quantification of hydrogen concentration in the specimen is significant in order to ascertain effective hydrogen diffusion into the sample as well as its removal after treatment.

3.3.2.2 Specimen Preparation for X-Ray Diffraction

The cylindrical specimens were ground and polished to a mirror finish using the following procedure:

Metalog method B from Struers Metalog Guide was used to grind and polish the specimens. The first step in the guide is grinding the specimen with the MD-Primo 220 grit pad at 300 rpm using water as a lubricant on the automatic polisher applying a force of 120N until the specimen is plane. The second step is further grinding of the specimen using the MD-Largo pad at 150 rpm using the diamond paste suspension with a grain size of 9 microns applying a force of 180N for 5 minutes. The final step is the polishing step that uses the MD-Nap pad at a speed of 150 rpm under a force of 60N for 2 minutes. The lubricant used in this final step is a mixture of 96 ml of the OP-U solution, 2 ml hydrogen peroxide and 2 ml of ammonia.

The XRD was carried out using a D8 ADVANCE X-ray apparatus shown in figure (3-8).

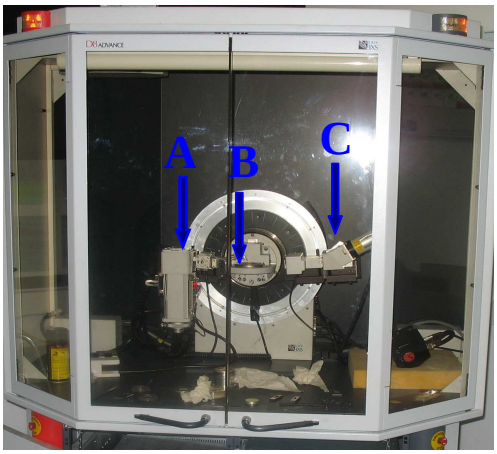

Figure 3-8: D8 ADVANCE X-Ray Diffraction Apparatus: A – X-ray Detector (Positioning sensitive detector (PSD)) B – Sample holder with the target specimen, C – x-ray source supplying CuK$_\alpha$ radiation

The measurement details are as follows:

- The X-ray generator operated at 40mA and 40kV
- The starting 2Θ angle was at 20^o and finish at 80^o
- Step size was at 0.02 degrees
- Time per step was 3.2 seconds
- The sample rotation was set on and the speed was 15 rpm

.

3.3.2.3 Specimen Preparation for Microhardness Measurements

Microhardness measurements were done on the as-received Ti-6-4 specimen, the hydrogenated specimen as well as the dehydrogenated specimens. The cylindrical test coupons were sectioned normal to the flat surface using a precision cutting machine shown in figure (3-5).

The specimens were subsequently mounted in Specifast resin using the Struers lab-press 3. Metalog method B from Struers Metalog Guide was used to grind and polish the specimens. The sequence was exactly as specified for XRD specimen preparation.

Finally, the Zwick microhardness tester shown in Figure 3-9 was used to measure the hardness of the bulk portion of all the specimens. The hydrogenation treatment affects the bulk of the specimen hence the bulk hardness measurements.

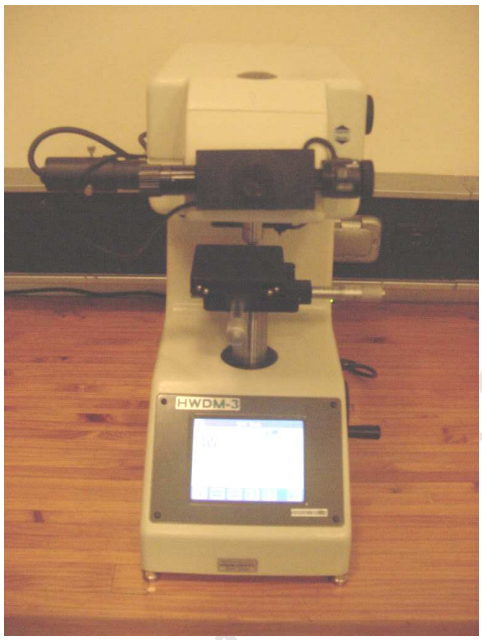

Figure 3-9: Zwick hardness tester

Seventeen random hardness measurements were made per specimen using a standard Vickers diamond indenter with a load of 500 gf. Then, the average hardness values as well as the standard deviation for the seventeen measurements were computed for all the specimens measured.

3.3.2.4 Specimen Preparation for Light Microscopy

The cylindrical test coupons prepared for microhardness were subsequently used for the light microscopy.

However, the specimens were first dip etched with the solution of the following etchant listed below:

- 10 ml hydrogen fluoride
- 30 ml nitric acid
- 50 ml of water

The samples were dip-etched in the solution for 15-20 seconds. The revealed microstructure was then examined under the light microscope. The microstructure in figure (3-9) was obtained from the as-received annealed specimen. All microstructures obtained in this research except otherwise stated, were taken at x50 magnification of the objective lens.

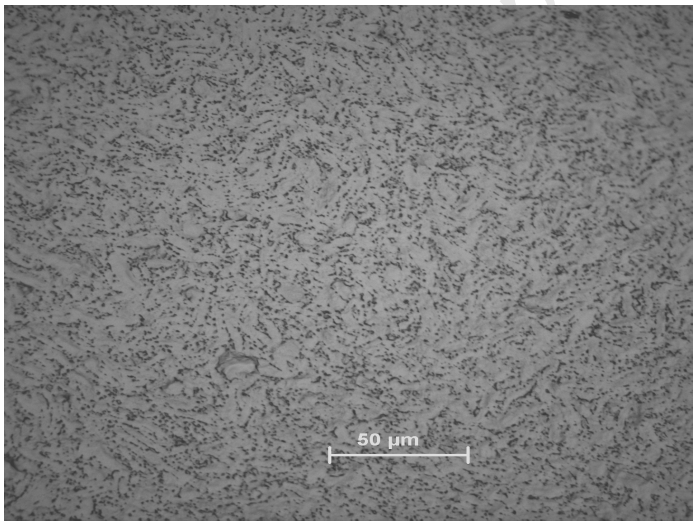

Figure 3-9: Microstructure of the as-received annealed specimen taken from the bulk after sectioning.

3.3.2.5 Scanning Electron Microscopy (SEM)

The cylindrical test coupons that were used for the light microscopy were used for the scanning electron microscopy. The specimens were additionally coated with silver on the surface in order to make the specimens more conductive during measurement. Then, the examination was done with the LEO Stroscan 440 scanning electron microscope at higher magnifications of 1500 and 5000 per specimen. An accelerating voltage of 20 kV was used in order to achieve optimum secondary and backscattered electron signal. The working distance between pole piece and sample was 20mm. The micrograph was captured with the secondary electron detector.

3.3.2.6 Grain size measurements

The grain sizes of the prior β-grains for the dehydrogenated specimens have been measured using the mean lineal intercept method. The mean intercept length gives the average length of a line segment that crosses a sufficiently large number of grains. It is proportional to the equivalent diameter of a spherical grain. The mean linear intercept length was determined for the hydrogenated specimens by laying a number of randomly placed test lines on the micrographs and counting the number of times that the grain boundaries were intercepted. It is expressed mathematically as:

$$\overline{L_L} = \frac{1}{\overline{N}_L} = \frac{L_T}{PM}$$

Where NL is the number of intercepts per total length of the test lines LT, P is the total number of grain boundary intersections and M is the magnification. The average grain size and standard deviation for each micrograph were calculated.

Chapter Four

Experimental Results and Discussion

4.1 Introduction

This chapter presents the results and the discussion of data obtained from the measurement of hydrogen concentration in the specimens, light microscopy, scanning electron microscopy, x-ray diffraction and microhardness testing.

4.2 Hydrogen Measurement

Table 4-1, shows the results of an attempt to measure the bulk concentrations of hydrogen by a process of mass changes for the hydrogenated and the dehydrogenated specimens respectively. These results were obtained by weighing specimens to the nearest 0.1mg before and after hydrogenation for weight gain and the subsequent reweighing after dehydrogenation for weight losses. The detailed experimental values are contained in Appendix E.

Table 4-1: Calculated Hydrogen concentration in Ti-6-4 cylinders following hydrogenation and dehydrogenation treatments

Sample	Hydrogenation treatment at 850°C for 3 hours		Dehydrogenation treatment at 750°C for 18 hours		Dehydrogenation at 650°C for 18 hours	
	Increase in hydrogen (wt. %)	Standard deviation	Decrease in hydrogen (wt. %)	Standard deviation	Decrease in hydrogen (wt. %)	Standard deviation
A	0.812	0.001	0.348	0.002		
B	0.538	0.001	0.095	0.001		
C	0.695	0.002	0.107	0.002		
D	0.486	0.001				
E	0.618	0.002				
F	0.765	0.002				
G	0.707	0.000			0.060	0.003
H	0.506	0.000			0.004	0.001
I	0.780	0.001			0.128	0.001
J	0.556	0.001			0.090	0.002

However, the calculated values are unreliable due to inconsistency in the mass values resulting from the oxide layers that were formed after each treatment (hydrogenation or dehydrogenation) due to insufficient vacuum achieved during heat treatments. It was difficult to reconcile the additional weight on the specimen due to the oxide layer; considering also that the weight of hydrogen molecule is very little relative to the oxide layers. Additional efforts were made to weigh the specimens after grinding off the oxide layers but the fact that diffusion of hydrogen into the bulk titanium specimen is not

homogeneous; there were chances that the greater portion of the hydrogen could have been lost in the course of the grinding. Hence, it was incorrect to relate the calculated hydrogen concentrations (after grinding) to the treatment period.

4.3 Light Microscopy

This section reveals the underlying microstructures of the Ti-6-4 specimen after heat treatment with hydrogen and the comparative control treatments following each heat treatment cycle.

4.3.1 Hydrogenation of Titanium specimen

Hydrogen has successfully been diffused into Ti-6-4 alloy using the procedure outlined in the previous chapter and the microstructure in figure (4-1) is a cross-section of microstructure that was obtained. The microstructure shows a fully modified grain structure with plate-like structures that are typical of martensite formation. The structure formed is typical of structures reported by researchers [4, 5, 41, 49, 73] that are evident after successful thermal diffusion of hydrogen into titanium alloys. Martensitic formation in titanium alloys during hydrogen heat treatment is reported to be dependent on the processing temperature, concentration of hydrogen in-diffused and the cooling rate after processing.

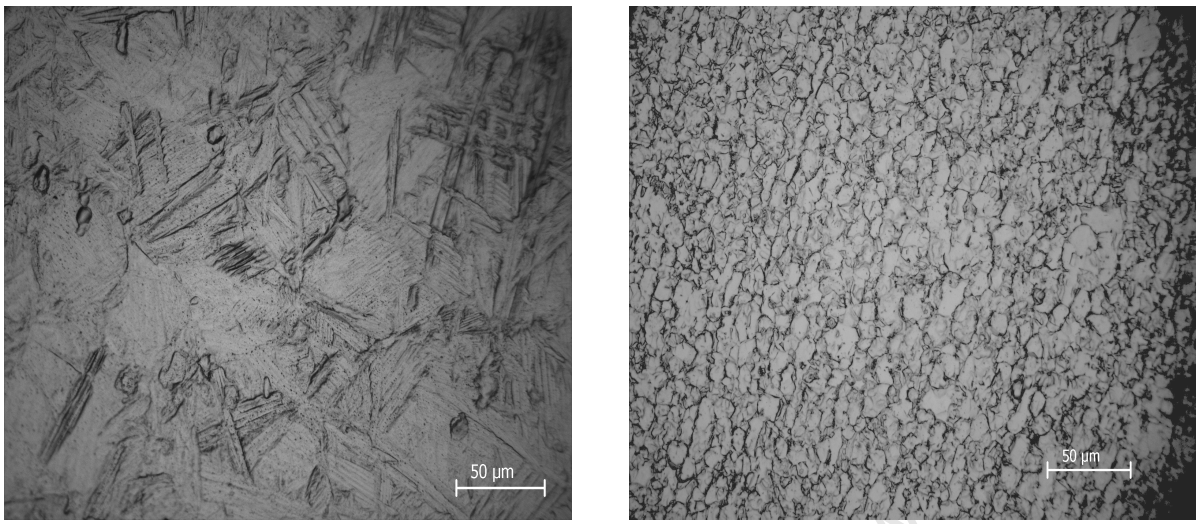

Figure 4-1: Light microscopy of Ti64 alloy: (A) hydrogenated showing the martensite plates and (B) Argon treated both at 850^{o}C for 3 hours and furnace cool to 430^{o}C and air cooled respectively showing the α -phase (light) and β-phase (dark)

4.3.1.1 Martensite formation in Ti-6Al-4V alloy with hydrogen

Hydrogen alloying destabilises the low-temperature hcp α-phase and stabilizes the more ductile high-temperature bcc β-phase in α and α+β titanium alloys [44]. It has the potential to increase the volume fraction of the β-phase and decrease that of the α-phase respectively. It brings about the redistribution of the alloying elements with respect to their favouring phase in the alloy. In a scientific review paper by F.H. Froes et al [5] , it was reported that there was a decrease in the diffusion coefficient of the alloying elements in the β-phase resulting from the hydrogen alloying of titanium, suggesting that the kinetics of the β-α phase transformation will slow down. Hydrogen alloying has been reported to have enabled the lowering of the β-phase transus temperature of titanium which subsequently facilitates the formation of martensite. F.H. Froes et al [5], reported that an increase in hydrogen concentration from 0 to 30 at.-% slows down the kinetics of the β phase transformation considerably, resulting to an increase in nose time for the start of transformation from 12 seconds to 42 minutes, figures (2-6 and 2-7). The large increase in nose time leads to a considerable decrease in the quenching rate necessary to

produce a 100% martensite structure. A cooling rate as low as 5 K min^{-1} in the alloy with 30 at-%H is sufficient while a cooling rate of 1000 K min^{-1} is required to produce a 100% martensite structure in the alloy with 0%H.

Considering the high diffusivity of hydrogen at elevated temperatures the three hour isothermal hydrogenation for the present research could have been sufficient to achieve up to about 30 at-% H for the martensite formation.

4.3.1.2 Hydrogenation Control Specimen

The specimen that was subjected to the same heat treatment cycle for the hydrogenation process but in argon environment instead of hydrogen revealed the microstructure shown in figure (4-1B). The relevance of this approach is to compare the resultant microstructure in a non-hydrogenated specimen under the same isothermal heat treatment process of hydrogenation. The microstructure revealed in figure (4-1B) shows an equiaxed coarse α grain structure with an intergranular untransformed β-phase within the grain boundaries. The α-phase structures appeared white and β-phase dark with the etching effect on the metal. The large grains are evidence of the grain growth that occurred during the heat treatment process. The grain growth was driven by the release of the grain boundary surface energy due to high temperature and the long duration of the treatment as the amount of total grain boundary surface is reduced. This leads to grain boundary mobility and grain growth.

There was no evidence of martensite plate-like structures as was the case with the hydrogenated specimen. Martensites are only formed in a non-hydrogenated titanium alloy when quenched at a very fast rate from above the beta transus [39]. The β-phase transus temperature ((α+β) → β transition) for Ti-6Al-4V alloy is reported to exist around 1000^{o}C [16, 17]. The temperature of 850^{o}C with which this experiment was done does not contain the needed homogeneous single β-phase which is required to facilitate the diffusionless phase transformation of β-phase to martensite formation in a non-hydrogenated specimen. Thus, the disclosure from the heat treatment points out to say

that the martensitic structures in the hydrogenated specimen were contributed by phase transformation enabled by hydrogen addition and not the thermal cycle itself.

4.4.2 Dehydrogenation of Ti-6Al-4V alloy Specimen

Various heat treatment procedures have been used to remove the in-diffused hydrogen in the titanium sample so as to preserve and/or enhance the mechanical integrity of the titanium alloy and to investigate the resultant novel microstructures after hydrogen removal in vacuum. Besides, according to an earlier report by D .H. Kohn et al [49], the removal of hydrogen is necessary because the residual hydrogen concentrations in-diffused into titanium alloys compromise the mechanical integrity, since hydrides can fracture and act as crack nuclei in the alloy. They reported also that as long as hydrogen concentrations are less than 140 p.p.m (0.014 wt.-%), there's no effect of hydrogen on dynamic properties. The maximum allowable hydrogen concentration in wrought Ti-6Al-4V is 120 p.p.m (0.012 wt. - %).

In line with these backdrops, isothermal dehydrogenation heat treatments for 18 hours at different elevated temperatures have been carried out in this research and the results obtained and the discussion of the results are presented next.

4.4.2.1 Isothermal Dehydrogenation Heat Treatments for 18 hours at Different Temperatures

4.4.2.1.1 Isothermal Dehydrogenation Heat Treatment at 750^{o}C

The dehydrogenation heat treatment carried out on the Ti-6-4 specimen in vacuum at 750^{o}C for 18 hours and furnace cooled to room temperature produced the microstructure shown in figure (4-2 A).

The microstructure shows a lenticular-like structure that is typical of a Widmanstätten structure with grain boundary allotriormorphs and some α-phase precipitates (light) within the prior β grains. The dark phase in-between the Widmanstätten α-phase plates are identified as residual β-phase.

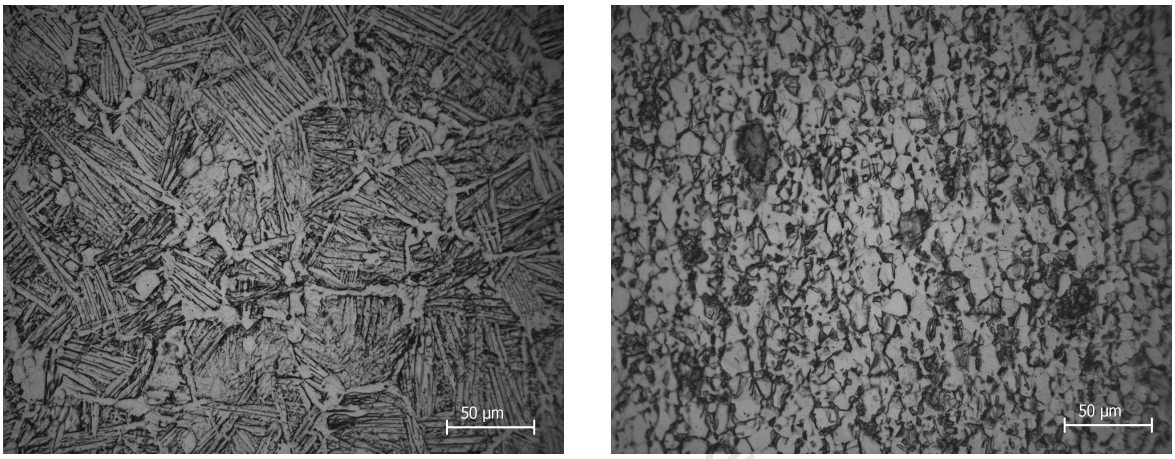

(A) **(B)**

Figure 4-2: Light microscopy of Ti64 alloy: (A) hydrogenated and (B) Argon treated both at 850°C for 3 hours and furnace cooled to 430°C and air cooled, then, (A) dehydrogenated and (B) vacuum treated, both at 750°C for 18 hours and furnace cooled to room temperature respectively.

It is particularly interesting to see the Widmanstätten structures formed after this dehydrogenation heat treatment. This is because Widmanstätten structures are only formed in a non-hydrogenated Ti-6-4 alloy on slow cooling after a solution heat treatment above the beta transus at about 1020°C [14]. Widmanstätten structures are formed in titanium alloys by heterogeneous nucleation and growth events occurring on pre-existing prior β grain boundary with each growing α plate maintaining a Burgers' relationship with its parent β matrix [74]. The nucleation and growth of Widmanstätten structures during the dehydrogenation heat treatment shows that there was a lowering of the β-phase transus by hydrogen alloying of Ti-6-4. Thus, a β-phase region can be thought to have existed around the temperature of 750°C used for the dehydrogenation process hence the Widmanstätten structures were formed. A similar cycle heat treatment done on another titanium specimen but without hydrogen supports the belief that the

Widmanstätten structures were initiated by hydrogen alloying and not heat treatment cycle. This is revealed by the microstructure shown in figure (4-2B). The microstructure shows a well dispersed coarse equilibrium α and intergranular β. The coarse α grains are evidence of grain growth during the heat treatment. The grain growth was driven by the release of the grain boundary surface energy due to high temperature and the long period of the treatment as the amount of total grain boundary surface is reduced. This leads to grain boundary mobility and grain growth of the specimen.

4.4.2.1.2 Isothermal Dehydrogenation Heat Treatment at 650°C

Following dehydrogenation heat treatment at 650°C for 18 hours and furnace cooled to room temperature, a microstructure typical to the morphology obtained for dehydrogenation at 750°C was obtained as shown in figure (4-3).
The microstructure shows a Widmanstätten microstructure with α+β phases. The Widmanstätten structures have shorter α plates and smaller prior β-grain boundaries of 27μm ± 4.53 relative to dehydrogenation treatment at 750°C which formed prior β-grain boundaries of 38μm ± 7.50; the ± values are the standard deviations. The prior β grain boundaries formed colony boundaries for the α-phase, which nucleated preferentially from the prior β grain boundaries. Besides, there are evidences of more primary-α grains (light) in the microstructure after the dehydrogenation at 650°C, figure (4-3), than those obtained after dehydrogenation at 750°C, figure (4-2).

This observation could be due to a greater expulsion of hydrogen at 650°C thereby enabling the β → α phase transformation to occur more easily, thus obviating the growth of Widmanstätten structures that are seen in the 750°C treatment. Also, the lower temperature of 650°C could have hindered the growth of Widmanstätten structures on cooling compared to the higher temperature of 750°C which favours growth and thickening of Widmanstätten plates on cooling.

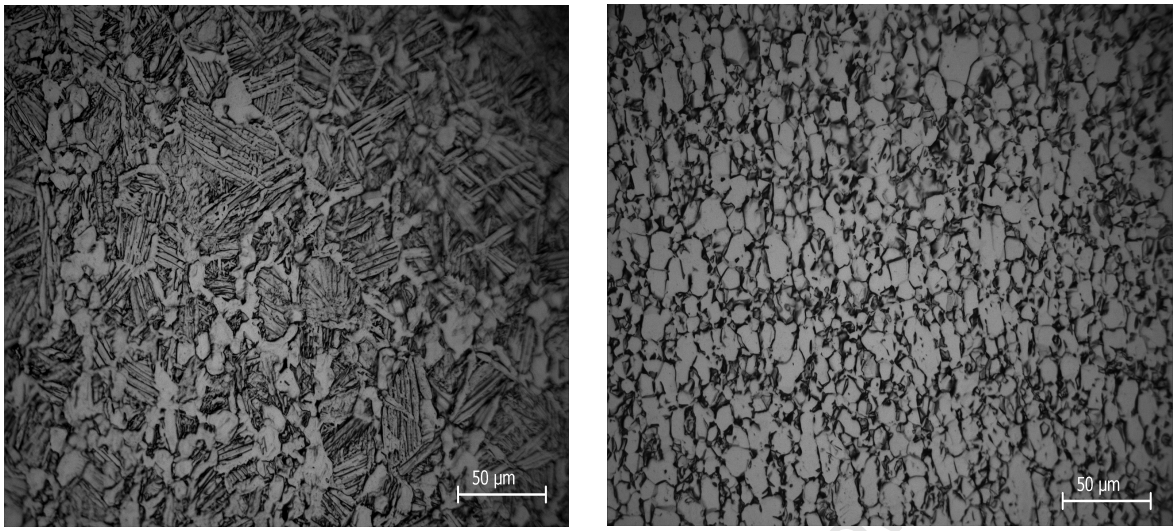

(A) **(B)**

Figure 4-3: Light microscopy of Ti-6-4 alloy: (A) hydrogenated and (B) Argon treated both at 850^{o}C for 3 hours and furnace cooled to 430^{o}C and air cooled, then, (A) dehydrogenated and (B) vacuum treated, both at 650^{o}C for 18 hours and furnace cooled to room temperature respectively.

Figure (4-3B) shows a control heat treatment done on a Ti-6-4 specimen at the same heat treatment cycle for dehydrogenation at 650^{o}C but without hydrogen. The microstructure shows a well dispersed coarse equilibrium α and intergranular β. The coarse alpha grains show evidence of grain growth during the heat treatment. The grain growth was driven by the release of the grain boundary surface energy due to high temperature and the long period of the treatment as the amount of total grain boundary surface is reduced. This leads to grain boundary mobility and grain growth of the specimen. The stored energy released was formed due to imperfections at the grain boundaries. There is no evidence of Widmanstätten structures in the microstructure.

4.4.2.1.3 Isothermal Dehydrogenation Heat Treatment at 550°C

A dehydrogenation heat treatment that was carried out at 550°C for 18 hours and furnace cooled to room temperature produced the microstructure shown in figure (4-4). It shows a microstructure that resembles a broken-down Widmanstätten microstructure with a well dispersed globular-like primary-α grain structures (light). The microstructure compares with the microstructure revealed at figure 4-3A though the grain boundary allotriormorphs seem to have nucleated more and grown bigger in the 550°C treatment than in figure 4-3A. The prior β-grain boundaries formed were 15μm ± 1.84; the ± values are the standard deviations. This could be indicative of effective dehydrogenation at 550°C. However, there are reservations to this observation due to the previous contributions by researchers that hydrides are formed within this treatment temperature of dehydrogenation. The temperature of dehydrogenation is believed to be low for effective dehydrogenation due to the stability of hydrides within lower temperatures as suggested by phase diagram done by Qazi et al [41]. Thus, it is not clear whether the microstructure is nearing a full decomposition of the reported hydride phases. Probably the long period of dehydrogenation (18 hours) may have enabled hydrogen removal in vacuum and partial decomposition of hydrides and subsequent precipitation of α-phase and some residual β-phase. Therefore, a mixture of (α+ β+δ) phases could be anticipated in the microstructure obtained. More scientific work needs to be done in order to confirm this observation. However, the SEM and the X-ray diffraction analysis done on the treated specimen which is discussed in the following sections will bring some more understanding.

Figure 4-4: Light microscopy of Ti-6-4 alloy hydrogenated at 850^{o}C for 3 hours and furnace cooled to 430^{o}C and air cooled, then, dehydrogenated at 550^{o}C for 18 hours and furnace cooled to room temperature

4.4 Scanning Electron Microscopy

This section reveals the microstructure of the treated specimens taken at higher magnifications (1500 and 5000 respectively for each specimen) in order to investigate the presence of phases that are possibly not visible from the optical microscopy.

Figures (4-5 to 4-8) reveal these microstructures treated as specified at their respective figures. Generally, there is no clear evidence of additional phase(s) order than those seen from the optical microscopy. The hydrogenated specimen, figure (4-5) reveals the martensite plates in the matrix of the fine equiaxed alpha structures.

The specimen dehydrogenated at 550^{o}C, figure 4-6, reveals the broken down Widmanstätten structures with the residual β-phase appearing white in-between the α-plates and the grain boundaries. The globular-like alpha structures are also revealed. No hydride phase is revealed. The presence of hydrides phase normally appears dark from the electron radiation along the α-grain boundaries.

Figure 4-7, reveals the Widmanstätten structures and the alpha globular grain structures as was seen from the light microscopy, figure 4-3. The residual β-phase appears white along the grain boundaries.

Figure 4-8, reveals the elongated Widmanstätten structures with the grain boundary residual β-phase.

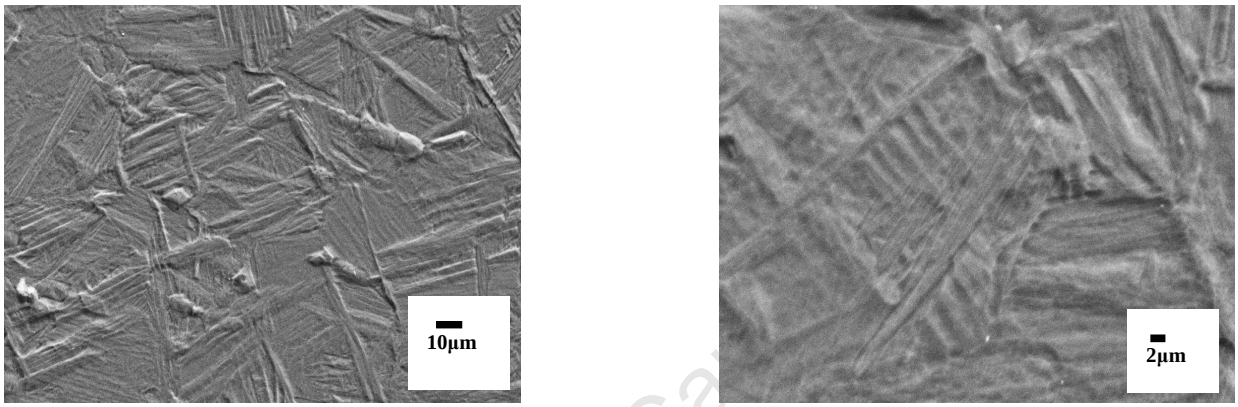

x 1500 **x 5000**

Figure 4-5: Scanning Electron Microscopy of Ti-6-4 alloy hydrogenated at 850°C for 3 hours and furnace cooled to 430°C and air cooled

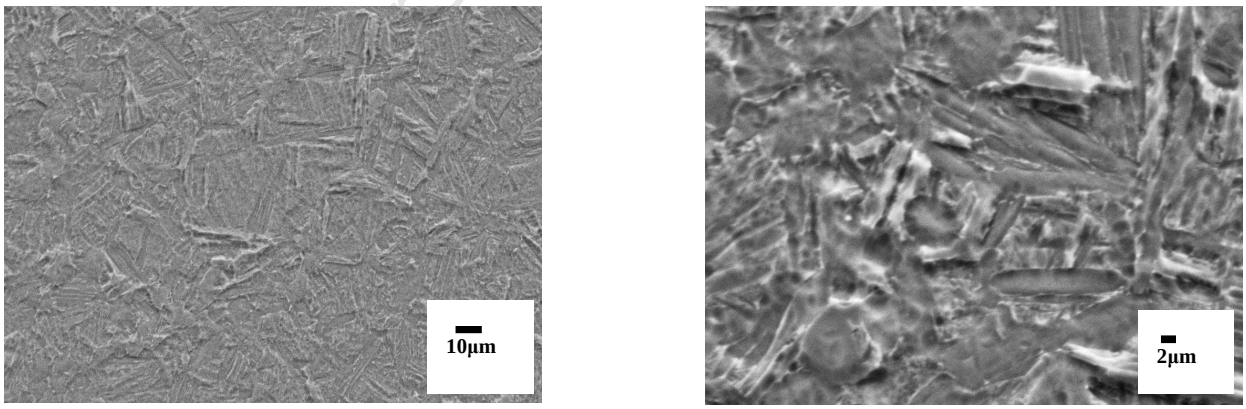

x 1500 **x 5000**

Figure 4-6: Scanning Electron Microscopy of Ti-6-4 alloy hydrogenated at 850°C for 3 hours and furnace cooled to 430°C and air cooled, then, dehydrogenated at 550°C for 18 hours and furnace cooled to room temperature

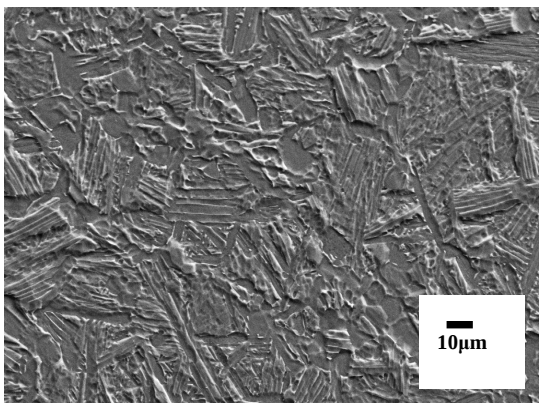

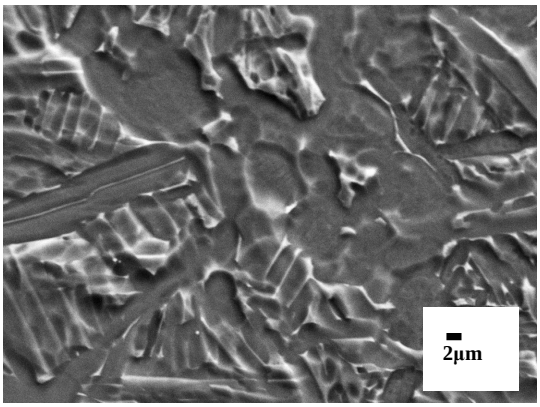

x 1500 **x 5000**

Figure 4-7: Scanning Electron Microscopy of Ti-6-4 alloy hydrogenated at 850^{o}C for 3 hours and furnace cooled to 430^{o}C and air cooled, then, dehydrogenated at 650^{o}C for 18 hours and furnace cooled to room temperature

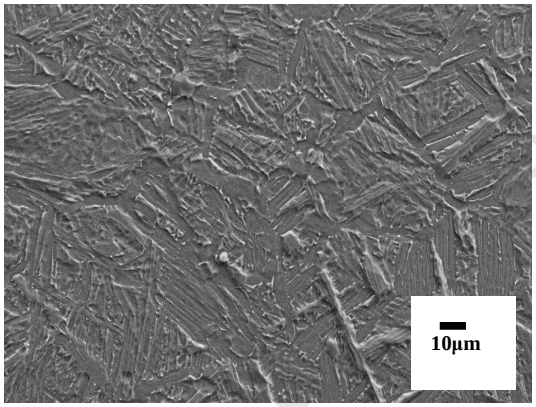

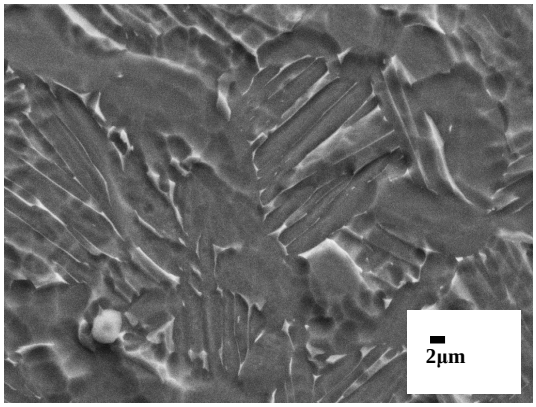

x 1500 **x 5000**

Figure 4-8: Scanning Electron Microscopy of Ti-6-4 alloy hydrogenated at 850^{o}C for 3 hours and furnace cooled to 430^{o}C and air cooled, then, dehydrogenated at 750^{o}C for 18 hours and furnace cooled to room temperature

4.5 X-Ray Diffraction

This section gives the X-ray diffraction spectra of the as-received annealed Ti-6Al-4V alloy specimen, hydrogenated specimen at specified heat treatment parameters, dehydrogenated specimens at specified heat treatment variables and control specimens that experienced the same cycle treatments for hydrogenation and dehydrogenation but in argon for the hydrogenation stage.

The X-ray peaks of this work were identified by measuring and comparing peak positions of the same alloy, Ti-6Al-4V, measured with Cu-k_α as X-ray source and published in scientific journals. Tables (1- 8) in Appendix (C) give the referred work as measured.

The spectra have been presented on the same scale for proper assessment hence some X-ray peaks revealed are cut off. The full spectra peak heights are found in Appendix (D).

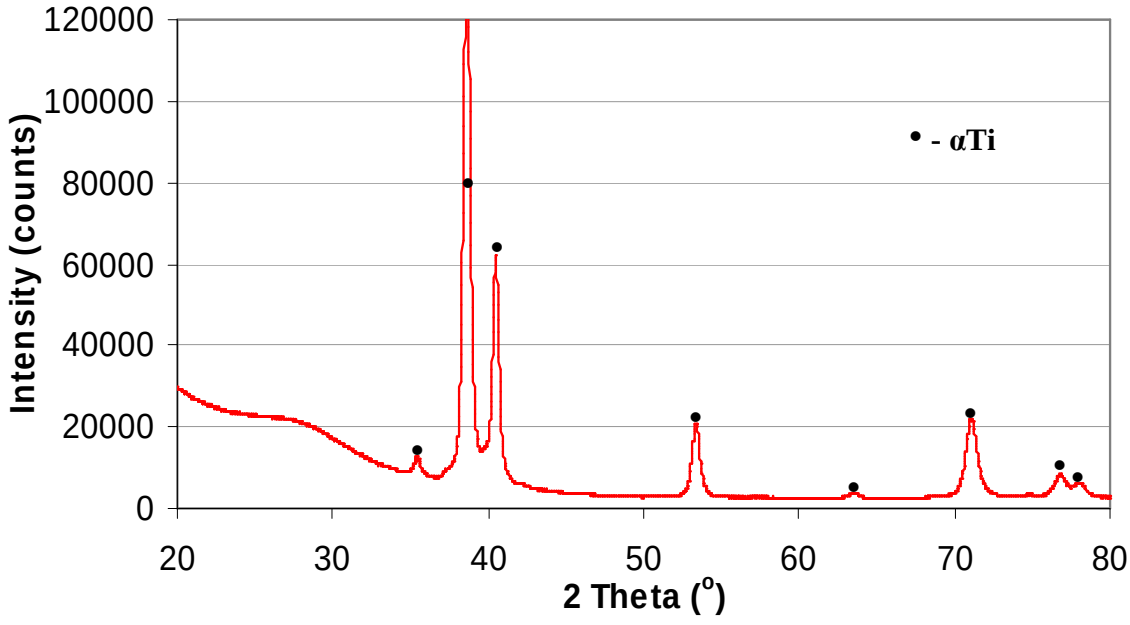

Figure 4-9: X-ray diffraction spectrum of Cold rolled annealed Ti-6-4 (As-Received)

Figure 4-9 shows the x-ray diffraction spectrum of the as-received annealed specimen. It revealed peaks that correspond to α-phase positions only. Beta phases were not present as would have been expected in an annealed condition. This suggests that the as-received specimen is probably not in the full annealed condition or the volume fraction of the β-phase was too low to be detected.

After hydrogenation heat treatment at 850°C for 3 hours of the annealed specimen, the intensity increased at some peak positions as shown in figure 4-10. The spectrum also reveals coexistence of a martensitic phase α″ (alpha double prime), and an α-phase at peak position 35°. Besides, a primary martensitic phase α′ (alpha prime) coexisted with α-phase at peak positions 38°, 41° and 53.5° respectively. No β-phase peak was revealed by the spectrum. The absence of β-phase peak for the hydrogenated specimen could be explained by the role hydrogen plays in phase transformation and kinetics of titanium alloys; hydrogen as a β-phase stabilizing element has the potential to lower the β-phase transus and transform the prior beta grains into martensite.

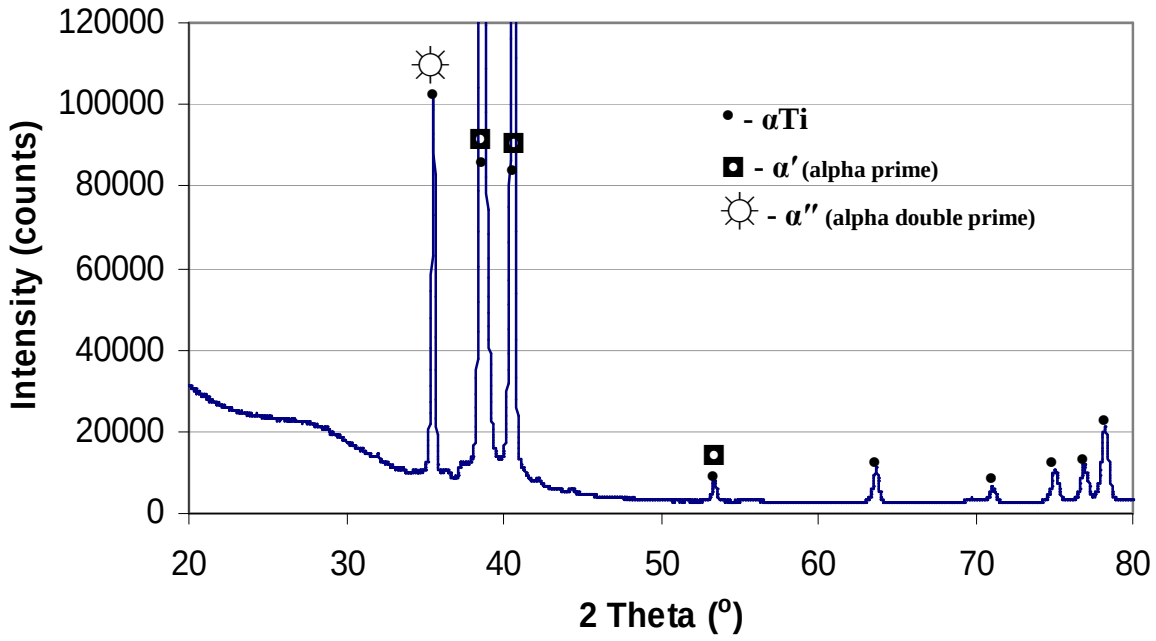

Figure 4-10: X-ray diffraction spectrum of Ti-6-4 hydrogenated at 850°C for 3 hours and furnace cooled to 430°C and air cooled: (Step 1)

The martensite phase formed by cooling from the beta phase region is reported to be either the α′ (alpha prime) phase (hcp) or α″ (alpha double prime) phase (orthorhombic), depending on the hydrogen content [56]. The formation of orthorhombic martensite is typical in α+β titanium alloys containing a large amount of β stabilizing alloying elements, such as V and Mo [41]. It is therefore not surprising to have similar effect from the addition of hydrogen, which is also a strong β stabilizer as revealed in the spectrum. Hydrogen is reported to have increased the nose time necessary to decompose the β-phase which subsequently enabled the formation of martensite in untreated specimens. In a scientific review paper by F.H. Froes et al [5], it is reported that an increase in hydrogen concentration from 0 to 30 at.-% slowed down the kinetics of beta phase transformation considerably, resulting in an increase in the nose time for start of transformation from 12secs to 42mins, figures (2-6) and (2-7) . The nose temperature decreased linearly from 725 to 580^{o}C with an increase in hydrogen concentration from 0 to 30 at.-%. The substantial increase in nose time leads to a considerable decrease in the quenching rate necessary to produce a 100% martensite structure. A cooling rate as low as 5 K min^{-1} in the alloy with 30 at.-%H is sufficient while a cooling rate of 1000 K min^{-1} is required to produce a 100% martensite structure in the alloy with 0%H. Therefore, given the 3 hour hydrogenation treatment which is a long period to achieve hydrogen diffusion and saturation considering the high diffusivity of hydrogen in titanium at elevated temperatures, the martensite phases revealed in the hydrogenated spectrum of this present work is anticipated.

The Hydrogenated specimen that was subsequently subjected to a dehydrogenation treatment at 550^{o}C for 18 hours and furnace cooled to room temperature revealed a spectrum with β-phase peaks at position 39.5^{o} and smaller peaks at positions 58^{o} and 72^{o} respectively. The α-phase exists at peak position 35^{o}, figure 4-11. Also, primary α′-phase coexists with α-phase at peak position 71.5^{o}.

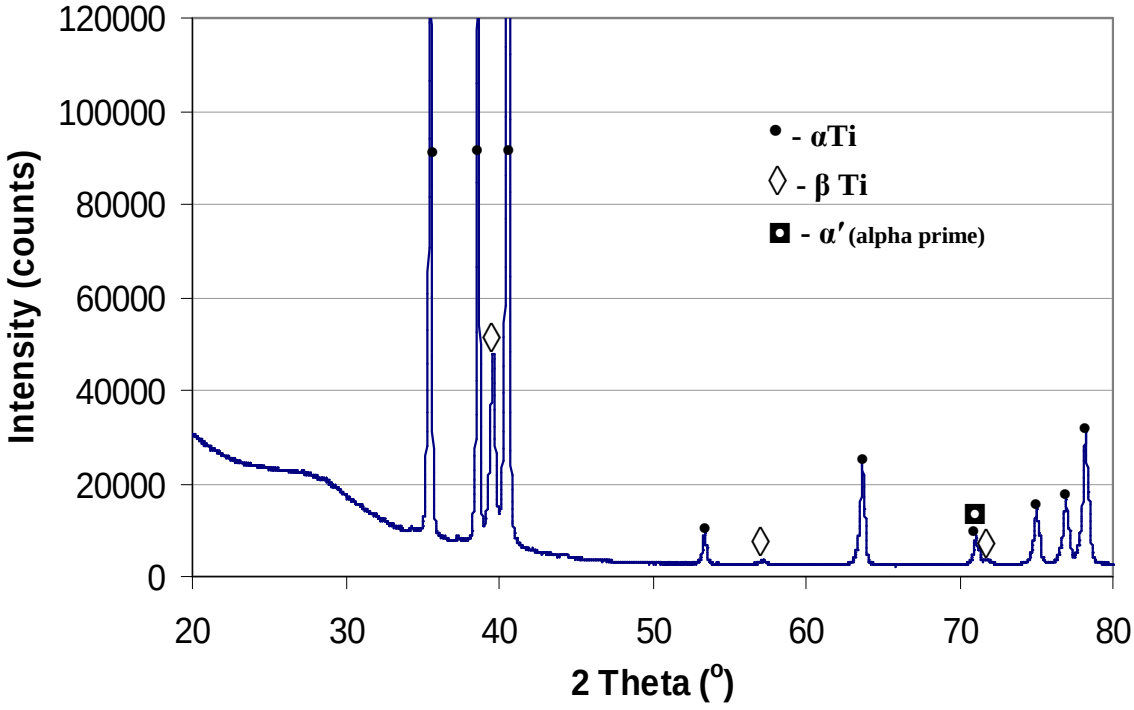

Figure 4-11: X-ray diffraction spectrum of Ti-6-4 hydrogenated at 850°C for 3 hours as in (Step 1) then, dehydrogenated at 550°C for 18 hours and furnace cooled to room temperature

The primary martensite in figure 4-11 could possibly be a residual martensite phase from the hydrogenated specimen which on dehydrogenation at 550°C could not achieve complete decomposition within the treatment time. Also, it is important to note that the β-phases that are revealed from this spectrum are conspicuously absent at the as- received specimen, figure 4-9.

The specimen dehydrogenated at 650°C for 18 hours after the hydrogenation stage revealed a spectrum as shown in figure 4-12. The spectrum indicates the same type of peak distribution revealed for the dehydrogenation treatment at 550°C. However, there is a significant increase in intensity for peaks at positions 38° and 41° respectively under constant acquisition time for all the spectra revealed in this work. There is about 47% increase in intensity for the β peak at position 39.5° relative to figure 4-11. The peaks

revealed are identified as alpha phase except the corresponding peaks for the β-phases. The α and β phases revealed in this spectrum are anticipated considering that the dehydrogenation temperature is high enough within the 18 hours treatment to achieve effective dehydrogenation. This is in accordance with the Ti-6Al-4V-xH alloy phase diagram done by J. I. Qazi et al [41]. In a similar work done by D. H. Kohn et al [49], they reported that dehydrogenation occurred more readily at higher temperatures and at longer treatment times. However, the dehydrogenation temperature and times must be chosen within the constraint of minimizing α – grain growth. Grain growth is minimized if shorter times are used, the opposite requirement of efficient dehydrogenation [49] .

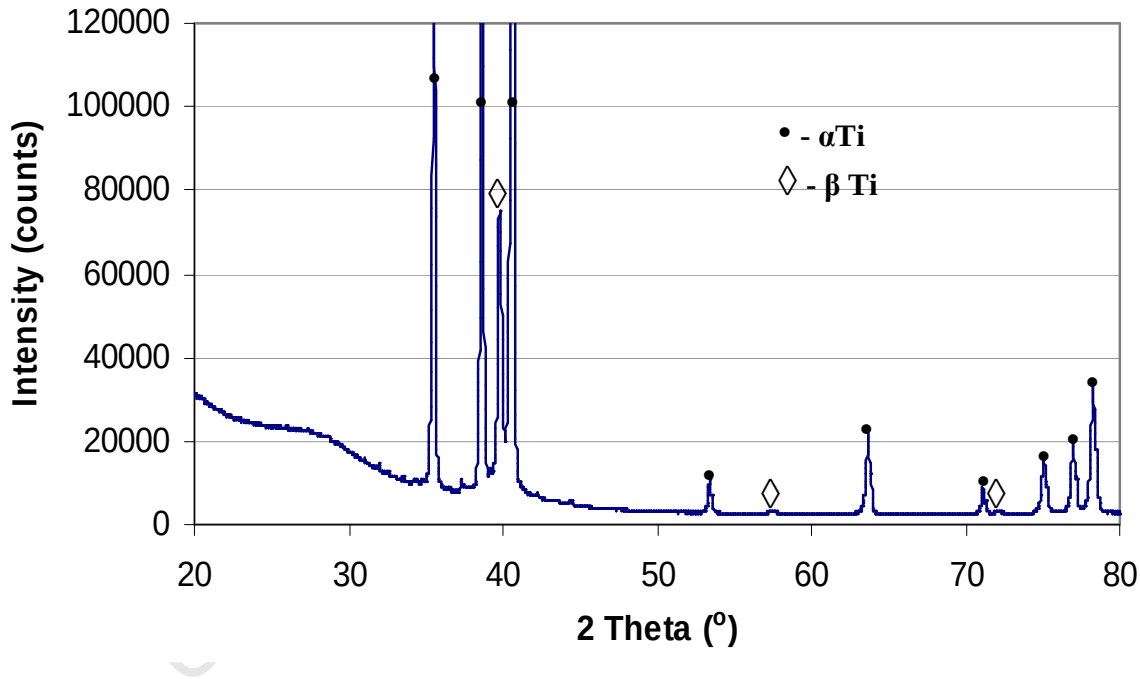

Figure 4-12: X-ray diffraction spectrum of Ti64 hydrogenated at 850°C for 3 hours as in (Step 1) then, dehydrogenated at 650°C for 18 hours and furnace cooled to room temperature

The specimen dehydrogenated at 750°C and furnace cooled to room temperature revealed the spectrum shown in figure 4-13. It displayed similar peak distribution as shown for dehydrogenation at 650°C, figure 4-12. The phases identified were once again anticipated based on the higher temperature and sufficient time used for the dehydrogenation

process. However, further work is needed in order to understand what contributes to the high peaks in all the spectra revealed for the hydrogen treated specimens. Apparently, samples were rotated during x-ray measurements in order to prevent problems of preferred orientation. Additionally, samples that were x-rayed without rotation showed no change in peak heights. Therefore, a possible contribution from preferred orientation was not observed.

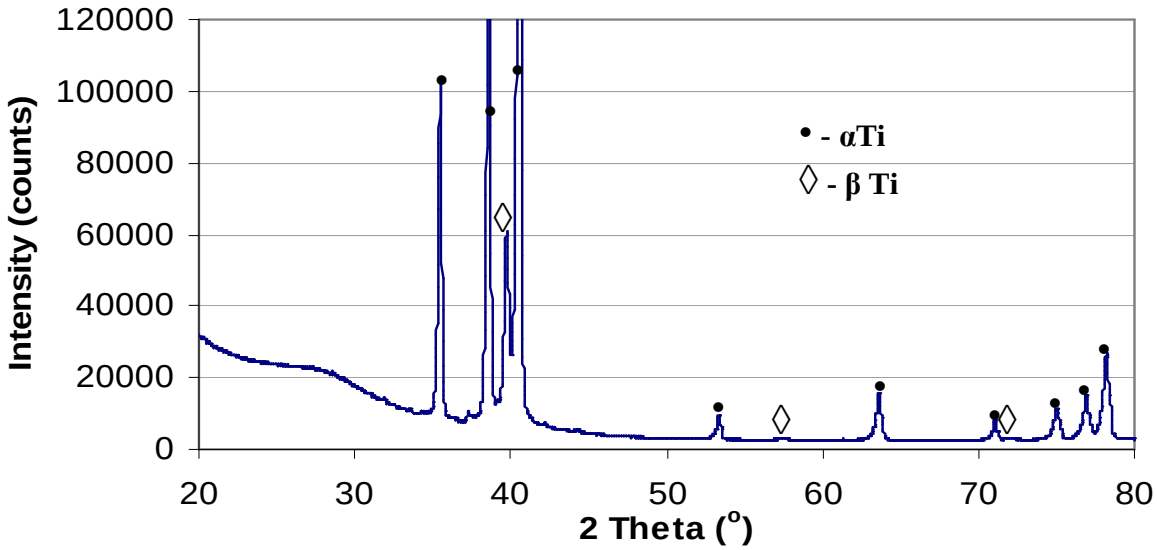

Figure 4-13: X-ray diffraction spectrum of Ti-6-4 hydrogenated for 3 hours as in (step 1) then, dehydrogenated at 750°C for 18 hours and Furnace cooled to room temperature

Figures (4-14, 4-15 and 4-16) show the spectra for control specimens treated as specified by their respective descriptions at each figure. They have common peak distributions and intensities. The spectra revealed corresponding β-phases peaks at positions 39.5°, 57° and 71.5° respectively. The α-phase peak distributions for the control specimens are the same as the dehydrogenated spectra but the control peaks are not as strong in intensity as the dehydrogenated spectra considering that their acquisition time was the same in all cases. The absence of β-phases in the as-received specimen which precipitated significantly at the control specimen suggests that the as-received material was probably not in a full annealed condition. The uniform distributions and intensity of the phases at the control

specimens could probably mean that the specimens have attended their equilibrium states during the heat treatments. Ti-6Al-4V alloy is reported to have about 10% β-phase and 90% α-phase by volume fraction at room temperature under equilibrium conditions.

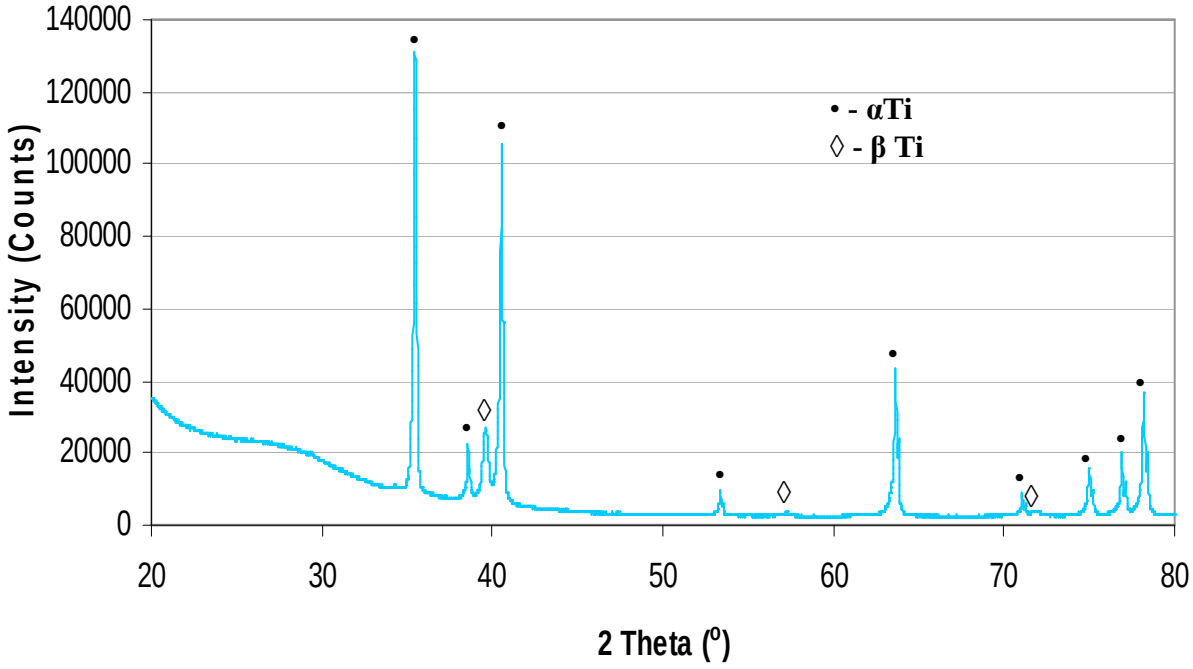

Figure 4-14: X-ray diffraction spectrum of Ti-6-4 treated in Argon at 850°C for 3 hours and furnace cooled to 430°C and air cooled

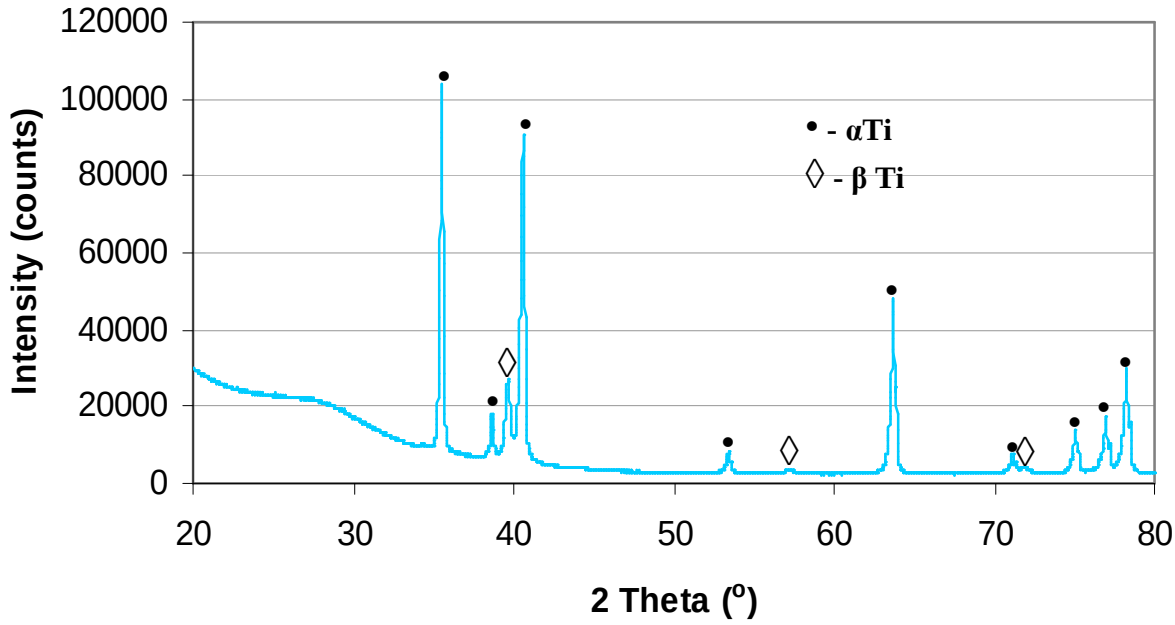

Figure 4-15: X-ray diffraction spectrum of Ti-6-4 treated in Argon at 850°C for 3 hours and furnace cooled to 430°C and air cooled, then, vacuum treated at 650°C for 18 hours and furnace cooled to room temperature

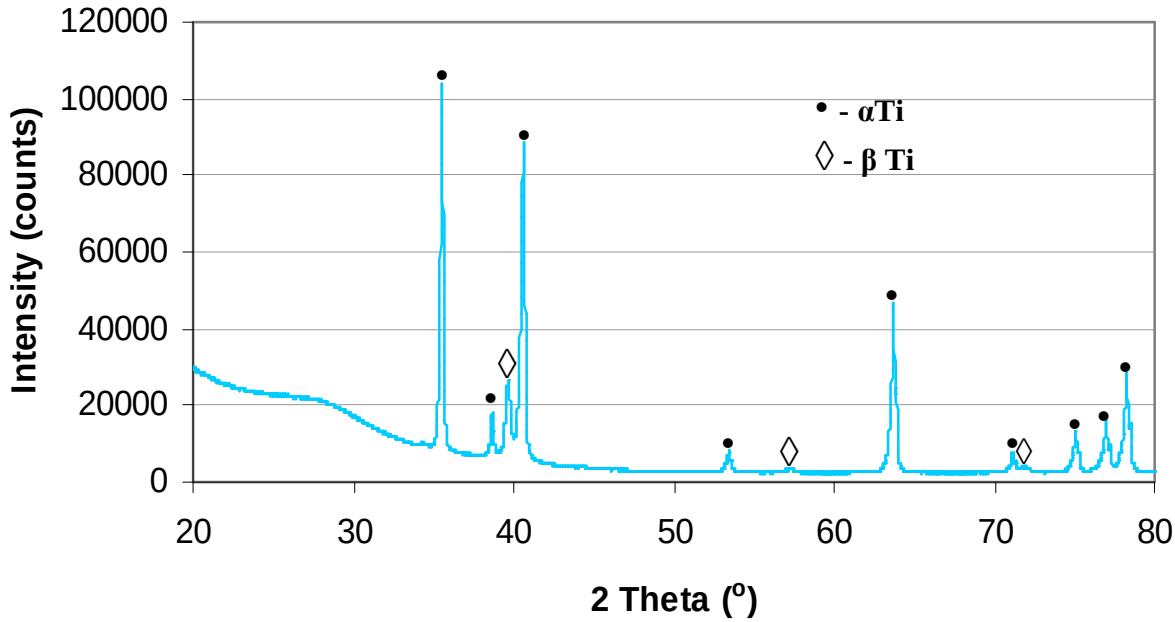

Figure 4-16: X-ray diffraction spectrum of Ti-6-4 treated in Argon at 850°C for 3 hours and furnace cooled to 430°C and air cooled, then, vacuum treated at 750°C for 18 hours and furnace cooled to room temperature

4.6 Microhardness measurements

Microhardness profiles have been done on the bulk section of the as-received Ti-6-4 specimen, the hydrogenated specimen as well as the dehydrogenated specimens. As indicated in the previous chapter seventeen random hardness measurements were made per specimen using a standard Vickers diamond indenter with a load of 500 gf..

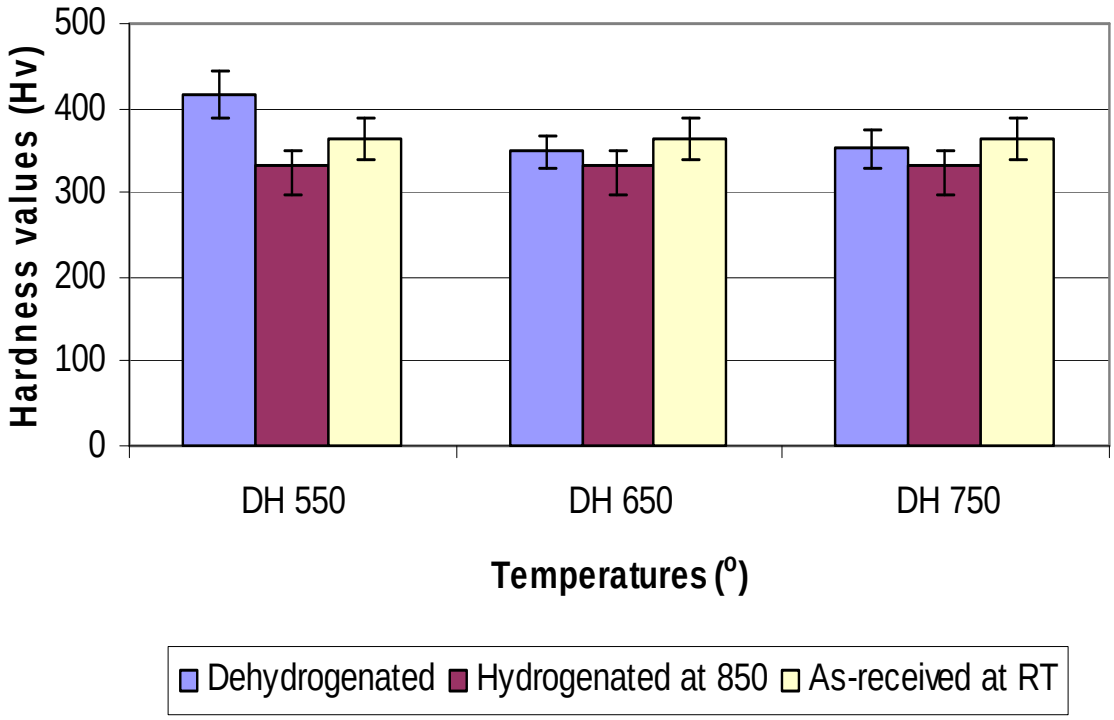

Figure 4-17: Bar chart for the microhardness vs starting temperature for the Ti-6-4 alloy specimens: as-received at room temperature, hydrogenated specimen treated at 850°C for 3 hours and furnace cooled to 430°C and air cooled, dehydrogenated specimens treated at 550°C, 650°C and 750°C for 18 hours respectively and furnace cooled to room temperature

Figure 4-17, shows the comparative hardness measurements for the as-received specimen, hydrogenated specimen and dehydrogenated specimens at the specified temperatures. Inspection at the figure shows an average drop in hardness in the hydrogenated specimen after the hydrogenation treatment relative to the as received condition. This drop in hardness could be due to the two martensite phases α′ and α″ that

were formed after the 3 hour hydrogenation period. The α″-phase is reported to be softer than the primary martensite α′ –phase. The hardness spread at the error bars (plotted with the minimum and maximum values) could be attributed to contributions from the two phases present.

The microhardness measurements on the dehydrogenated specimen at the various treatment temperatures (550^{o}C, 650^{o}C and 750^{o}C for 18 hours) respectively revealed a significant increase in hardness after dehydrogenation at 550^{o}C while specimens dehydrogenated at 650^{o}C and 750^{o}C respectively resulted to equal hardness which is slightly higher than the hydrogenated specimen. The hardness achieved after the dehydrogenation at 550^{o}C is seen to be higher than hardness achieved for the as-received specimen as well as the hydrogenated and dehydrogenated specimens respectively. The higher hardness achieved at 550^{o}C could be due to the higher presence of equiaxed globular alpha precipitates that resulted after the dehydrogenation treatment at 550^{o}C. Alpha grains are reported to have higher hardness than the β grains. The residual martensite phase detected with the x-ray diffraction could also have contributed to the hardness. Besides, the hardening behaviour could also have resulted from the short range ordering, which occurs at high hydrogen concentrations in titanium alloys as was reported in the scientific review paper by F.H. Froes et al [5]

The equal hardness achieved after dehydrogenation at 650^{o}C and 750^{o}C respectively were not significantly high relative to the hydrogenated and the as-received specimen respectively. This could possibly be due the high residual β-phase that precipitated after the respective dehydrogenation treatment. β-phase has minimal hardness relative to the α-phase.

Chapter Five

Conclusions

The following conclusions can be made from the results obtained for this research:

- The apparatus for the hydrogenation and dehydrogenation of Ti-6-4 alloy has been designed and it has been experimentally tested as safe and reliable for use under laboratory conditions.

- The hydrogenation technique carried out in this research produced fine α-grain structures and martensite plates. The investigation with X-ray diffraction analysis on the treated specimens revealed the presence of martensite. This martensite could possibly be hexagonal α′ (alpha prime) phase or orthorhombic α″ (alpha double prime) phase or both.

- The microstructural changes or modifications seen after the three hour hydrogenation cycle which were not evident in the control specimen are attributed to phase transformations brought about by hydrogen alloying in the sample and not the heat treatment cycle.

- Dehydrogenation at 550^{o}C, 650^{o}C and 750^{o}C for 18 hours produced at least partial hydrogen removal considering that no trace of hydrides was detected with the scanning electron microscopy. X-ray diffraction was particularly not very reliable towards identifying possible hydride phase due to problems of peak overlaps in the spectra.

- The measurement of hydrogen concentrations in the specimens was unsuccessful due to additional weight from the oxide layers formed on the specimens after each heat treatment. The vacuum achieved for the experiment was insufficient hence the oxide formation.

- There was a significant β-phase precipitation in the dehydrogenated samples compared to the control samples. Moreover, the β-phase was not detected in the as-received specimen. This implies that hydrogen being a β-phase stabilizing element increased the volume fraction of the β-phase at room temperature after processing.

- Upon dehydrogenation at 750^{o}C and 650^{o}C respectively, Widmanstätten structures with continuous grain boundary allotriormorphs and α-phase colonies are formed while similar treatment at 550^{o}C produced more nucleation and further growth of the grain boundary allotriormorphs and a homogeneous microstructure consisting of globular α-grains in a β matrix.

- Dehydrogenation at 550^{o}C for 18 hours achieves greater hardness compared to similar treatment at 650^{o}C and 750^{o}C respectively. The higher hardness achieved after the dehydrogenation treatment is an indication of enhancement in mechanical strength of Ti-6-4 alloy achieved with the hydrogen treatment.

- Although effective dehydrogenation was achieved at 750^{o}C for 18 hours, dehydrogenation at 550^{o}C and 650^{o}C for 18 hours can be seen as more desirable processing variables due to the fact that a greater volume fraction of equiaxed α-grains were produced after this particular dehydrogenation treatment compare to the structure achieved from the 750^{o}C. Besides, minimal grain growth is possible at the lower temperatures. It is also more cost effective to process at the temperatures of 550^{o}C and 650^{o}C respectively.

Chapter Six

Recommendations

The following recommendations are made in the anticipation that, with further investigations into the new technique of using hydrogen as a temporary alloying element, its potentials of microstructural modifications and mechanical property enhancement will be fully understood and utilized.

- The process of mass changes for the hydrogenated and the dehydrogenated specimens was unreliable due to the additional weight from the oxide layers from the oxide layers formed after each heat treatment. It is suggested that a higher vacuum pump should be used during processing in order to achieve better vacuum thereby preventing the oxidation on the specimen.

- Additional mechanical tests other than hardness could be carried out in order to investigate materials response to properties such as tensile strength, fatigue and fracture toughness.

- The hydrogenation could be processed at varying time periods in order to investigate the influence of hydrogenation time on microstructure.

- To vary hydrogenation temperatures in order to investigate the influence of temperatures to hydrogenation and the microstructure thereof.

- The dehydrogenation at 550^{o}C and 650^{o}C for 18 hours produced more homogeneous α+β grain structures which more mechanical property enhancements are expected compare to the structure obtained from the 750^{o}C. Therefore, it is suggested that lower dehydrogenation temperatures be used.

- Investigation into the phase transformation characteristics, eg. Change in lattice parameters, during hydrogenation and dehydrogenation treatments could be carried out with the dilatometer.

- To perform repeated HG and DH cycles in order to investigate the influence of repeated cycles on microstructure and the resultant mechanical properties.

References

1 R. Ding, Z. X. Guo, and A. Wilson, *Materials Science and Engineering* vol. A327, pp. 233-245, 2002.

2 G.Domizzi, M.I. Luppo, and G. Vigna, "Microstructural features of the hydrogenation process in Ti grade 2," *Journal of Alloys and Compounds*, vol. 424, pp. 193 - 198, 2006.

3 R. R. Boyer, "An overview on the use of titanium in the aerospace industry," *Materials Science and Engineering*, vol. A213, pp. 103-114, 1996.

4 C.Y. Yu, C.C. Shen, and T. P. Perng, "Microstructure of Ti-6Al-4V processed by hydrogenation," *Scripta Materialia*, vol. 55, pp. 1023-1026, 2006.

5 F. H. Sam Froes, O. N. Senkov, and J. I. Qazi, *International Materials Review*, vol. 49, pp. 227, 2004.

6 J. I. Qazi, O. N. Senkov, J. Rahim, A. Genc, and F. H. Froes, *Met. Mat. Trans. A*, vol. 32A, pp. 2453-2463, 2001.

7 O. N. Senkov and J. J. Jonas, *Metal. & Mater. Trans. A*, vol. 27A, pp. 1878-1887, 1996.

8 D.B. Shan, Y.Y. Zong, T.F. Lu, and Y. Lv, "Microstructural evolution and formation mechanism of FCC titanium hydride in Ti-6Al-4V-xH alloys," *Journal of Alloys and Compounds*, vol. 423, pp. 229-234, 2006.

9 K. E. Thiehsen and et al., "The effect of nickel, Chromium, and primary alpha phase on the creep behaviour of Ti-6242Si," *Met. Trans. A*, vol. 24A, pp. 1819-1826, 1993.

10 S. R. Seagle, G. S. Hall, and H. B. Bomberger, *Met. Eng. Q*, pp. 48-54, 1972.

11 P. F. Barbosa and S. T. Button, *Proc Instn Mech Engrs*, vol. 214, pp. 23-32, 2000.

12 J. L. Murray, "The Al-Ti (aluminium-titanium) system. Phase diagrams of binary titanium alloys," *ASM*, pp. 12-24, 1987.

13 D. R. Askerland, "The Science and Engineering of Materials," 3rd S. I. ed: Stanely Thornes Ltd, 1998, pp. 424-430.

14 "Atlas of Microstructures of Industrial Alloys, Metals Handbook," vol. 7, 8th ed, 1972, pp. 321-334.

15 R. Shivpuri, J. Hua, P. Mittal, and A. K. Srivastava, "Industrial,Welding and Systems Engineering ": The Ohio State University, Columbus, USA, 2002, pp. 1-4.

16 W. R. Kerr, R. R. Smith, M. E. Rosenblum, F. J. Gurney, Y. R. Mahajan, and L. R. Bidwell, "'Titanium 80: Science and Technology', (ed. H.Kimura and O.Izumi)," *TMS-AIME,Warrendale, PA* vol. 4, pp. 2477-2486, 1980.

17 A. A. Ilyn, B. A. Kolachev, and A. M. Mamonov, in *Titanium '92: Science and Technology*, vol. 1, F. H. Froes and I. Caplan, Eds.: TMS, Warrendale, PA, 1993, pp. 941-947.

18 M. T. Jovanovic, S. Tadic, S. Zec, Z. Miskovic, and I. Bobic, *Materials and design*, vol. 27, pp. 192-199, 2006.

19 D. R. Askerland, "The Science and Engineering of Materials", S. I. ed: Van Nostrand (International) Co. Ltd, 1988, pp. 338-350.

20 P. A. Dearnerley, *Proc Instn Mech Engrs*, vol. 213, pp. 107-135, 1999.

21 R. R. Boyer and H. W. Rosenberg, "Beta titanium on the SR-71; Historical note 1, Beta Titanium Alloys in the 1980's" *TMS, Warrendale, PA*, pp. 1-8, 1984.

22 A. A. Ilyn and A. M. Mamonov, *Russian Metallurgy*, vol. 5, pp. 52-57, 1994.

23 H. Yoshimura, K. Kimura, M. Hayashi, M. Ishii, T. Hanamura, and J. Takamura, *Mat. Trans. JIM*, vol. 35, pp. 266-272, 1994.

24 O. N. Senkov and I. O. Bashkin, "'Metallurgical Processes for the Year 2000 and Beyond' (ed. H.Y.Sohn) " *TMS, Warrendale, PA*, vol. 1, pp. 271-280, 1994

25 O. N. Senkov, E. V. Konopleva, and E. G. Ponyatovsky, " 'Microstructure/Properties Relationships of Titanium Alloys', (ed. S. Ankem and J.A. Hall)," *TMS*, pp. 207-214, 1994.

26 A. A. Ilyn, I. S. Polkin, A. M. Mamonov, and V. K. Nosov, " " in *Titanium '95:Science and Technology*, vol. 4, P. A. Blenkinsop, W. J. Evans, and H. M. Flower, Eds.: The Institute of Materials, London, UK 1995, pp. 2462-2469.

27 O. N. Senkov, J. J. Jonas, and F. H. Froes, *JOM*, vol. 48, pp. 42-47, 1996.

28 W. R. Kerr, *Metall. Trans. A*, vol. 16A, pp. 1077-1087, 1981.

29 N. E. Paton, B. S. Hickman, and D. H. Leslie, *Metall. Trans. A*, vol. 2, pp. 2791-2796, 1971.

30 A. A. Ilyn, A. M. Mamonov, V. K. Nosov, and V. M. Majstrov, *Russian Metallurgy*, vol. 5, pp. 74-77, 1994.

31 V. E. Arkhipov, S. F. Dubinin, V. E. Naish, T. V. Novoselova, S. B. Pupyshev, N. H. Ratslav, I. V. Sagradze, and S. G. Teploukhov, *Phy. Metals Metallography*, vol. 78, pp. 573-578, 1994.

32 O. N. Senkov, M. Dubois, and J. J. Jonas, *Metal. & Mater. Trans. A*, vol. 27, pp. 3963-3970, 1996.

33 J. H. Li, P. S. Grant, M. L. Jenkins, and B. Cantor, *J. Microscopy*, vol. 185, pp. 132-145, 1997.

34 J. H. Li, P. S. Grant, M. L. Jenkins, and B. Cantor, " 'Control of Interfaces in Metal and Ceramics Composites', (ed. R.Y. Lin and S.G. Flashman)," pp. 357-370, 1993.

35 N. Machida, K. Funami, and M. Kobayashi, *Mat. Sci. Forum*, pp. 539-544, 357-359, 2001.

36 L. I. Anisimova, Y. A. Aksenov, M. G. Badaeva, N. V. Vas'ko, V. L. Kolmogorov, and V. S. Mozhaiskii, *Metal Sci Heat Treatment (Russia) (USA)*, vol. 34, pp. 143-147, 1992.

37 R. J. Wasilewski and G. L. Kehl, "METALLURGIA," *Manchr* vol. 50, pp. 225, 1954.

38 San-Martin and F. D. Manchester, "The H-Ti (Hydrogen- Titanium) System," *Bulletin of Alloy Phase Diagrams* vol. 8, pp. 30-42, 1987.

39 A. D. Mcquillan and M. K. Mcquillan, *Titanium*. London: Butterworths, 1956.

40 I. J. Polmear, *Light Alloys:Metallurgy of the Light Metals*, 3rd edition ed. New York: John Wiley and Sons, 1995.

41 J.I.Qazi, O.N.Senkov, J. Rahim, and F. H. S. Froes, "Kinetics of martensite decomposition in Ti-6Al-4V-xH alloys," *Materials Science and Engineering*, vol. A359, pp. 137-149, 2003.

42 B. Gong, Z. H. Lai, and M. Kobayashi, *Acta Metallurgica Sinica A, (English Edition)*, vol. 28, pp. A431-A434, 1992.

43 C. Zhang, W. Bian, Z. Lai, and B. Gong, *Acta Metallurgica Sinica A, (English Edition)*, vol. 5, pp. 362-368, 1992.

44 O. N. Senkov and F. H. Froes, *Int. J. Hydrogen Energy*, vol. 24, pp. 565-576, 1999.

45 O. N. Senkov and J. J. Jonas, *Metal. & Mater. Trans. A*, vol. 27, pp. 1869-1877, 1996.

46 O. N. Senkov and J. J. Jonas, *Metal. & Mater. Trans. A*, vol. 27, pp. 1303-1312, 1996.

47 I. O. Bashkin, V. Y. Malyshev, and Y. A. Aksenov, *Phys. Metals & Metallography* vol. 69, pp. 158-164, 1990.

48 O. N. Senkov and J. J. Jonas, "Titanium 95: Science and Technology, (ed. P.A. Blenkinsop, W.J. Evans, and H.M. Flower)," *The Institute of Materials, London, UK*, vol. 2, pp. 1026-1033, 1995.

49 D. H. Kohn and P. Ducheyne, "Microstructural refinement of beta-sintered and Ti-6Al-4V porous-coated by temporary alloying with hydrogen," *J. Mat. Sci.*, vol. 26, pp. 534-544, 1991.

50 O. N. Senkov and E. G. Ponyatovsky, "'Strength of Materials (ICSMA 10)' (ed. H. Oikawa, K. Maruyama, S. Takeuchi, and M. Yamaguchi)," *The Japan Institute of Metals, Japan*, pp. 639-642, 1994.

51 O. N. Senkov, J. J. Jonas, and F. H. Froes, *Philosophical Magazine A*, vol. 80, pp. 2813-2825, 2000.

52 Y. A. Aksyonov, I. O. Bashkin, and V. L. Kolmogorov, *Phys. Metals & Metallography* vol. 67, pp. 157-163, 1989.

53 A. D. Mcquillan, *Royal Society of London,Series A* vol. 204, pp. 309-322, 1951.

54 B. A. Kolachev, Y. B. Egorova, and V. D. Talalaev, in *Advances in the Science and Technology of Titanium Alloy Processing*, I. Weiss, R. Srinivasan, P. J. Bania, D. Eylon, and S. L. Semiatin, Eds. Warrendale, PA: TMS 1997, pp. 339-346.

55 M. Niinomi, B. Gong, T. Kobayashi, T. Ohyabu, and O. Toriyama, *Metall. Mater. Trans. A*, pp. 1141-1151, 1995.

56 H. Yoshimura, M. Hayashi, and K. Kimura, "Nippon Steel Tech. Report," vol. 62, pp. 80-84, 1994.

57 S. Abkowitz, G. J. Kardys, S. Fujishiro, F. H. Froes, and D. Eylon, "Titanium Net Shape Technologies," in *The Metallurgical Society of AIME*, 1984, pp. 107-120.

58 F. H. Froes, in *1991 P/M in Aerospace and Defence Technology*. Princeton, NJ: MPIF 1991, pp. 5-33.

59 B. Gong, Z. H. Lai, and M. Kobayashi, *Acta Metallurgica Sinica A*, vol. 28, pp. A431-A434, 1992.

60 D. Zhongquan, W. Gaochao, C. Yuxin, W. Chunlie, and Z. Zhifang, in *Titanium'92 Science and Technology*, vol. I, F. H. S. Froes and I. Caplan, Eds.: TMS,Warrendale, PA 1993, pp. 871-877.

61 O. N. Senkov, "'Strength of Materials (ICSMA 10)', (ed. H. Oikawa, K. Maruyama, S. Takeuchi, and M. Yamaguchi)," *The Japan Institute of Metals, Japan*, pp. 635-638, 1994.

62 L. S. Apgar and D. Eylon, presented at 1990 Advances in Powder Metallurgy, Princeton, NJ, 1990.
63 D. H. Kohn and P. Ducheyne, "Tensile and fatigue strength of hydrogen-treated Ti-6Al-4V alloy," *J. Mat. Sci.*, vol. 26, pp. 328-334, 1991.
64 S. Abkowitz and D. Rowell, *J. Metals*, vol. 38, pp. 36-39, 1986.
65 W. H. Kao and L. M. Orsborn, "Powder Metallurgy of Titanium Alloys, (ed. F.H. Froes and J.E. Smugeresky)," *TMS-AIME*, pp. 163 1980.
66 F. H. Froes, D. Eylon, and C. Suryanarayana, *JOM*, vol. 42, pp. 26-29, 1990.
67 K. Ameyama, Y. Kaneko, H. Iwasaki, and M. Tokizane, in *1989 Advances in Powder Metallurgy*vol. 3. Princeton, NJ: MPIF 1989, pp. 121-126.
68 S. Abkowitz and D. Rowell, "Progress in Powder Metallurgy," vol. 42, pp. 611-624, 1986.
69 W. H. Kao, D. Eylon, C. F. Yolton, and F. H. Froes, "Progress in Powder Metallurgy," vol. 37, pp. 289-301, 1982.
70 K. Yong, Z. X. Guo, and D. V. Edmonds, *Scripta Metall. Mater.*, vol. 27, pp. 1695-1700, 1992.
71 K. Yang, Z. X. Guo, and D. V. Edmonds, *Scripta. Metall. Mater.*, vol. 27, pp. 1021-1026, 1992.
72 Z. X. Guo, J. H. Li, K. Yang, and B. Derby, "Composites," vol. 25, pp. 881-886, 1994.
73 Liangshun Luo, Yanqing Su, Jingjie Guo, and H. Fu, "Formation of titanium hydride in Ti-6Al-4V alloy," *Journal of Alloys and Compounds*, vol. 425, pp. 140-144, 2006.
74 T.Ahmed and H.J.Rack, "Phase transformation during cooling in α +β titanium alloys," *Materials Science and Engineering A*, vol. 243, pp. 206-211, 1999.
75 D.Eliezer, E.Tal-Gutelmacher, C.E.Cross, and T. Boellinghaus, "Hydrogen absorption and desorption in the duplex-annealed Ti-6Al-4V alloy during exposure to different hydrogen-containing environments," *Materials Science and Engineering* vol. A 433, pp. 298-304, 2006.
76 E.Tal-Gutelmacher and D. Eliezer, "High fugacity hydrogen effects at room temperature in titanium based alloys," *Journal of Alloys and Compounds*, vol. 404-406, pp. 613-616, 2005.

Appendix A

Component design of Experimental Apparatus

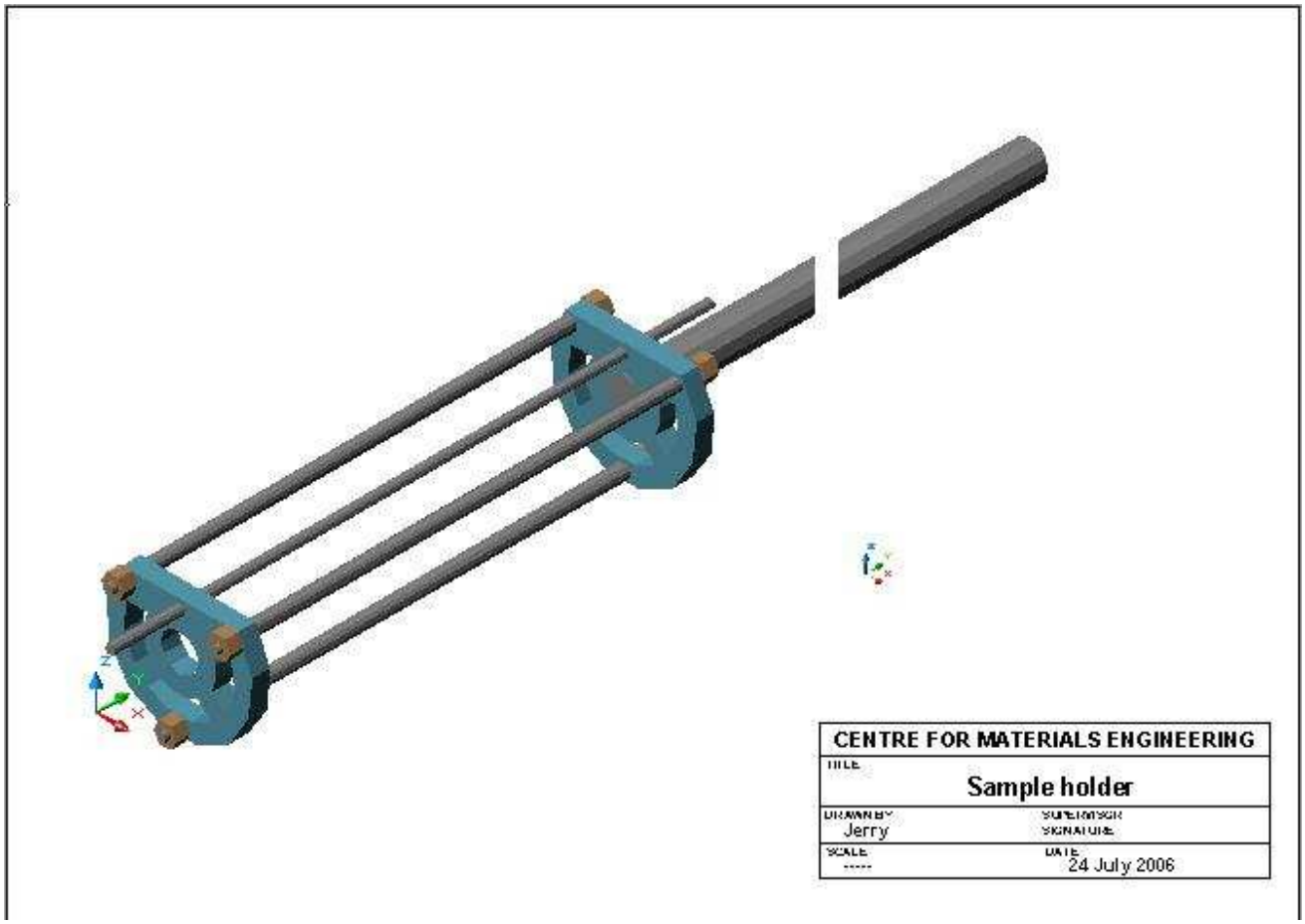

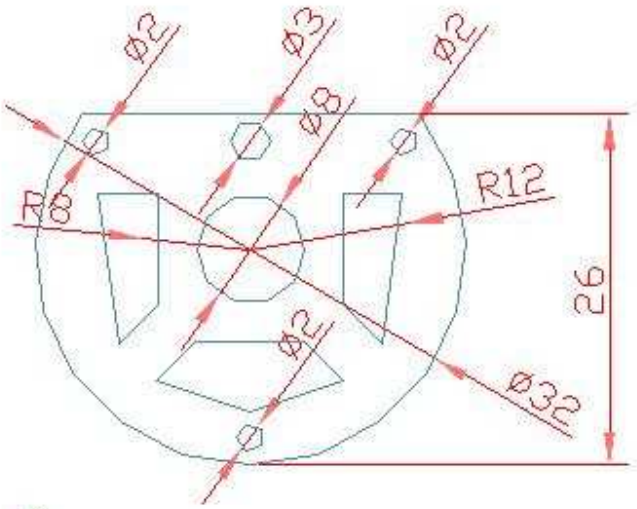

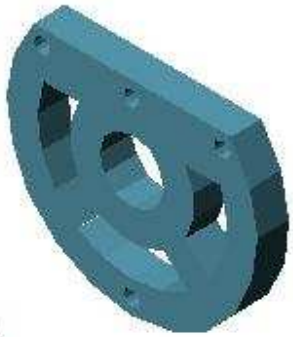

NOTES:
2 x cradles to be made
Cradle to be made from AISI 316 s/steel, 4mm thick plate
3mm dia. hole to be threaded for standard 3mm s/steel ready bar
1x cradle to have 8mm dia. central hole threaded for 8mm s/steel tube connection
Ventilation hole sizes not critical

CENTRE FOR MATERIALS ENGINEERING	
TITLE: 2 x Cradles	
DRAWN BY: Jerry	SUPERVISOR SIGNATURE:
SCALE: -----	DATE: 24 July 2006

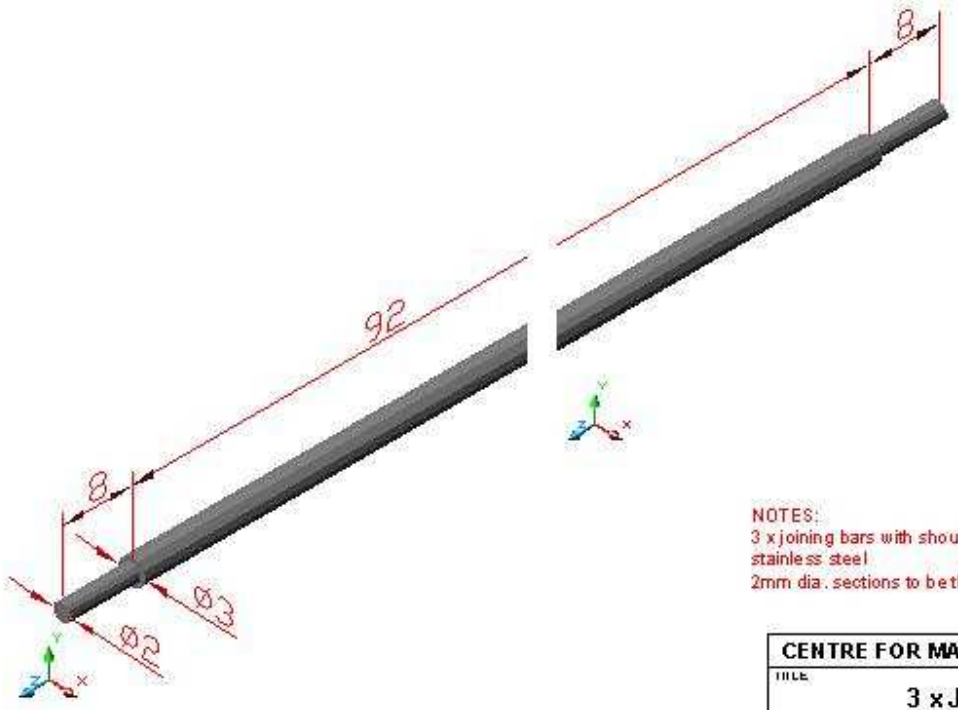

NOTES:
3 x joining bars with shoulders to be made from stainless steel
2mm dia. sections to be threaded for nuts

CENTRE FOR MATERIALS ENGINEERING	
TITLE: 3 x Joining rods	
DRAWN BY: Jerry	SUPERVISOR SIGNATURE:
SCALE: -----	DATE: 24 July 2006

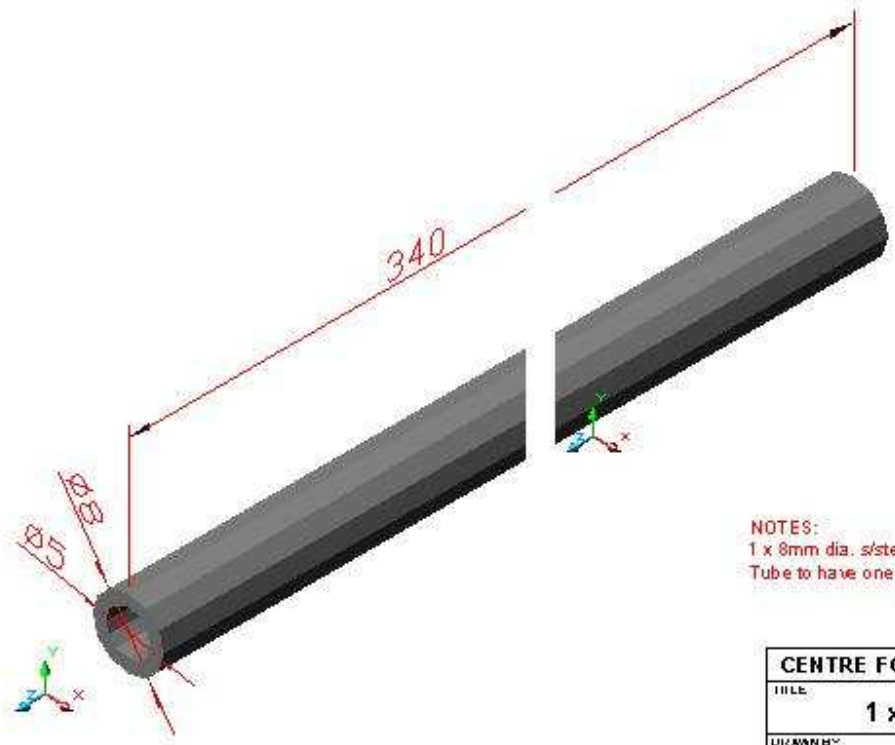

NOTES:
1 x 8mm dia. s/steel tube handle
Tube to have one end threaded to fit cradle

CENTRE FOR MATERIALS ENGINEERING	
TITLE: 1 x S/Steel tube handle	
DRAWN BY: Jerry	SUPERVISOR SIGNATURE:
SCALE: -----	DATE: 24 July 2006

Appendix B

Preliminary Tests and Operating Procedure

Because of the danger associated with the use of hydrogen, an operational performance assessment was done on the test rig for it to be certified safe for use. The following steps and procedures were followed in conducting experiments in the test rig.

a. Preliminary Safety Checks

- Ensure that all the Gas Cylinder knobs on the cylinders are closed;
- Ensure that the Gas Regulator knobs are closed;
- Ensure that the correct Cylinder is used and not misplaced in position;
- Ensure that there are no leaks from any of the Cylinders and hose ends to the Gas Cylinders and vacuum furnace;
- Ensure procedure check for tightness;
- Ensure that there are no vacuum leaks on the furnace assembly;
- Ensure that the power switches are initially off;
- Ensure that the extractor fan in the fume cupboard is on throughout the experiment. This helps in addition to the main extractor to evacuate any gas leak during the experiment.

b. Placement of Samples into the Furnace

- In order to open the sample inlet, ensure that the pressure gauge at the furnace is at atmospheric (0kPa) otherwise introduce argon from its bottle to achieve 0kPa;
- Open the argon gas cylinder knob and set pressure with the gas regulator at 100kPa;
- Open the gas inlet valve slightly and watch the pressure gauge on the furnace until it reaches just below 10kPa;
- Turn off the argon flow from the bottle and close the gas inlet on the furnace;
- Open the sample inlet carefully and insert your sample;
- Close the sample inlet carefully afterwards.

c. Obtaining Furnace Vacuum and Initiating Furnace Heat up

- Keeping the cylinder knobs and gas regulators closed, open the gas inlet valve on the furnace, open the Speedivalve, switch on the Peroni gauge and then switch on the pump;
- Close the gas inlet valve after about 2 to 3 minutes of pumping down;
- Set furnace to heat up to $500^{o}C$;
- Leave the pump on until pressure is below 10^{-1} Torr;
- Then, close the Speedivalve, switch off the PIRANI gauge and finally, switch off the pump.

d. <u>Introduction of 5% Hydrogen & Argon mix (Reaction Gas)</u>

- Ensure that the reaction gas cylinder is connected;
- When furnace temperature reaches 500^{o}C, open the reaction gas knob and set the pressure with the regulator to 100kPa;
- Set your desired flow rate on the flow meter;
- Open the gas inlet valve on the furnace and maintain pressure in the furnace system to not more than 20kPa;
- Set furnace set point to 950^{o}C;
- When 950^{o}C is reached, furnace must remain isothermally at this temperature for a duration of 3hours;
- After the isothermal treatment, the furnace is switched off to cool down with the sample up to 500^{o}C (furnace temperature) with the reaction gas still flowing. This was to attend a complete cycle from the point of hydrogen introduction;
- Switch off the reaction gas flow at the gas cylinder knob and the flow meter;
- Switch on the pump and open the Speedivalve to quickly pump down the reaction gas in the vacuum system, and open the gas hose;
- Put off the pump after about 2 minutes and close the Speedivalve and the gas inlet valve;
- Remove gas hose from the reaction gas cylinder and connect the gas hose to the argon cylinder;
- Open the argon gas cylinder knob and set pressure with the Gas regulator at 100kPa;
- Open the gas inlet valve slightly and watch the pressure gauge on the furnace to reach just less than 10kPa;
- Put off the argon flow;
- Remove sample carefully from the furnace at 500^{o}C (furnace temperature) and allow it to cool in air.

Appendix C

X-ray diffraction measurements as measured from the published scientific papers (references attached)

Table C- 1

XRD PATTERN OF UNCHARGED & GAS-PHASE CHARGED (500^{o}C, 5atm, 10h) Ti-6Al-4V SPECIMENS BETWEEN AND AFTER TDS (at 5^{o}C/Min, up to 700^{o}C) [75]			
2 THETA (2Θ)	α Ti	β Ti	δ TiH_2
35.5^{o} (uncharged)	*		
35.5^{o} (charged 10hrs)			*
38.5^{o} (uncharged)	*		
40^{o} (uncharged)		*	
42^{o}(charged 10hrs)			*
42^{o} (uncharged)	*		
53.5^{o} (uncharged)	*		
58^{o} (uncharged)		*	
58.5^{o} (charged)			*
64^{o} (uncharged)	*		
70.5^{o} (charged)			*
71.5^{o} (uncharged)	*		
72.5^{o} (uncharged)		*	
75.5^{o} (uncharged)		*	
77^{o} (uncharged)	*		

Table C- 2

XRD PATTERNS OF Ti-6Al-4V: as β-solution treated; hydrogenated at 600°C; and hydrogenated/dehydrogenated for five cycles [4]					
2 THETA (2Θ)	α Ti	β Ti	β_H	δ	α_2
26° (HG/DH x5)					*
36°					*
38°			*		
40° (as-β-soln.)		*			
41° (as-β-soln.)	*				
42°				*	
53.5° (as-β-soln.)	*				
56°			*		
57.5° (as-β-soln.)		*			
60°				*	
63.5° (as-β-soln.)	*				
64°					*
71°	*				

Table C- 3

XRD PATTERNS OF UNCHARGED AND ELECTROCHEMICALLY HYDROGENATED Ti-6Al-4V ALLOY, AFTER 12 & 48hrs OF CHARGING AT 50mA/ CM^2 [75]					
2 THETA (2Θ)	α Ti				
35.5°(0hrs)	*				
36°(12hrs)				*	
38°(12hrs)					*
38.5°(0hrs)	*				
40°(12hrs)		*			
40.5°(0hrs)	*				
42.5°(12hrs)			*		
53.5°(0hr, 12hrs)	*				
58°(0hr)		*			
61°(0hr, 12hrs)				*	
64°(0hrs, 12hrs)	*				
71°(0hr, 12hrs)	*				
72.5°(0hr)		*			
75° – 80°	*				

Table C- 4

XRD PATTERNS OF Ti-6Al-4V ALLOY WITH DIFFERENT HYDROGEN CONTENT: (a) AS-RECEIVED, (b)0.106 wt.-%, (c) 0.302 wt.-%, AND (d) 0.490 wt.-% [[73]]				
2 THETA (^{o})	PHASES PRESENT			
	α Ti	β Ti	α″	δ
35.5 (a) (b)	*			
35.5 (c)	*		*	
35.5 (d)	*		*	*
38.5 (a)	*			
38.5 (b)	*	*		
38.5 (c)	*	*		
38.5 (d)	*	*		*
39.5 (a)		*		
40.5 (a - d)	*			
53.5 (a) (b)	*			
53.5 (c)	*		*	
53.5 (d)	*	*	*	
56 (b) (c)		*		
56.5 (a)		*		
64 (a – d)	*			
65 (c) (d)			*	
69 (d)				*
71.5 (a – d)	*			
75 (a) (b)	*			
77 (a – d)	*			
78.5 (a – d)	*			

Table C- 5

XRD PATTERNS OF UNCHARGED AND ELECTROCHEMICALLY HYDROGENATED AT ROOM TEMPERATURE (a) FULLY LAMELLAR Ti- 6Al-4V [[76]]					
2 THETA (^{o})	PHASES PRESENT				
	α Ti	β Ti	γ TiH	δ TiH_2	TiO
35.5 (48hrs)	*				
36 (48hrs)			*		
38 (hrs)					*
39 (12 & 48hrs)	*				
40(0,12,48hrs)	*				
42(48hrs)			*		
53.5(0,12,48hrs)	*				
57.5(0,12hrs)		*			
71.5(0,12,48hrs)	*				
77 (48hrs)	*				
84 (48hrs)					*

Table C- 6

XRD PATTERNS OF UNCHARGED AND ELECTROCHEMICALLY HYDROGENATED AT ROOM TEMPERATURE: DUPLEX Ti-6Al-4V SPECIMENS [[76]]					
2 THETA (^{o})	PHASES PRESENT				
	α Ti	β Ti	γ TiH	δ TiH_2	TiO
35.5(0,12,48hrs)				*	
36(12hrs,48hrs)			*		
37.5(0,12,48hrs)					*
38.5(0,12,48hrs)	*				
40(0,12,48hrs)		*			
40.5(0,12,48hrs)	*				
42(12,48hrs)			*		
43.5(48hrs)				*	
53.5(0,12,48hrs)	*				
57.5(0,12,48hrs)		*			
61.5(0,12,48hrs)				*	
63.5(0,12,48hrs)	*				
71(0,12,48hrs)	*				
72.5(0,12,48hrs)		*			
75 (0,12,48hrs)	*				
77 (0,12,48hrs)	*				
78.5(0,12,48hrs)	*				

Table C- 7

XRD PATTERNS OF THE Ti-6Al-4V ALLOY: (a) BEFORE HYDROGENATION; (b) HG 0.2 wt.-%; (c) HG 0.3 wt. -%; (d) HG 0.5 wt.-% [8]				
2 THETA (°)	PHASES PRESENT			
	α	β	α′	δ
35.5 (a)	*			
35.5 (b)	*			*
35.5 (c) (d)	*		*	*
38 (c)				*
38 (d)	*			*
38.5 (a) (b)	*			
38.5 (c)	*		*	
38.5 (d)			*	
40 (a – d)		*		
40.5 (a)	*			
40.5 (b)	*			*
40.5 (c) (d)	*		*	*
44.5 (a – d)		*		
53.5 (a) (b)	*			
53.5 (c) (d)	*		*	
55 (d)				*
63 (d)	*		*	
63.5 (a) (b)	*			
63.5 (c)	*		*	
65 (a – d)		*		
69 (b – d)				*
71 (a) (b)	*			
71(c) (d)	*		*	
77 (a) (b)	*			
77 (c)	*	*		
77 (d)	*			
78 (a) (b)	*			
78 (c) (d)	*			

Table C- 8

XRD PATTERNS OF SAMPLES CONTAINING: 0at. -%H, 10 at.-%H, 20 at.-%H, 30 at.-%H ANNEALED AT 1050^{o}C, 890^{o}C, 855^{o}C, 850^{o}C FOR 1 HOUR AND WATER QUENCHED [[41]]								
	0at.-%H at 1050^{o}C		10at.-%H at 890^{o}C		20at.-%H at 855^{o}C		30at.-%H at 850^{o}C	
2 THETA (^{o})	α′	α″	α′	α″	α′	α″	α′	α″
35.1	*		*				*	*
36				*				
38.5	*		*	*	*	*		*
39							*	
40.5					*		*	*
41	*		*	*		*		
53	*		*				*	*
55				*				
64			*	*				
64.5							*	
65								*
69								*
71	*							
72			*				*	
77	*							
78	*							*
78.5						*		

Appendix D

X-ray diffraction peaks as measured on the Ti-6-4 specimen (Full peak heights)

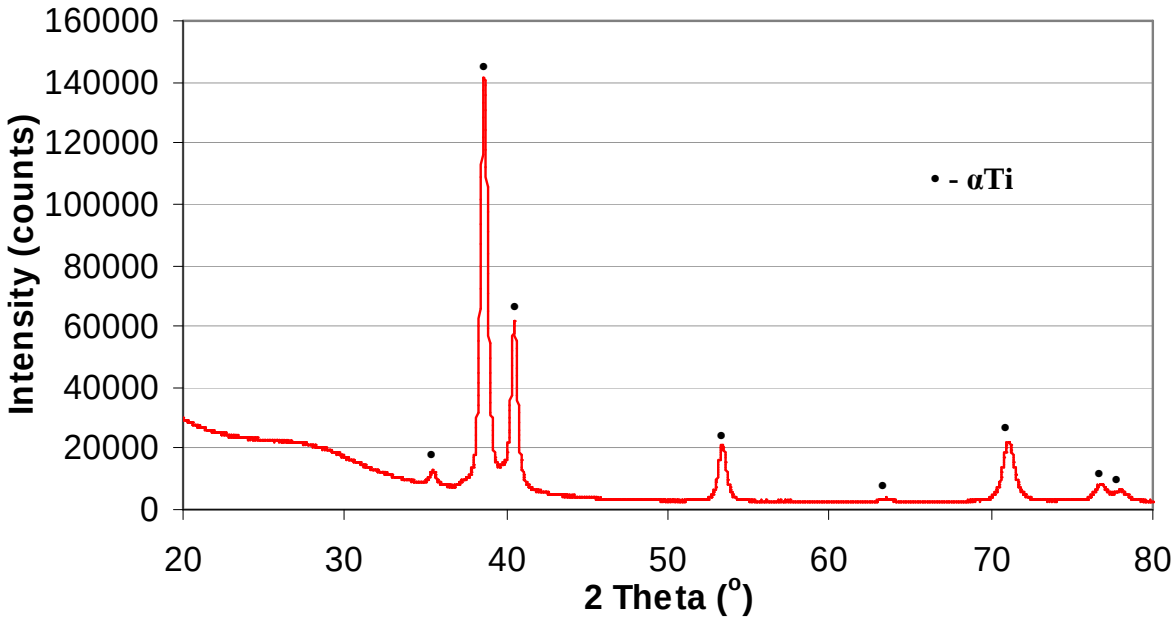

Figure D-1: X-ray diffraction spectrum of Cold rolled annealed Ti64 (As-Received)

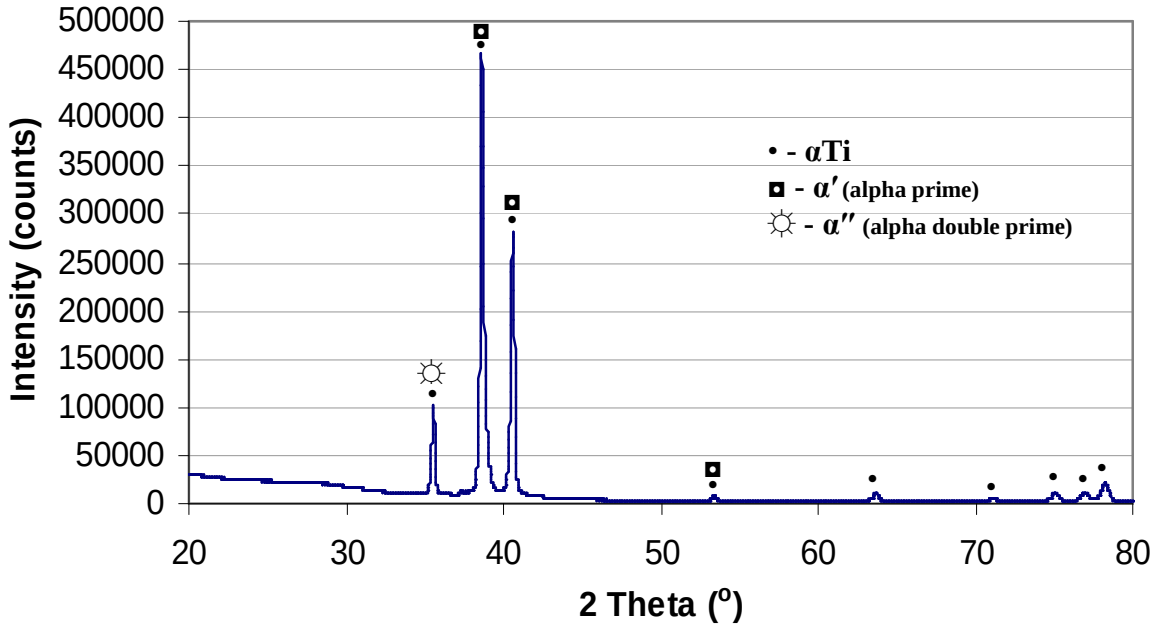

Figure D- 2: X-ray diffraction spectrum of Ti64 hydrogenated at 850°C for 3 hours and furnace cooled to 430°C and air cooled: (Step 1)

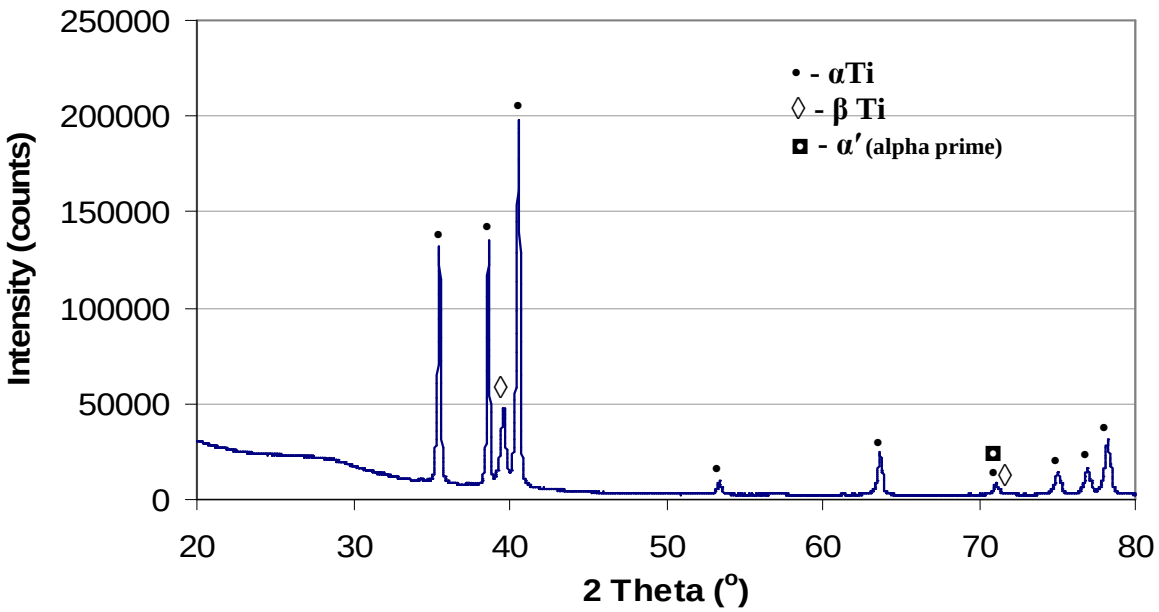

Figure D- 3: X-ray diffraction spectrum of Ti64 hydrogenated at 850°C for 3 hours as in (step 1) then, dehydrogenated at 550°C for 18 hours and furnace cooled to room temperature

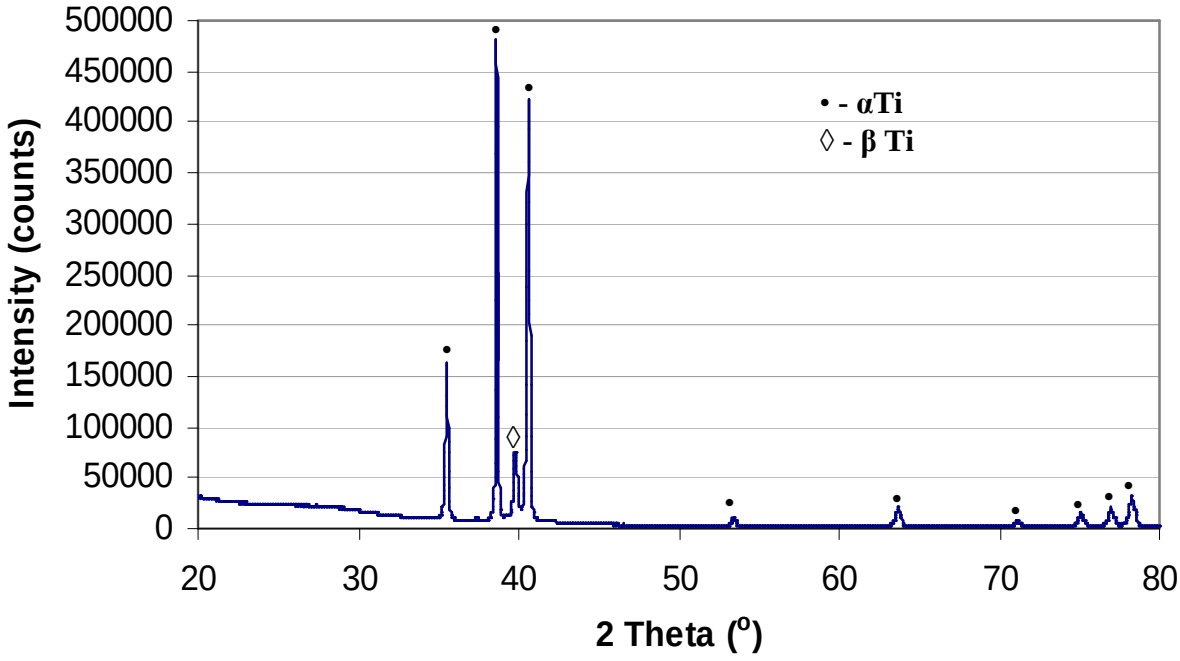

Figure D- 4: X-ray diffraction spectrum of Ti64 hydrogenated at 850°C for 3 hours as in (step 1) then, dehydrogenated at 650°C for 18 hours and furnace cooled to room temperature

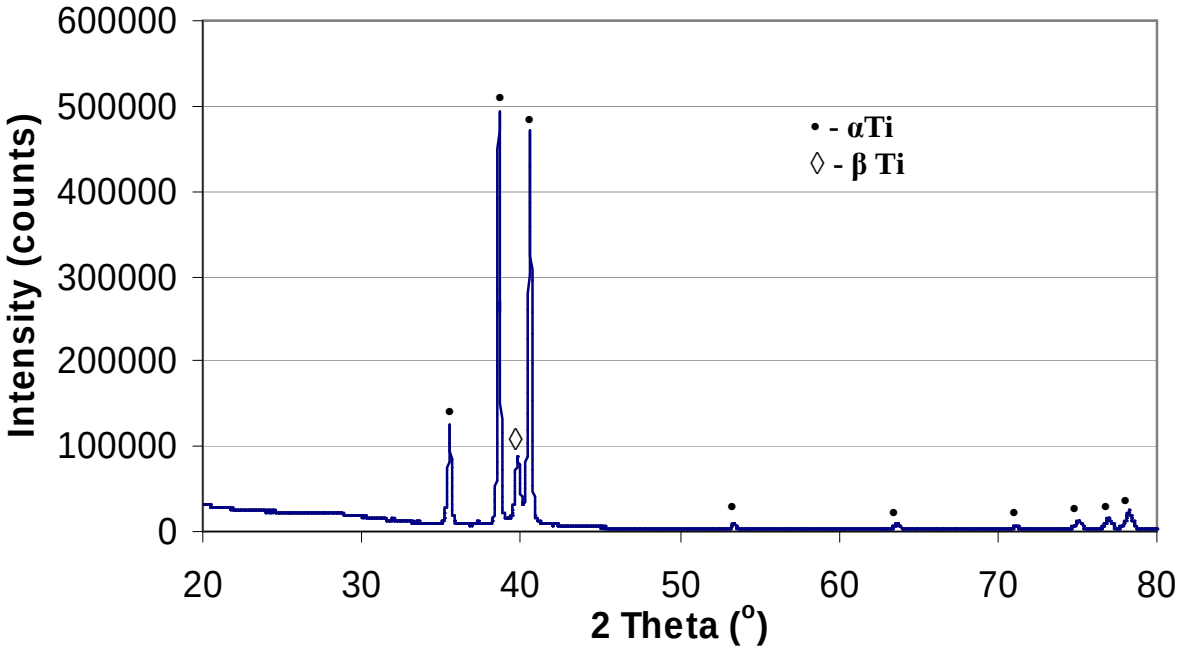

Figure D- 5: X-ray diffraction spectrum of Ti64 hydrogenated for 3 hours as in (step 1) then, dehydrogenated at 750°C for 18 hours and furnace cooled to room temperature

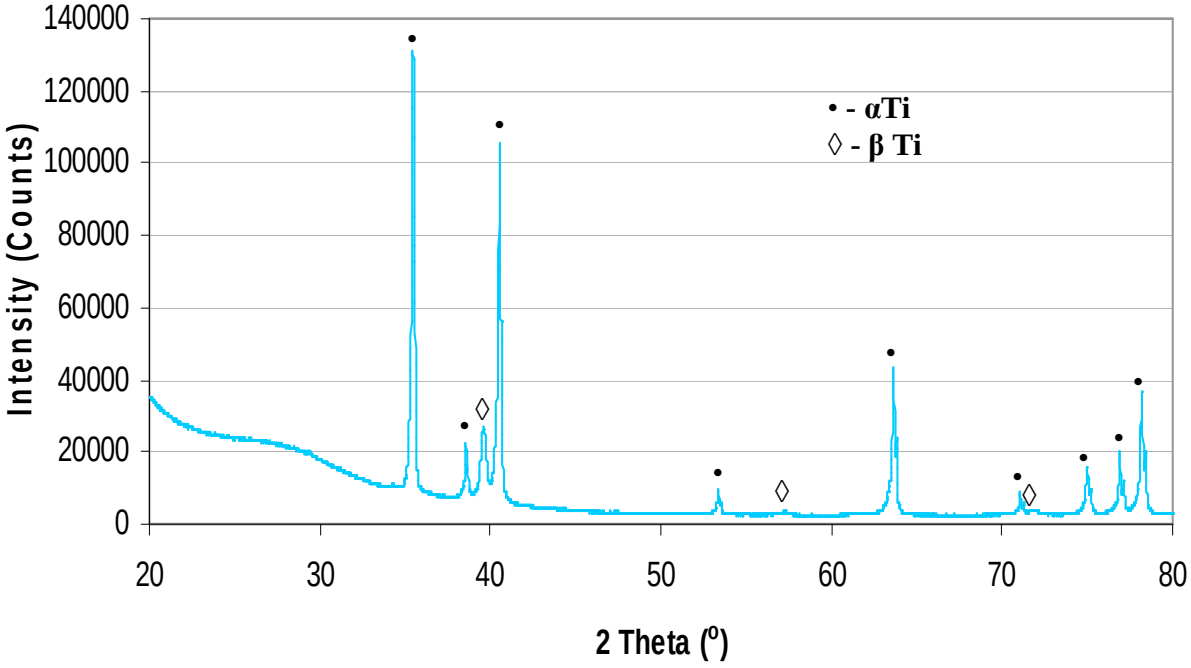

Figure D- 6: X-ray diffraction spectrum of Ti64 treated in Argon at 850°C for 3 hours and furnace cooled to 430°C and air cooled

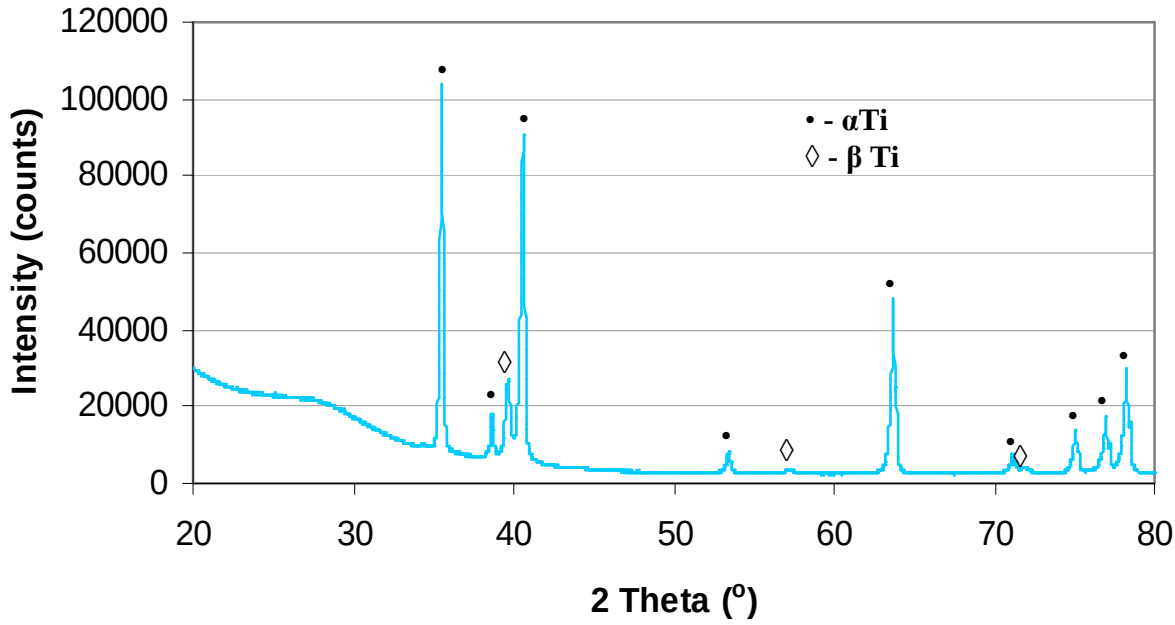

Figure D- 7: X-ray diffraction spectrum of Ti64 treated in Argon at 850°C for 3 hours and furnace cooled to 430°C and air cooled, then, vacuum treated at 650°C for 18 hours and furnace cooled to room temperature

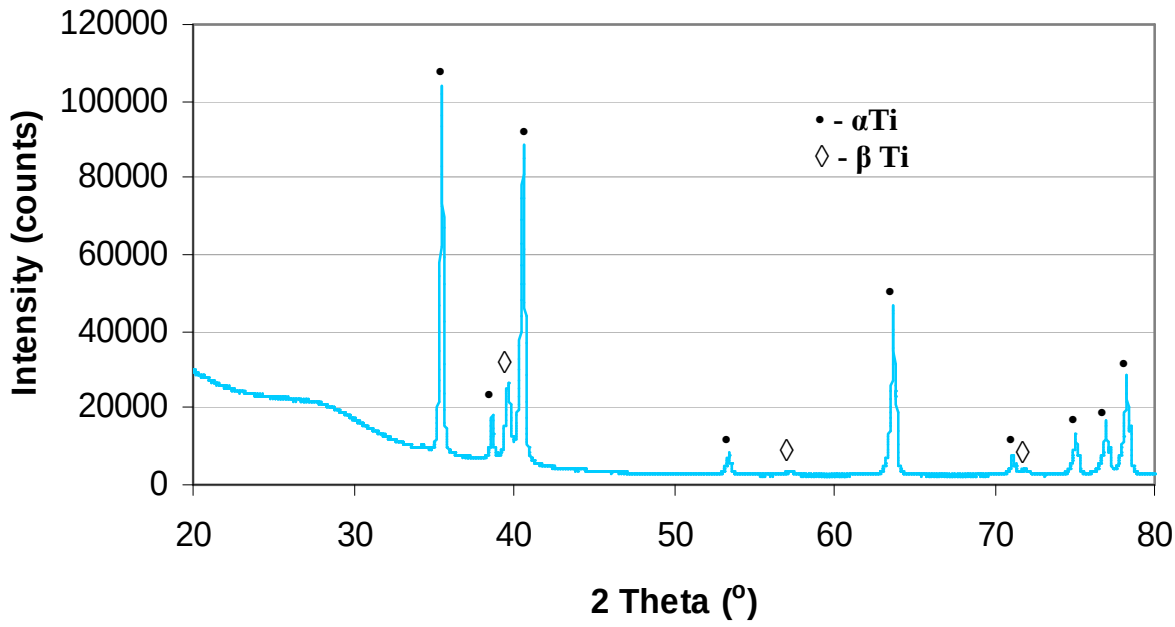

Figure D-8: X-ray diffraction spectrum of Ti64 treated in Argon at 850°C for 3 hours and furnace cooled to 430°C and air cooled, then, vacuum treated at 750°C for 18 hours and furnace cooled to room temperature

Appendix E

Calculated Hydrogen concentration in Ti-6-4 cylinders following hydrogenation and dehydrogenation treatments

Experiment Sample A				
	Mass As-received (M_{ar})	Mass After HG at 850°C for 3hrs (M_{hg})	Mass Loss/Gain (M_{hg} - M_{ar})	Weight % Loss/Gain: [(M_{hg} - M_{ar})/ (M_{ar})] x 100%
X_1	1.68416	1.69783	0.01367	0.811681
X_2	1.6842	1.69788	0.01368	0.812255
X_3	1.68418	1.69788	0.0137	0.813452
X_4	1.68417	1.69785	0.01368	0.81227
Mean	1.6841775	1.69786	0.013683	0.812414
Std. Dev.	1.70783E-05	2.45E-05	1.26E-05	0.000744

Experiment Sample A				
	Mass After HG at 850°C for 3hrs (M_{hg}	Mass After DH at 750°C for 18hrs (M_{dh}))	Mass Loss/Gain (M_{dh} – M_{hg})	Weight % Loss/Gain: [(M_{dh} – M_{hg})/ (M_{hg})] x 100%
X_1	1.69783	1.69196	-0.00587	-0.34574
X_2	1.69788	1.69196	-0.00592	-0.34867
X_3	1.69788	1.69192	-0.00596	-0.35103
X_4	1.69785	1.69194	-0.00591	-0.34809
Mean	1.69786	1.691945	-0.00592	-0.34838
Std. Dev.	2.45E-05	1.91E-05	3.7E-05	0.002173

Experiment Sample B				
	Mass As-received (M_{ar})	Mass After HG at 850°C for 3hrs (M_{hg})	Mass Loss/Gain (M_{hg} - M_{ar})	Weight % Loss/Gain: [(M_{hg} - M_{ar})/ (M_{ar})] x 100%
X_1	1.68354	1.69261	0.00907	0.538746
X_2	1.68351	1.69258	0.00907	0.538755
X_3	1.68356	1.69259	0.00903	0.536363
X_4	1.68352	1.69258	0.00906	0.538158
Mean	1.6835325	1.69259	0.009058	0.538006
Std. Dev.	2.21736E-05	1.41E-05	1.89E-05	0.00113

Experiment Sample B				
	Mass After HG at 850°C for 3hrs (M_{hg})	Mass After DH at 750°C for 18hrs (M_{dh}))	Mass Loss/Gain (M_{dh} – M_{hg})	Weight % Loss/Gain: [(M_{dh} – M_{hg})/ (M_{hg})] x 100%
X_1	1.69261	1.69101	-0.0016	-0.09453
X_2	1.69258	1.691	-0.00158	-0.09335
X_3	1.69259	1.69099	-0.0016	-0.09453
X_4	1.69258	1.69095	-0.00163	-0.0963
Mean	1.69259	1.690988	-0.0016	-0.09468
Std. Dev.	1.41E-05	2.63E-05	2.06E-05	0.001218

Experiment Sample C				
	Mass As-received (M_{ar})	Mass After HG at 850°C for 3hrs (M_{hg})	Mass Loss/Gain (M_{hg} - M_{ar})	Weight % Loss/Gain: [(M_{hg} - M_{ar})/ (M_{ar})] x 100%
X_1	1.68221	1.69387	0.01166	0.693136
X_2	1.68218	1.69389	0.01171	0.696121
X_3	1.6822	1.69392	0.01172	0.696707
X_4	1.6822	1.69389	0.01169	0.694923
Mean	1.6821975	1.693893	0.011695	0.695222
Std. Dev.	1.25831E-05	2.06E-05	2.65E-05	0.001576

Experiment Sample C				
	Mass After HG at 850°C for 3hrs (M_{hg})	Mass After DH at 750°C for 18hrs (M_{dh}))	Mass Loss/Gain ($M_{dh} - M_{hg}$)	Weight % Loss/Gain: [($M_{dh} - M_{hg}$)/ (M_{hg})] x 100%
X_1	1.69387	1.69208	-0.00179	-0.10568
X_2	1.69389	1.69209	-0.0018	-0.10626
X_3	1.69392	1.69206	-0.00186	-0.1098
X_4	1.69389	1.69209	-0.0018	-0.10626
Mean	1.693893	1.69208	-0.00181	-0.107
Std. Dev.	2.06E-05	1.41E-05	3.2E-05	0.001889

Experiment Sample D				
	Mass As-received (M_{ar})	Mass After HG at 850°C for 3hrs (M_{hg})	Mass Loss/Gain ($M_{hg} - M_{ar}$)	Weight % Loss/Gain: [($M_{hg} - M_{ar}$)/ (M_{ar})] x 100%
X_1	1.6799	1.68805	0.00815	0.485148
X_2	1.67986	1.68806	0.0082	0.488136
X_3	1.67989	1.68805	0.00816	0.485746
X_4	1.67989	1.68804	0.00815	0.485151
Mean	1.67989	1.68805	0.008165	0.486045
Std. Dev.	1.73205E-05	8.16E-06	2.38E-05	0.001422

Experiment Sample E				
	Mass As-received (M_{ar})	Mass After HG at 850°C for 3hrs (M_{hg})	Mass Loss/Gain ($M_{hg} - M_{ar}$)	Weight % Loss/Gain: [($M_{hg} - M_{ar}$)/ (M_{ar})] x 100%
X_1	1.67584	1.68618	0.01034	0.617004
X_2	1.67583	1.68619	0.01036	0.618201
X_3	1.67582	1.68615	0.01033	0.616415
X_4	1.67582	1.68622	0.0104	0.620592
Mean	1.6758275	1.686185	0.010358	0.618053
Std. Dev.	9.57427E-06	2.89E-05	3.1E-05	0.001849

Experiment Sample F				
	Mass As-received (M_{ar})	Mass After HG at 850°C for 3hrs (M_{hg})	Mass Loss/Gain (M_{hg} - M_{ar})	Weight % Loss/Gain: [(M_{hg} - M_{ar})/ (M_{ar})] x 100%
X_1	1.67507	1.68784	0.01277	0.762356
X_2	1.67504	1.68785	0.01281	0.764758
X_3	1.67506	1.68787	0.01281	0.764749
X_4	1.67505	1.68789	0.01284	0.766544
Mean	1.675055	1.687863	0.012808	0.764602
Std. Dev.	1.29099E-05	2.22E-05	2.87E-05	0.001719

Experiment Sample G				
	Mass As-received (M_{ar})	Mass After HG at 850°C for 3hrs (M_{hg})	Mass Loss/Gain (M_{hg} - M_{ar})	Weight % Loss/Gain: [(M_{hg} - M_{ar})/ (M_{ar})] x 100%
X_1	1.67295	1.68479	0.01184	0.707732
X_2	1.67295	1.68478	0.01183	0.707134
X_3	1.67294	1.68476	0.01182	0.706541
X_4	1.67295	1.68476	0.01183	0.707134
Mean	1.6729475	1.684778	0.01183	0.707135
Std. Dev.	5E-06	1.26E-05	8.16E-06	0.000486

Experiment Sample G				
	Mass After HG at 850°C for 3hrs (M_{hg})	Mass After DH at 650°C for 18hrs (M_{dh}))	Mass Loss/Gain (M_{dh} – M_{hg})	Weight % Loss/Gain: [(M_{dh} – M_{hg})/ (M_{hg})] x 100%
X_1	1.68479	1.68371	-0.00108	-0.0641
X_2	1.68478	1.68378	-0.001	-0.05935
X_3	1.68476	1.6838	-0.00096	-0.05698
X_4	1.68476	1.68378	-0.001	-0.05935
Mean	1.684778	1.683768	-0.00101	-0.05995
Std. Dev.	1.26E-05	3.95E-05	5.03E-05	0.002987

Experiment Sample H				
	Mass As-received (M_{ar})	Mass After HG at 850°C for 3hrs (M_{hg})	Mass Loss/Gain ($M_{hg} - M_{ar}$)	Weight % Loss/Gain: [($M_{hg} - M_{ar}$)/ (M_{ar})] x 100%
X_1	1.68534	1.69387	0.00853	0.506129
X_2	1.68535	1.69387	0.00852	0.505533
X_3	1.68534	1.69386	0.00852	0.505536
X_4	1.68534	1.69386	0.00852	0.505536
Mean	1.6853425	1.693865	0.008522	0.505684
Std. Dev.	5E-06	5.77E-06	5E-06	0.000297

Experiment Sample H				
	Mass After HG at 850°C for 3hrs (M_{hg})	Mass After DH at 650°C for 18hrs (M_{dh}))	Mass Loss/Gain ($M_{dh} – M_{hg}$)	Weight % Loss/Gain: [($M_{dh} – M_{hg}$)/ (M_{hg})] x 100%
X_1	1.69387	1.6938	-7E-05	-0.00413
X_2	1.69387	1.69376	-0.00011	-0.00649
X_3	1.69386	1.69381	-5E-05	-0.00295
X_4	1.69386	1.69379	-7E-05	-0.00413
Mean	1.693865	1.69379	-7.5E-05	-0.00443
Std. Dev.	5.77E-06	2.16E-05	2.52E-05	0.001486

Experiment Sample I				
	Mass As-received (M_{ar})	Mass After HG at 850°C for 3hrs (M_{hg})	Mass Loss/Gain ($M_{hg} - M_{ar}$)	Weight % Loss/Gain: [($M_{hg} - M_{ar}$)/ (M_{ar})] x 100%
X_1	1.6433	1.65614	0.01284	0.781355
X_2	1.64328	1.65611	0.01283	0.780756
X_3	1.64329	1.65609	0.0128	0.778925
X_4	1.64331	1.65612	0.01281	0.779524
Mean	1.643295	1.656115	0.01282	0.78014
Std. Dev.	1.29099E-05	2.08E-05	1.83E-05	0.001112

Experiment Sample I				
	Mass After HG at 850°C for 3hrs (M_{hg})	Mass After DH at 650°C for 18hrs (M_{dh})	Mass Loss/Gain ($M_{dh} - M_{hg}$)	Weight % Loss/Gain: [($M_{dh} - M_{hg}$)/ (M_{hg})] x 100%
X_1	1.65614	1.65400	-0.00214	-0.12922
X_2	1.65611	1.65398	-0.00213	-0.12861
X_3	1.65609	1.65399	-0.00210	-0.12680
X_4	1.65612	1.65400	-0.00212	-0.12801
Mean	1.656115	1.653993	-0.00212	-0.12816
Std. Dev.	2.08E-05	9.57E-06	1.71E-05	0.00103

Experiment Sample J				
	Mass As-received (M_{ar})	Mass After HG at 850°C for 3hrs (M_{hg})	Mass Loss/Gain ($M_{hg} - M_{ar}$)	Weight % Loss/Gain: [($M_{hg} - M_{ar}$)/ (M_{ar})] x 100%
X_1	1.69601	1.70546	0.00945	0.55719
X_2	1.69601	1.70543	0.00942	0.555421
X_3	1.69601	1.70543	0.00942	0.555421
X_4	1.69602	1.70543	0.00941	0.554828
Mean	1.6960125	1.705438	0.009425	0.555715
Std. Dev.	5E-06	1.5E-05	1.73E-05	0.001022

Experiment Sample J				
	Mass After HG at 850°C for 3hrs (M_{hg})	Mass After DH at 650°C for 18hrs (M_{dh})	Mass Loss/Gain ($M_{dh} - M_{hg}$)	Weight % Loss/Gain: [($M_{dh} - M_{hg}$)/ (M_{hg})] x 100%
X_1	1.70546	1.70388	-0.00158	-0.09264
X_2	1.70543	1.70391	-0.00152	-0.08913
X_3	1.70543	1.70391	-0.00152	-0.08913
X_4	1.70543	1.70391	-0.00152	-0.08913
Mean	1.7054375	1.703903	-0.00153	-0.09001
Std. Dev.	1.5E-05	1.5E-05	3E-05	0.001758